Digital measurement system for the LHC klystron high voltage modulator.

by
Anders Mikkelsen

Thesis submitted to Bergen University College
in partial fulfilment of the requirements for the degree of
Bachelor of Science

Department of Electronics
Bergen University College
March 2014

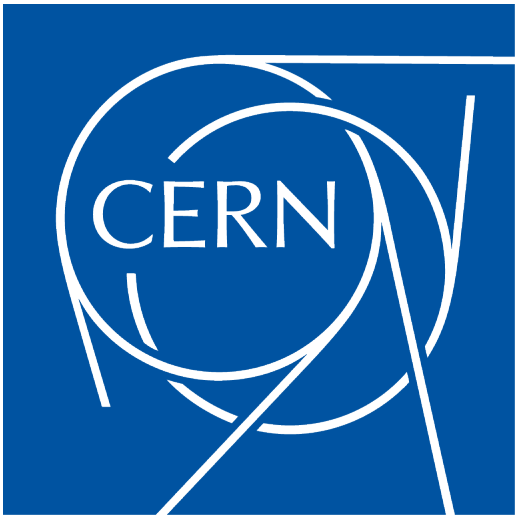

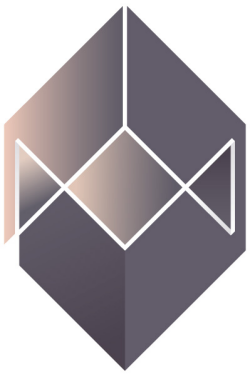

HØGSKOLEN
I BERGEN

BERGEN UNIVERSITY COLLEGE

CERN-THESIS-2014-033
26/03/2014

CERN Geneva

Abstract

"Accelerating voltage in the Large Hadron Collider (LHC) is created by a means of 16 superconducting standing wave RF cavities, each fed by a 400MHz/300kW continuous wave klystron amplifier. Part of the upgrade program for the LHC long shutdown one is to replace the obsolete analogue current and voltage measurement circuitry located in the high voltage bunkers by a new, digital system, using ADCs and optical fibres. A digital measurement card is implemented and integrated into the current HV modulator oil tank (floating at -58kV) and interfaced to the existing digital VME boards collecting the data for several klystrons at the ground potential. Measured signals are stored for the logging, diagnostics and post-mortem analysis purposes."

Acknowledgements

"First and foremost, I would like to thank my supervisor at CERN, Dr. Daniel Valuch and my professor at Bergen University College, Dr. Johan Alme for guidance and advice during this project. I would also like to thank all my colleagues in the BE-RF-FB group, the BE-RF-CS group and the BE-RF-KM group for their support and help, with special thanks to Tom Levens and Gianfranco Ravidà. Finally, I would like to thank my family and friends for moral support and encouragement."

—

Contents

List of Tables

List of Figures

1. Introduction to CERN

CERN is the European Organization for Nuclear Research, located near the French-Swiss border close to Geneva. The organization consists of 21 member states, with a few more currently in the process of joining. CERN was founded in 1954 by 12 nations, with a mission to perform fundamental research, advance the frontiers of technology, educate the scientists of tomorrow and bring together nations for international collaboration.

CERN experiments mainly revolve around particle accelerators, machines that accelerate charged particles up to high velocities, and collide them with fixed targets or other particles to observe the outcome. In such collisions, new particles are created, and by observing these particles and their decay products, the forces and building blocks of nature can be explored.

The experiments performed at CERN have resulted in a range of achievements, including the discovery of W and Z bosons in 1983, creation of antihydrogen atoms in 1995 and the discovery of a particle consistent with the Higgs boson in 2012.

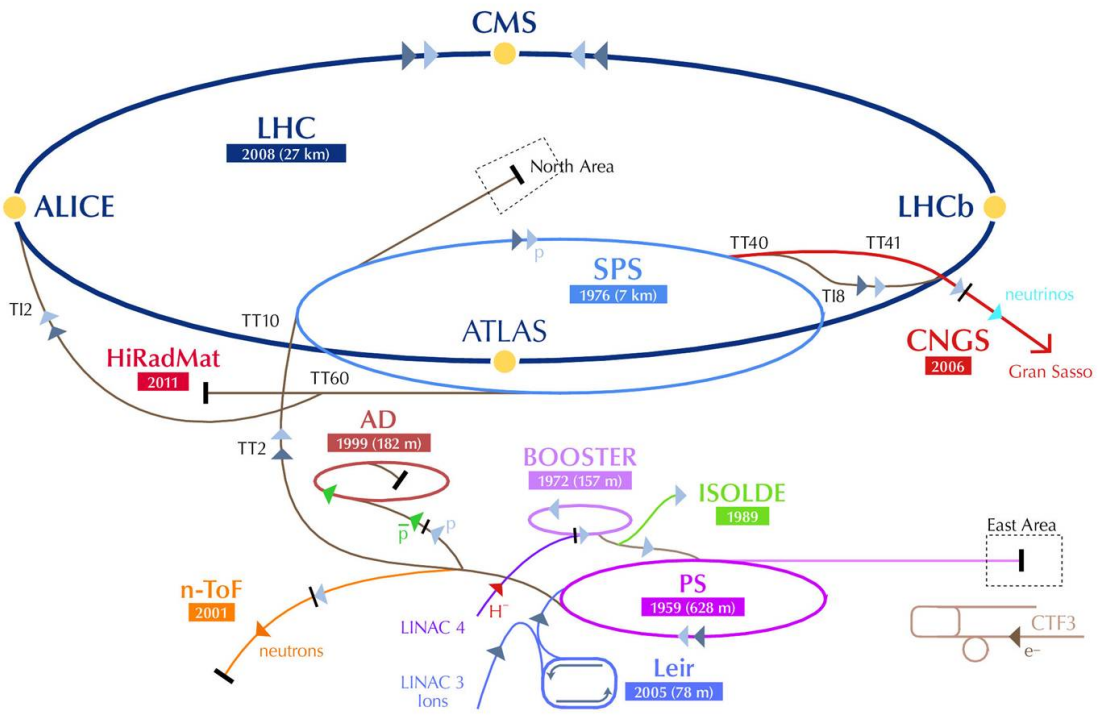

Figure 1.1: The CERN accelerator complex

The CERN accelerator complex consists of a number of linear and circular accelerators, shown in Figure 1.1, the biggest of which is the Large Hadron Collider, shown in Figure 1.2. The Large Hadron Collider is a circular particle accelerator and collider, 27 km in circumference. It is the largest and most complex machine built by mankind. The machine has a pair of beam pipes, each with particles being accelerated in opposite directions. Charged particles are steered in a closed circular orbit by the use of 1232 superconducting dipole magnets, each 15 meters long, cooled down to a few degrees above absolute zero. The particles are accelerated by radio frequency cavities, presently up to energies of 4 TeV per beam for protons. When the particles have been accelerated up to the desired energy, they are steered to collide with each other at several points along the machine. Each of these locations contain an experiment, consisting of a wide range of different detectors to measure the outcome of particle collisions. The four main experiments are ATLAS, CMS, ALICE and LHCb.

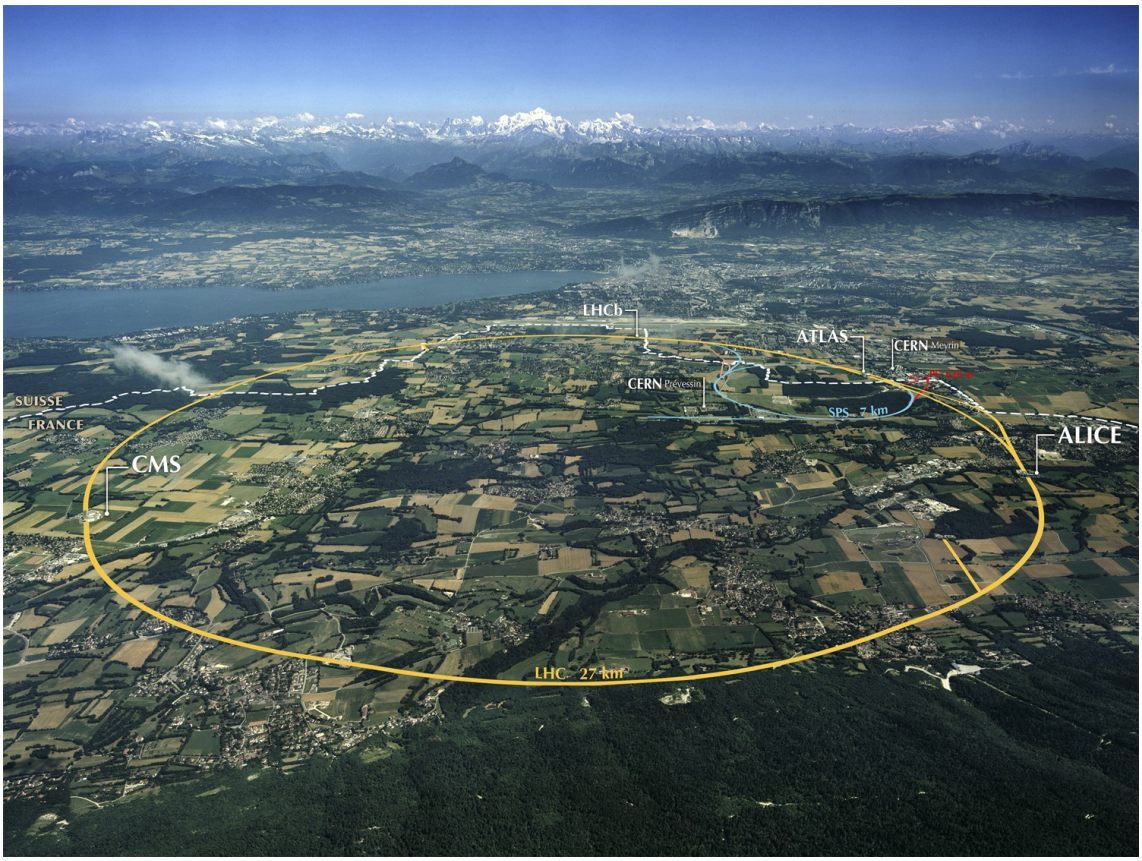

Figure 1.2: Aerial view of the Large Hadron Collider location

2. LHC RF power systems overview

2.1 LHC accelerating system overview

To accelerate charged particles, electric fields are used. In the LHC, these fields are generated inside superconducting RF cavities. There are eight cavities per beam, separated into a pair of cryomodules with four cavities in each. One of these modules is shown during assembly in Figure 2.1 and installed in the machine tunnel in Figure 2.2. Figure 2.3 shows an overview of the power RF systems in the LHC. Each cavity is powered from one klystron RF amplifier, which provides up to 330 kW of RF power at 400.8 MHz [5]. Waveguides transfer the RF power from the klystrons to the accelerating cavities. Reflected power from the cavities passes back through the waveguides, and is diverted into water-cooled ferrite loads by the circulators.

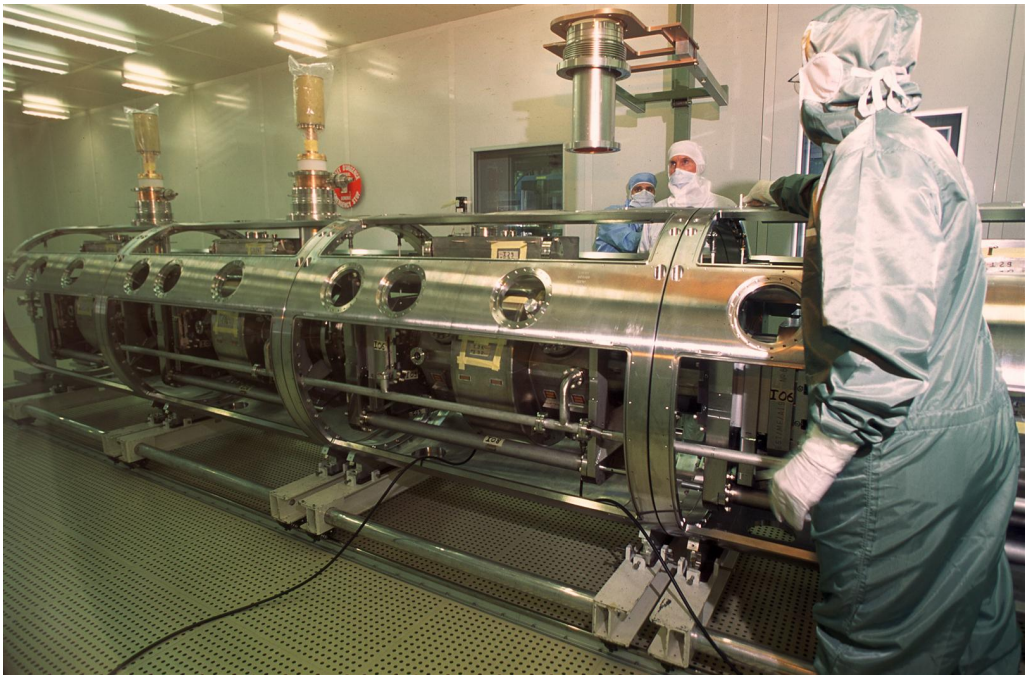

Figure 2.1: LHC cavity module being assembled in a clean-room [1]

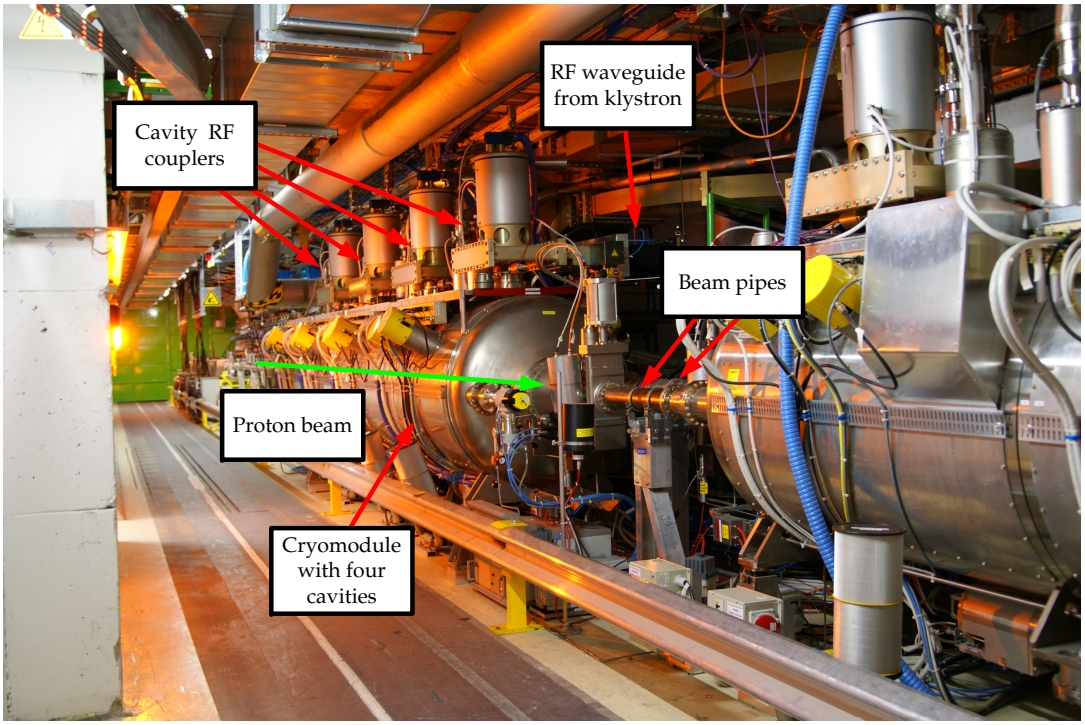

Figure 2.2: LHC cavity module in machine tunnel [2]

The RF drive signal for the klystron amplifier is generated by the Low Level RF system, based on feedback loops to keep the field in the cavities synchronized to the particles circling in the machine.

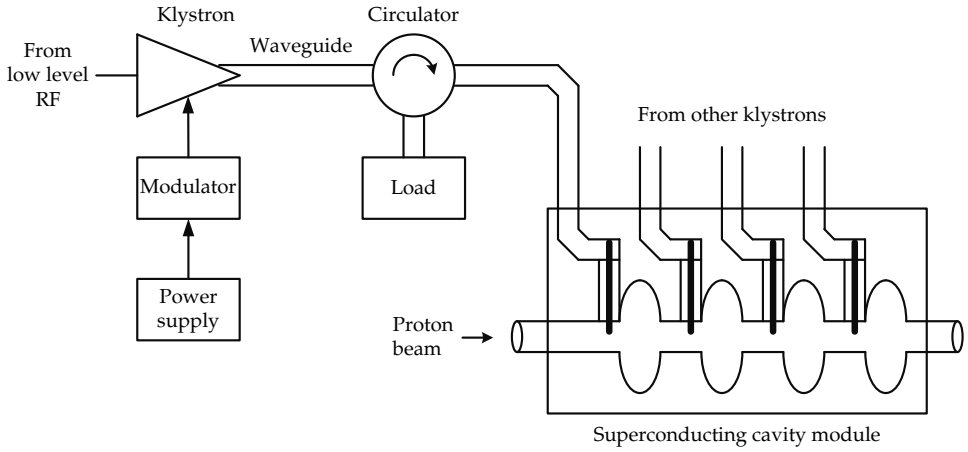

Figure 2.3: The acceleration RF systems in the LHC

2.2 High voltage generation and distribution

For the 16 klystrons in the LHC, there are four power converters, each supplying four klystrons. The power converters, shown in Figure 2.4, are supplied by the 18 kV three-phase grid at CERN. This voltage is stepped down to 1 kV by two transformers with the secondaries configured so that one advances the phase by 15 degrees and the other retards the phase by 15 degrees. This results in a six-phase output. Thyristor AC line controllers regulate the effective voltage. The output of the thyristor controllers goes to two step-up transformer that step up the voltage to 52 kV. The high voltage from the transformer secondaries is rectified, and the rectified output of the two transformers is put in series. The output of each power converter is smoothed using two 2.5 H inductors. Due to the phase offset between the transformers, the ripple on the output is reduced, and less output filter inductance is needed compared to a regular 3-phase system [3] [6] [7].

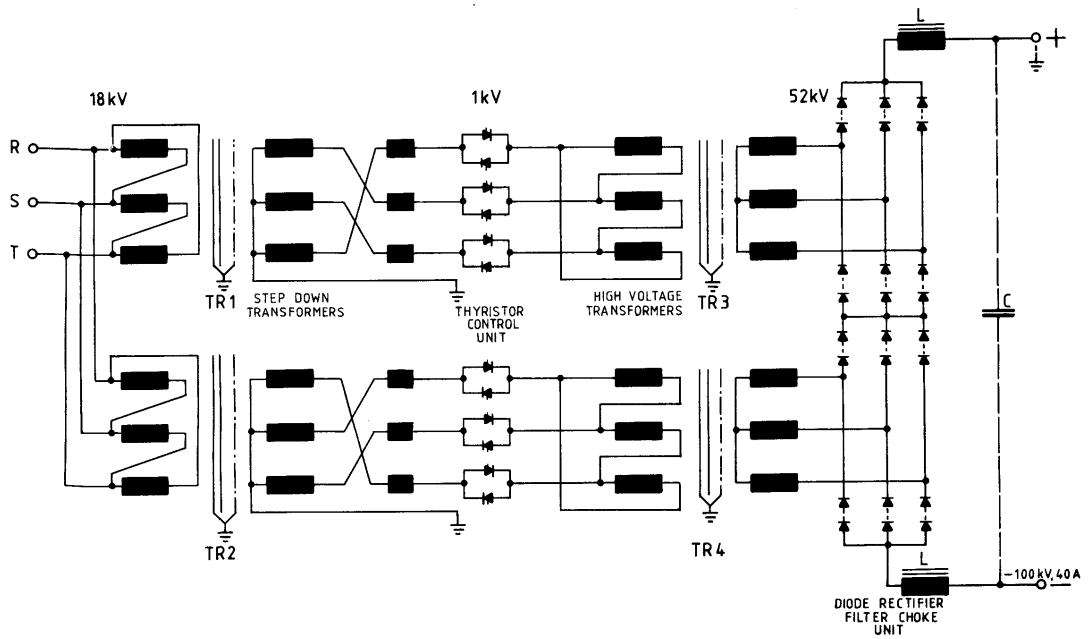

Figure 2.4: Diagram of the power converters for the LHC klystrons [3]

An overview of high voltage distribution for the LHC klystrons is shown in Figure 2.5. The power converters are installed on the surface, and the klystrons are at LHC point 4, underground cavern UX45. Shielded cables are used to bring the high voltage down to the klystrons. The output of each power converter goes to a separator, which distributes and switches power to the individual klystron modulators and interconnects the HV bus with the decoupling capacitor and crowbar. A 4 μF decoupling capacitor is used for each set of four klystrons. A

10 Ω resistor is placed in series with the capacitor to limit the peak current in case of klystron arcing and subsequent crowbar firing. The separator, crowbar, decoupling capacitor and modulators for a set of four klystrons are mounted in one high voltage bunker, shown in figure 2.6.

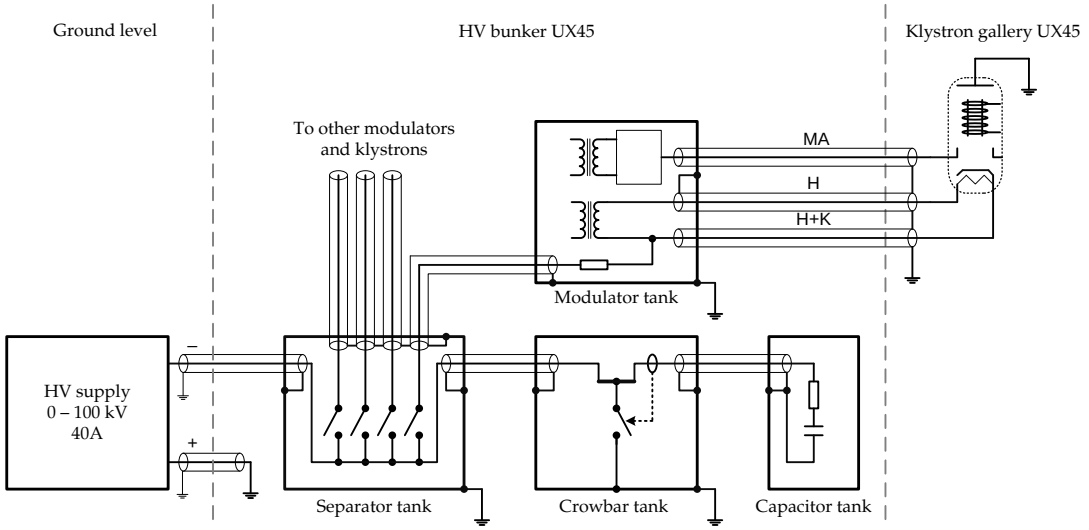

Figure 2.5: High voltage distribution and crowbar

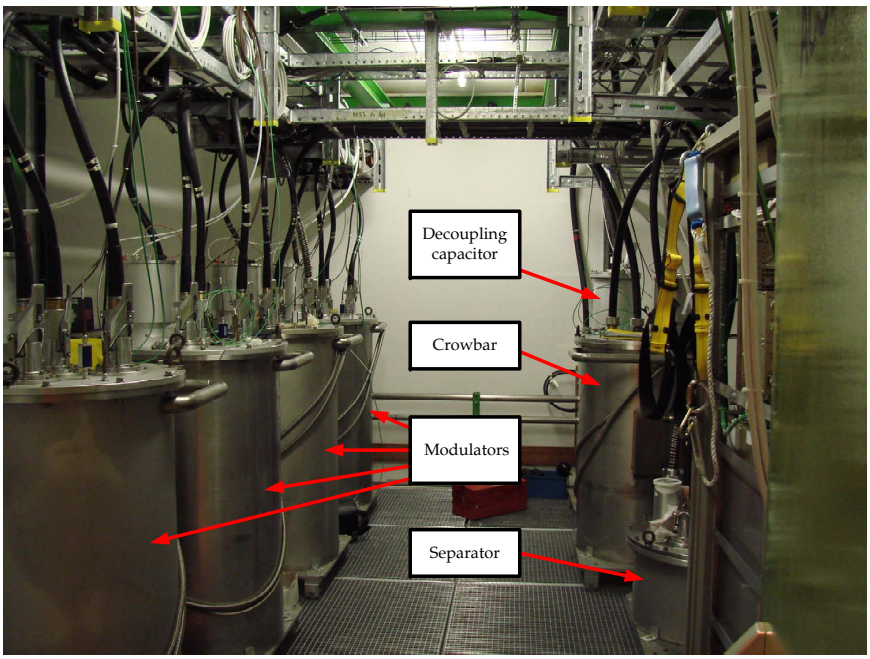

Figure 2.6: Interior of a high voltage bunker for four klystrons

2.3 Klystrons, modulators and crowbars

The klystrons used in the LHC are Thales type TH2167, shown in Figure 2.7 (a). Each klystron can deliver up to 330 kW CW of radio frequency power at 400.8 MHz, while operating with a cathode voltage of -58 kV and a cathode current of 9.2 A [8]. The klystrons are fitted with a modulation anode, which allows the cathode current to be varied without changing the cathode voltage. This permits the operating point of each klystron to be changed individually despite four klystrons sharing the same cathode supply. The modulation anode is typically at a positive voltage of between 5 kV and 35 kV relative to the cathode, depending on the desired cathode current. The cathode heater requires a current of approximately 30 A, and the voltage drop across the heater at this current is typically around 7 V.

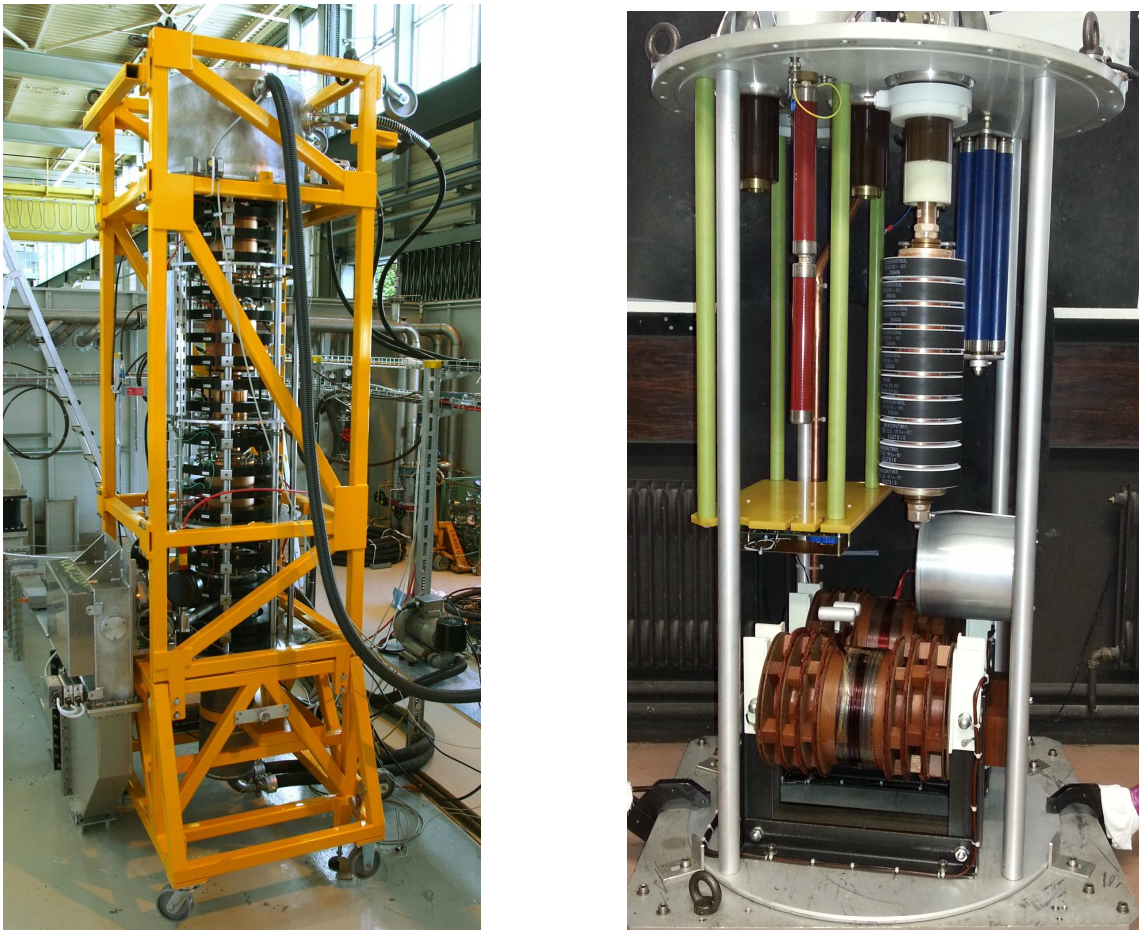

(a) (b)

Figure 2.7: Thales TH2167 klystron (a) and MAC10 modulator (b)

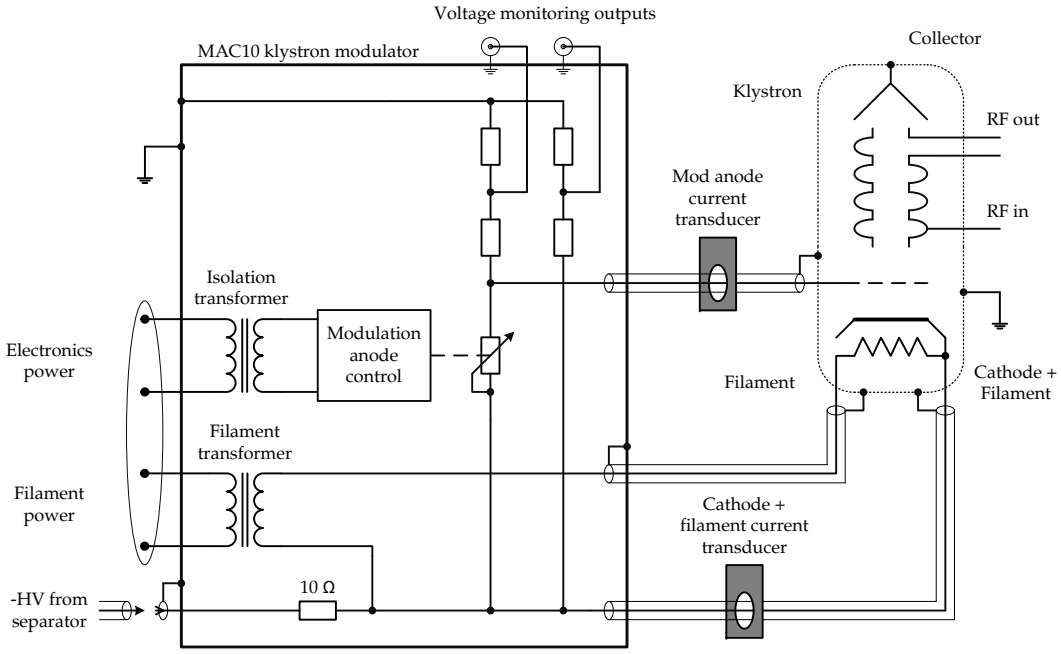

Figure 2.8: Modulator connected to klystron

The klystron modulator, shown in Figure 2.7 (b) and Figure 2.8, provides the heater power and the modulation anode voltage to the klystron, and connects the klystron cathode to high voltage from the separator. Voltage dividers in the modulator allow for external monitoring of the cathode and modulation anode voltages at ground potential. There is a 10 Ω resistor in series with the high voltage supply, to aid in decoupling and to limit peak currents through the klystron in case of arcing.

Heater voltage for the klystron is supplied by a 33 V transformer with an isolation rating of 100 kV between the primary and the secondary. Heater current is controlled at ground potential by a phase angle controller external to the modulator, the so called "gradateur", which regulates the primary current of the heater transformer based on feedback from an external heater current transducer.

The modulation anode voltage is generated by a variable voltage divider between the cathode and ground, with an adjustable element in one leg of the divider. This adjustable element is presently a power switching tetrode, Thales type TH5186 [9]. The tetrode control is galvanically isolated by means of frequency-to-voltage converters and optical fibres. This tetrode is not manufactured any more, so a replacement based on current technology is being investigated. One proposal is to use reed relays and resistors [10].

In the klystrons, there is a strong electrical field between the cathode, which sits at a high negative potential, and the body of the klystron, which is grounded. The space between the cathode and the body of the klystron can suffer an electri-

cal break down, leading to arcing inside the klystron. The electrical arc has a very low resistance, so the current drawn from the supply is much higher than in normal operation. This leads to high energy dissipation in the klystron cathode, the most delicate part of the tube. In this scenario, the cathode voltage of the klystron must be rapidly removed before permanent damage occurs to the klystron.

Even if the power supply is shut down immediately when an arc occurs, the energy stored in the decoupling capacitor, the high voltage cables and the power supply output inductors is sufficient to cause serious damage to the klystrons. A crowbar is installed to remove the high voltage supply in case of a klystron arc. The crowbar is a fast switch connected between the high voltage supply output and ground, which short circuits the high voltage bus to ground when excessive currents are detected flowing from the decoupling capacitor. In the system currently installed in the LHC, the switch is a hydrogen thyratron, but a replacement based on thyristors is being evaluated [4].

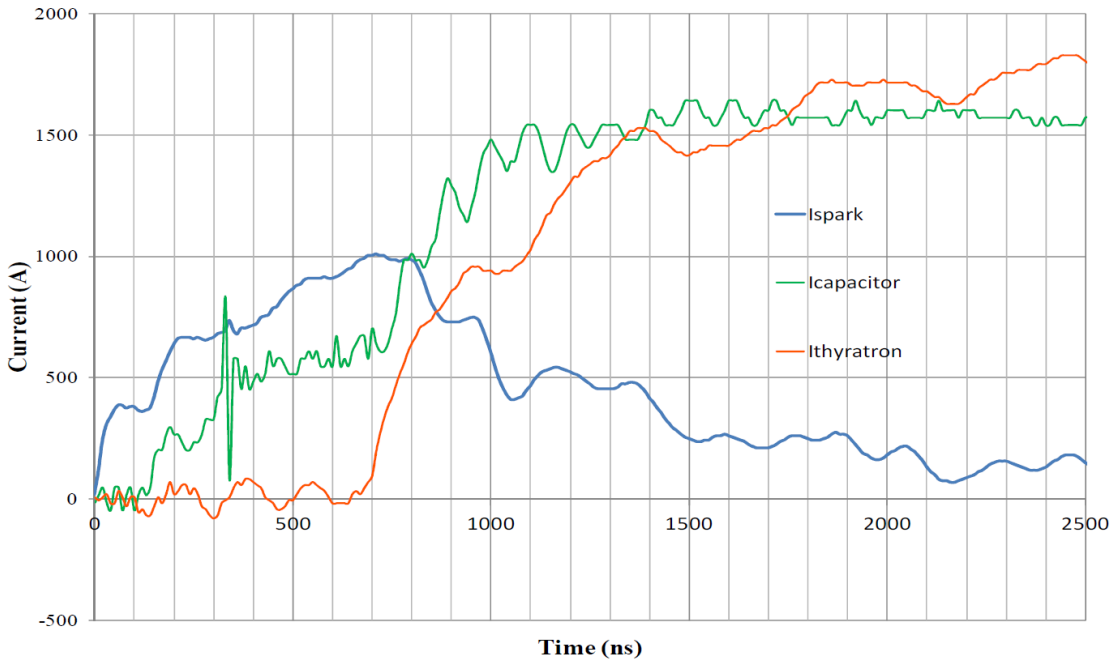

Figure 2.9: Klystron current (blue), crowbar current (orange) and capacitor current (green) during klystron arcing at low voltage [4]

Figure 2.9 shows the currents flowing in the high voltage system during klystron arcing and subsequent crowbar firing, when operating at a voltage lower than the typical operating voltage. The fault current paths are shown in Figure 2.10. The blue trace shows the current flowing in the klystron, which peaks at approximately 1 kA. This initial part of the fault current mainly comes from discharge of the coaxial high voltage cables. This current starts diminishing around 800 ns

after the arc occurs, as the crowbar turns on and diverts the current. The crowbar current (orange) can be seen to start rising when the crowbar fires around 700 ns. During crowbar firing at the full operating voltage of -58 kV, the waveforms are similar, but the klystron spark current peaks at 1.6 kA and the crowbar current peaks at 5.5 kA.

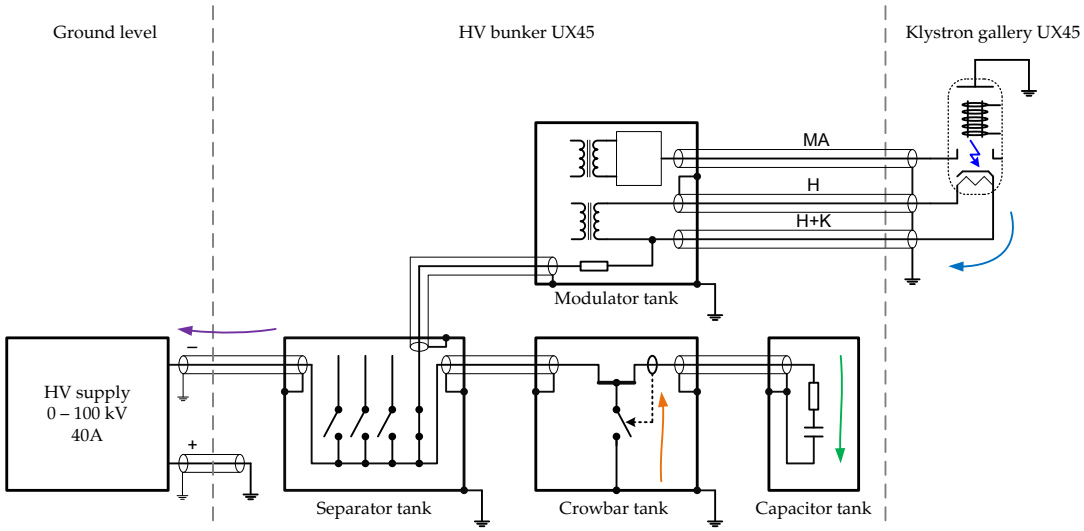

Figure 2.10: Current paths during klystron arcing and crowbar firing

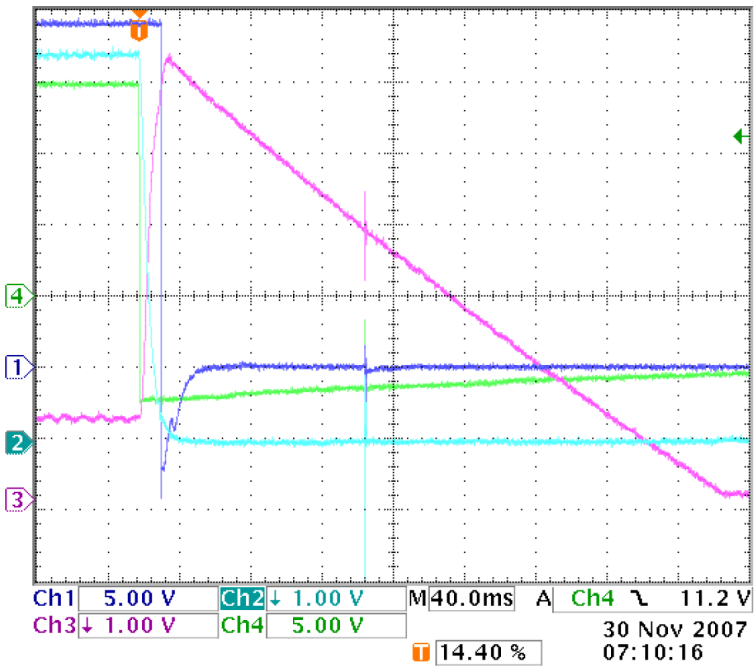

Figure 2.11: Slow part of the crowbar current at 58 kV, purple trace is crowbar current. 8 A per vertical division, 40 ms per horizontal division

The crowbar continues conducting as the decoupling capacitor discharges, with a time constant of 20 μs. After 100 μs, the decoupling capacitor is largely discharged, but the output inductors of the power supply still store a significant amount of energy. The discharge of these inductors has a much longer time constant, shown in Figure 2.11. This current also flows through the crowbar, which needs to keep conducting until this energy is dissipated.

2.4 Present klystron HV parameter measurements

As part of the control systems for the LHC high power RF, certain important parameters of the klystron operation are monitored and logged. Cathode voltage and modulation anode voltage are measured using voltage dividers mounted inside the modulator, with outputs at ground potential, shown in Figure 2.12. Modulation anode, cathode and filament current are measured by a pair of external current transducers mounted on the high voltage cables between the modulator and the klystron, shown in Figure 2.13. The shielding of high voltage cables between the modulator and the klystron must be left unconnected on the modulator side to avoid measurement errors caused by currents flowing in the shielding. This is not an ideal solution, as high voltages can appear on the cable shielding during klystron sparking and other transient events.

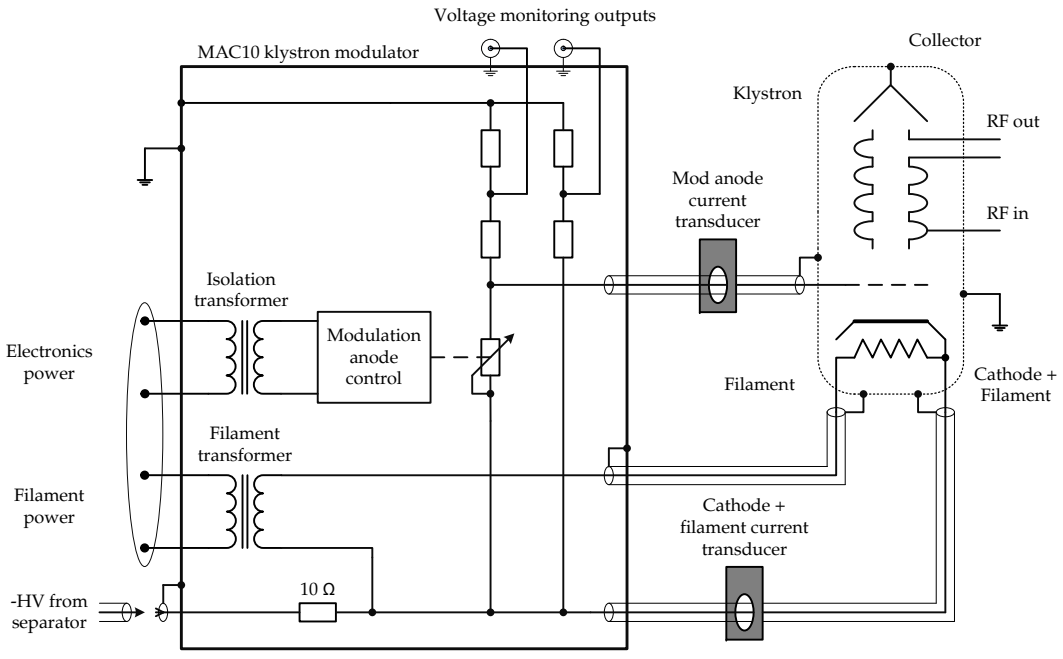

Figure 2.12: Present HV measurement system

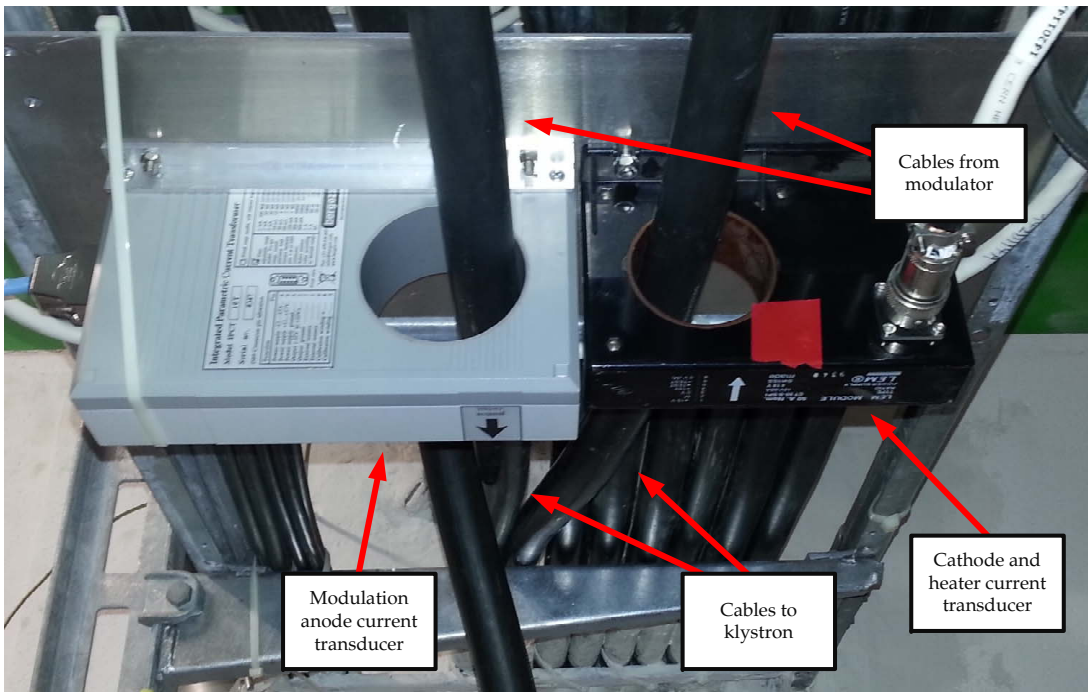

Figure 2.13: Current transducers in the existing installation

One source of uncertainty in the present measurement system is caused by the way the cathode current is measured. One common transducer is used to measure both the cathode current and the filament current, as shown in Figure 2.14. This current transducer is placed around the Filament/Cathode wire of the klystron, where both the filament current (AC) and the cathode current (DC) is flowing. To separate these two measurements, the filament current is taken as the AC component of the current and the cathode current is taken as the DC component. The problem is that not all of the cathode current flows in the Filament/Cathode connection to the klystron, part of it flows in the Filament wire, through the secondary of the filament transformer. This current represents around 10 % of the total cathode current. This fraction of the cathode current is therefore not measured in the present system. To correct for this, the measured current value is multiplied by a constant. This fraction is not necessarily identical between different klystrons, and it is not guaranteed to be stable with ageing of the klystrons. A further problem with the existing installation is that some of the equipment used is outdated and out of production. Some of the equipment is currently past its expected service life, and reliability can not be guaranteed.

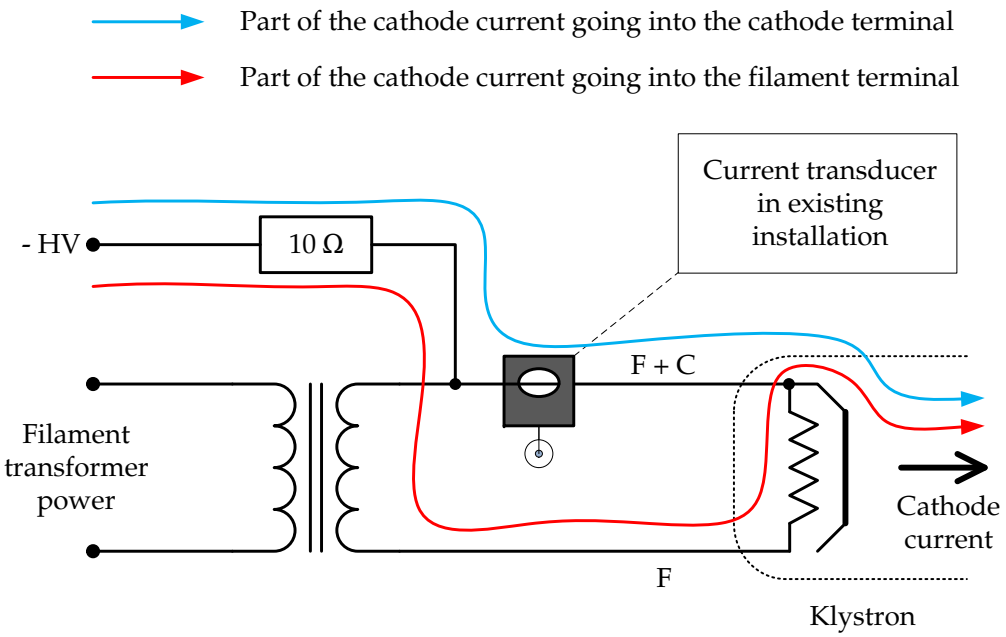

Figure 2.14: Cathode current path through filament transformer

Following is an example of a fault that occurred in the LHC RF power system on 20.09.2011 20:25:16, with all data available from the current measurement system. An entry in the machine log book for the LHC shows a beam dump triggered by a fault in the RF system:

```
Global Post Mortem Event

Event Timestamp: 20/09/11 20:25:16.053
Fill Number: 2129
Accelerator / beam mode: PROTON PHYSICS / STABLE BEAMS
Energy: 3500040 [GeV]
Intensity B1/B2: 15217 / 15570 [e^10 charges]
Event Category / Classification:
PROTECTION_DUMP / MULTIPLE_SYSTEM_DUMP
First BIC input Triggered:
First USR_PERMIT change:
Ch 8-RF-b1: B T -> F on CIB.UA47.R4.B1
```

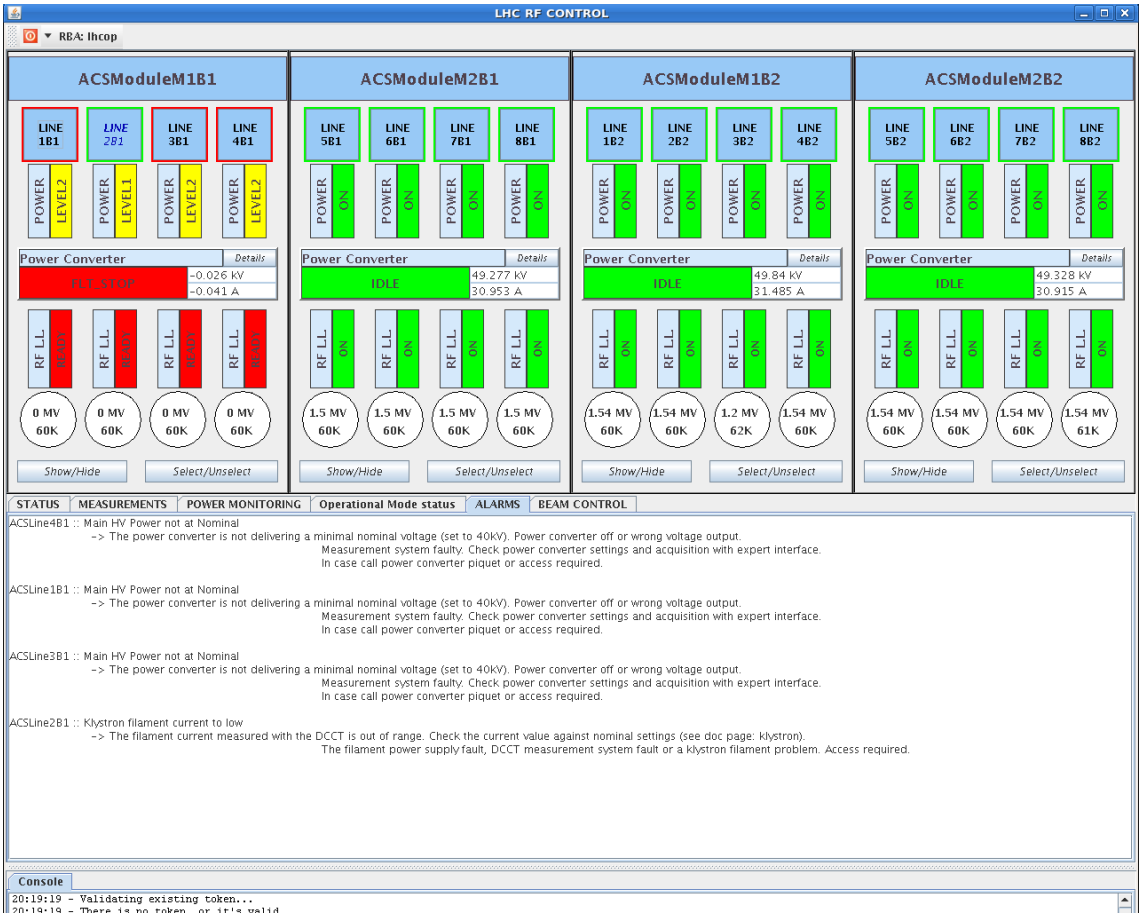

Figure 2.15: LHC RF control systems showing shut-down of one power converter and triggered interlocks

The RF high power status display, shown in Figure 2.15, shows that power converter 1 on beam 1 has been shut down. A ”Klystron filament current too low” error is indicated in ACSLine2B1 and ”Main HV power not at Nominal” errors are indicated for the other three klystrons. This indicates that the fault is most likely to be in klystron 2, the interlocks on the other klystrons are caused by the power converter shutting down in response to the fault with the klystron 2. Figure 2.16 shows the interlock chain for the RF systems. The interlocks needed to enable Level 2 for klystron 2 (LINE 2B1 LV2 ENABLE) are indicated to have fired. An examination of the individual interlocks indicates that the fault was triggered by the ”DCCT currents” interlock on klystron 2 in RF module 1 for beam 1.

Figure 2.16: LHC RF interlock system, showing fault is in LV2 interlocks, DCCT current

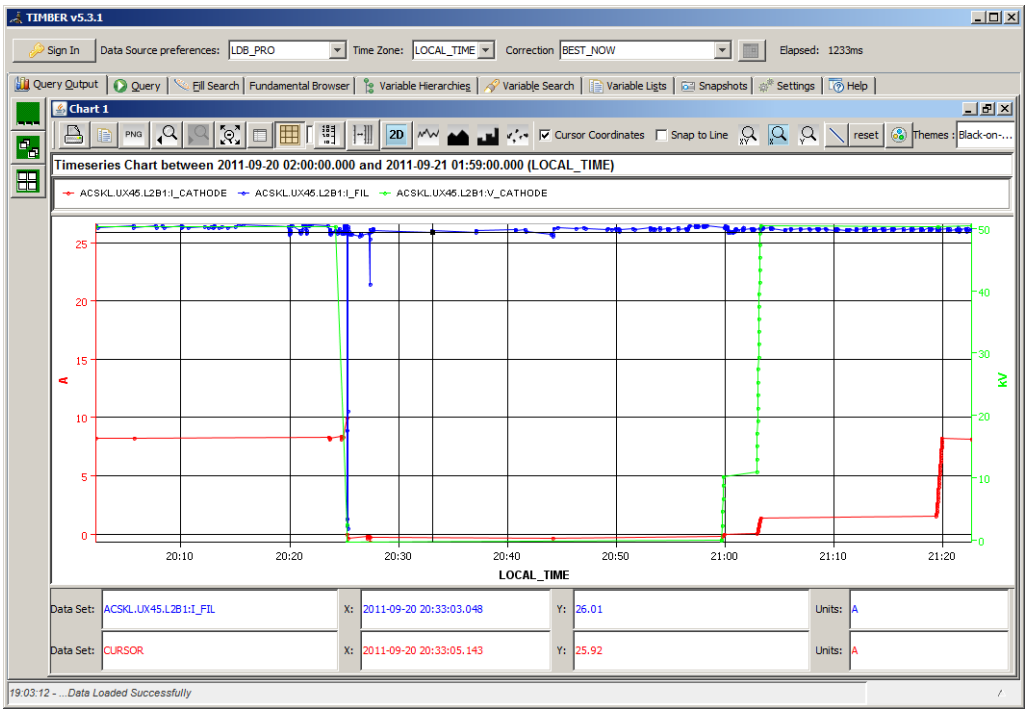

Figure 2.17: Logged measurement data plot showing filament current drop-out. Cathode current (red), filament current (blue) and cathode voltage (green)

Measurement data is logged in the central LHC logging database, "Timber", and stored permanently [11]. Figure 2.17 shows the logged cathode current in red, filament current in blue and cathode voltage in green. The dots on the plot lines indicate saved data points, and the lines are interpolated between these points. During periods with small changes in the measured values, measurements are stored every 15 minutes. Examination of the logged data shows a short interruption in the filament current for klystron 2 around 20:25, which corresponds with the time of the beam dump.

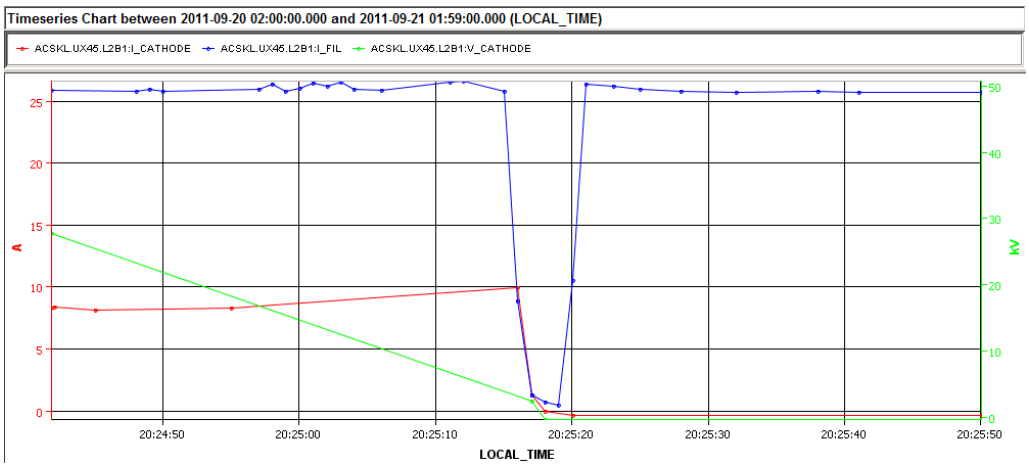

Figure 2.18: Measurement data plot showing filament current drop-out in closer detail. Cathode current (red), filament current (blue) and cathode voltage (green)

During periods with larger changes in measured values, measurements are stored every second. Due to the transient nature of the fault, it can be hard to analyse the post-mortem data to determine the cause. Figure 2.18 shows a close-up view of the event that triggered the interlock, the filament current drops to nearly zero for several seconds. The cathode current can be seen to fall at the same time as the filament current, but due to the granularity of the measurement it is hard to determine if this happens before or after, which could give vital clues as to the cause of the fault.

To overcome these problems, it is proposed to make a new state of the art measurement system. To allow direct measurements of filament voltage, filament current and cathode current, the measurement system should be directly connected to the klystron cathode. The proposed solution gives an increase in the sample rate by three orders of magnitude compared to the existing system, which will greatly facilitate post-mortem analysis. A side effect of the new system is also a 10-fold increase in measurement accuracy.

3. Prototype version

3.1 Requirements for the measurement system

The parameters that need to be measured are shown in table 3.1. All measurement channels should to have at least 10 bits of resolution and all channels should to be sampled at a rate of at least 1 kHz to allow observation and logging of short-lived events. All measured values need to be be stored in a buffer, at least one minute long, for diagnostics and post-mortem analysis. The measurement system needs to be compatible with the conditions encountered in normal modulator operation and it needs to survive the conditions during conceivable fault scenarios.

Measured parameter	Nominal value	Measurement range
Heater voltage	±20 V pk	±50 V pk
Heater voltage RMS	12 V RMS	50 V RMS
Heater current	±40 A pk	±50 A pk
Heater current RMS	30 A RMS	50 A RMS
Cathode current	9 A	15 A
Cathode voltage	-58 kV	-70 kV
Modulation anode voltage	-35 kV	-70 kV

Table 3.1: Parameters that will be measured

The klystron is operated with a grounded collector, and the measurement system is floating at the cathode potential, which is nominally -58 kV. The measurement system needs to be constructed in such a way that it can be integrated into the modulator without compromising the high voltage clearance distances inside the oil tank. The components used need to be able to work correctly while immersed in oil for long periods of time.

3.2 Measuring current

The chosen ADC measures unipolar voltage signals in the range of 0 V to 2 * Vref, which corresponds to 0 – 5 V. We want to measure AC and DC parameters, these need to be mapped to the unipolar input voltage range to the ADC. There are several approaches to measure currents and scale them to this range. A current

passing through a resistance leads to a voltage drop across the resistance according to ohm's law. This voltage can be scaled up to the input voltage range of the ADC using a differential amplifier, as shown in Figure 3.1 (a), but this method has several disadvantages. If a floating current measurement is needed, a differential amplifier needs to be used to sense the voltage across the resistor. In a noisy high voltage environment, this amplifier needs very good common-mode rejection. To measure larger currents, the voltage across the sense resistor needs to be kept low to minimize power dissipation in the sense resistor. This dictates that the amplifier needs considerable gain to amplify the sense voltage up to the ADC input voltage range.

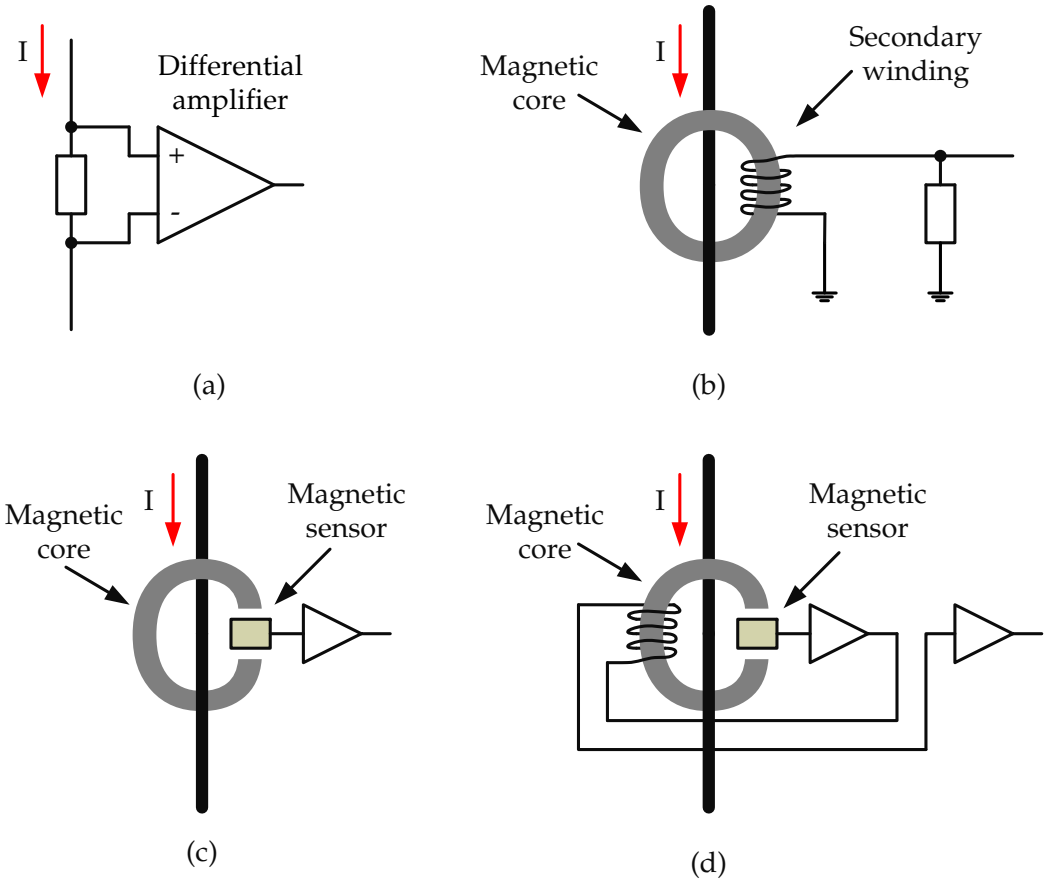

Figure 3.1: Resistive current sensing (a), traditional current transformer (b), open-loop (c) and closed-loop (d) current transducers

A current passing through a wire also leads to a magnetic field around the wire according to Ampere's law. By measuring this field, the current can be measured without a direct electrical connection to the circuit in which the current is flowing. This can be done using a regular transformer for AC currents, shown

in Figure 3.1 (b). Transformers have a finite lower frequency limit, so they can not be used to measure DC currents. To measure DC currents as well as AC currents, hall-effect and flux-gate sensors are used to sense the field in the core. Fully integrated magnetic current transducers are widely available with a range of different full-scale currents and accuracies, and a bandwidth of tens to hundreds of kilohertz.

Magnetic current transducers generally come in two varieties, open-loop and closed-loop. Open-loop transducers directly measure the magnetic field in the core, shown in Figure 3.1 (c), making the assumption that the field strength is directly proportional to the current . All high-permeability magnetic core materials used in these current transducers experience saturation, which leads to non-linearity errors in the current measurement. To avoid this error source, closed-loop current transducers inject a current in a second winding on the magnetic core, shown in Figure 3.1 (d). This current is adjusted by the transducer electronics to cancel out the main current, so the field in the core is close to zero [12]. Due to the fact that these transducers measure the field in the magnetic core, any remanent magnetism in the core will lead to an electrical offset on the output.

3.3 Proposed solution

The proposed measurement system consists of a measurement card integrated into the modulator, and a receiver card at ground potential, shown in Figure 3.2. Communication between the measurement card and the receiver is over optical fibre.

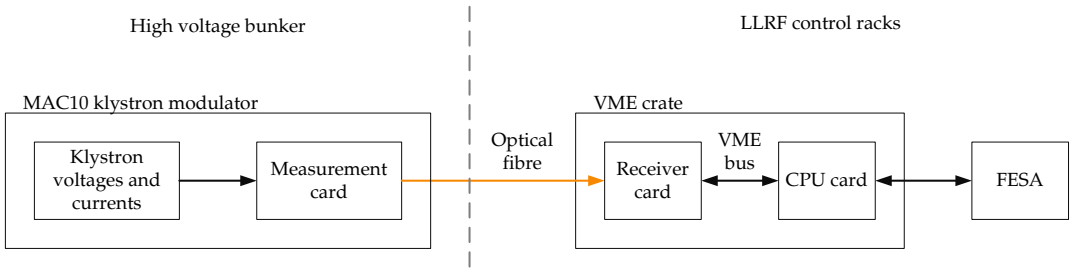

Figure 3.2: Overview of the measurement system

Existing ground-referenced resistor dividers in the modulator can be extended to also provide a voltage measurement referenced to the cathode potential, shown in Figure 3.3. Transient voltage suppressors are placed across the low-side voltage divider resistors to protect the measurement system from voltage spikes. Connections to the high voltage divider resistors are done using shielded cable, and

the low-side measurement resistors are placed on the measurement board. The cathode potential for the klystron is connected to the live terminal of the filament transformer. As the high voltage measurements are referenced to the klystron cathode, the heater voltage measurement should also be referenced to this potential, which is the live of the heater transformer. Power for the measurement card can be taken from the low voltage transformer that presently powers the modulation anode voltage control system.

Analogue-to-digital converters are available with standard serial interfaces like SPI and I^2C. These serial interfaces can be used directly over optical fibre, but this has some disadvantages. SPI requires four lines, which would mean four fibres to each modulator. I^2C uses only two lines, but one is bidirectional, which means that at least three fibres and additional electronics is needed to transmit I^2C over fibre.

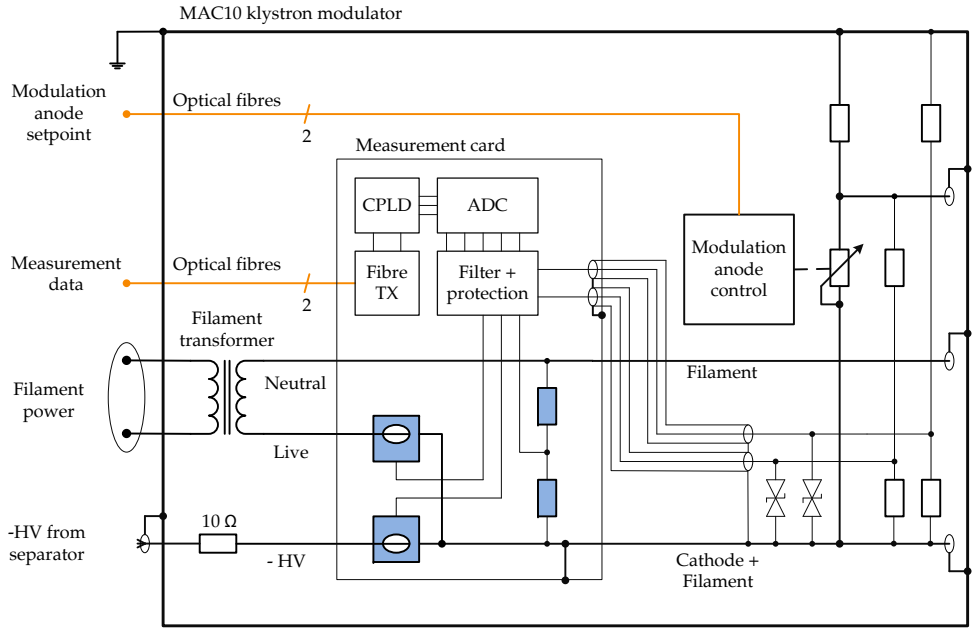

Figure 3.3: Measurement card integrated in the modulator

A programmable logic device is inserted between the ADC and the fibre link. Its purpose is to initialize the ADC, sequence and control the readout of the different measured channels, and encode and serialize the data for the fibre link. For the programmable logic device, FPGAs are considered too risky due to the harsh HV environment the measurement system is operating in. In theory, with proper encoding, a single optical fibre could be used to transmit the data. Full encoding of the measured data, clock signal and packet framing into a single fibre is

difficult to implement with the limited hardware resources available in CPLDs. In addition, a sophisticated link with the clock embedded in the data is prone to upset.

In the data link, there's a chance of data corruption due to interference or bad connections. If some bits get lost, the receiver needs to resynchronize to the serial stream so that subsequent bytes don't end up misaligned in the receiver. In the SPI bus, this is done using the Chip Select (CS) signal. This signal goes low before the start of each packet, resynchronizing the transmitter and receiver.

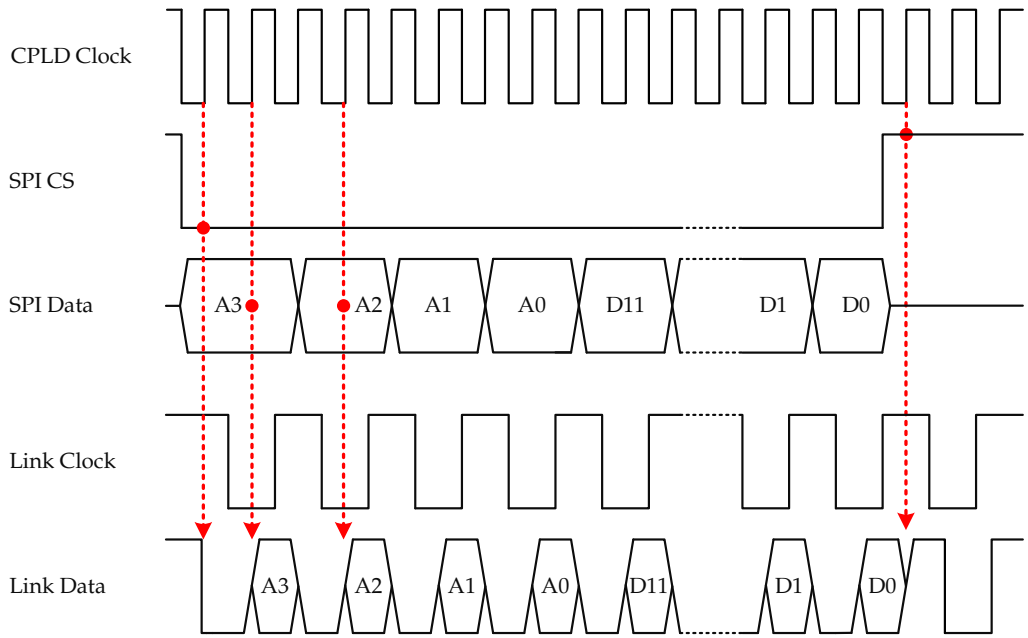

Figure 3.4: SPI interface and serial link that incorporates clock and CS into a single signal

A compromise is proposed, based on SPI, where the chip select is embedded in the data, and the clock is sent separately, requiring two fibres for the link. CS is transmitted on the falling edge of the clock and the data is transmitted on the rising edge, shown in Figure 3.4. In case of data corruption, the transmission should recover automatically by the next frame, due to the chip select embedded in the data signal. The proposed method is robust to interference, and simple and low cost due to the use of only two fibres between the measurement card and the receiver.

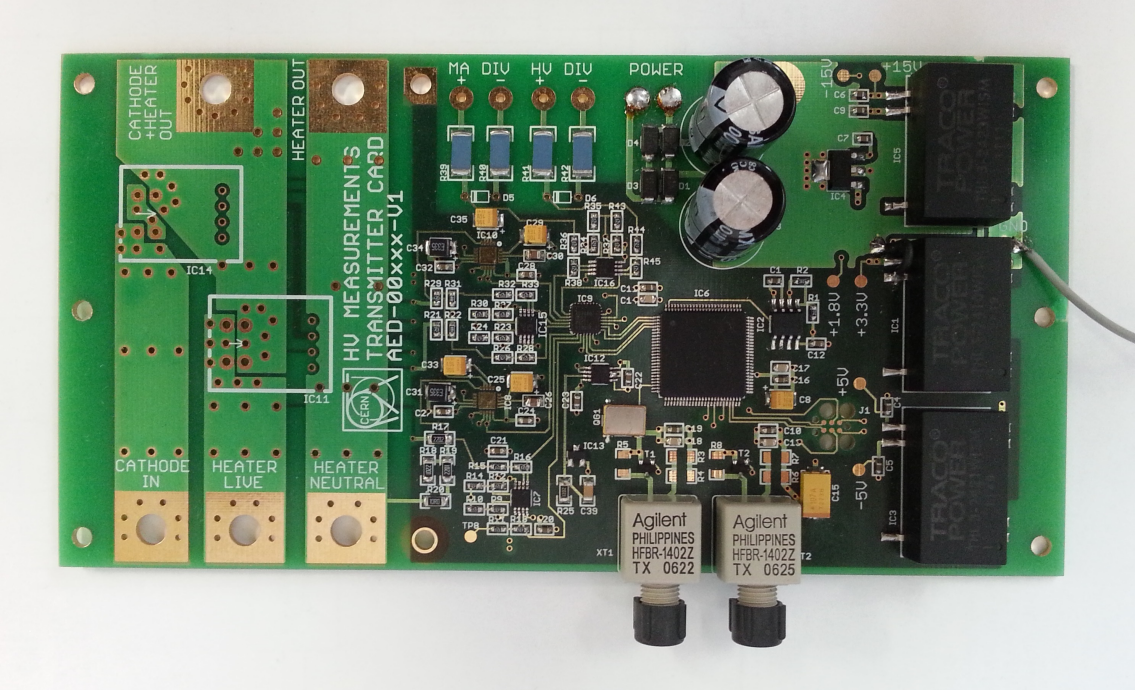

Figure 3.5: Measurement board prototype

A first feasibility study revision of the system was built before my arrival at CERN. The measurement board is shown in Figure 3.5.

The analogue signals from the voltage dividers and current transducers are digitized by an Analog Devices AD7490 digital-to-analog converter. This ADC has 16 input channels with a resolution of 12 bits each, but only the eight first are used in this application. Internally, it contains a single ADC with a maximum sample rate of 1 MSPS, that can be switched between the different input channels. The converter is configured for an input voltage range of 0 V to 2 * Vref, 0 – 5 V, corresponding to readings of -2048 and 2047 respectively [13]. A block diagram of the measurement system is shown in Figure 3.6.

The measurement board is controlled by a Xilinx CoolRunner II CPLD [14]. A block diagram of the CPLD code is shown in Figure 3.7. The first eight out of 16 available analogue-to-digital converter channels are read in sequence by the CPLD, starting with channel 7 and ending with channel 0. Each data packet from the ADC consists of 16 bits, where the upper four are the channel number and the lower 12 are the measurement value in two's complement format. The serial data from the ADC is transmitted over an SPI interface. Once a complete data packet has been received by the ADC sequencer in the CPLD, it is moved to the link sequencer (LinkSeq block), which serializes and frames it for the fibre optic interface. Once all eight measurement channels have been transmitted, the CPLD waits for a time determined by the desired sample rate, then the process is repeated.

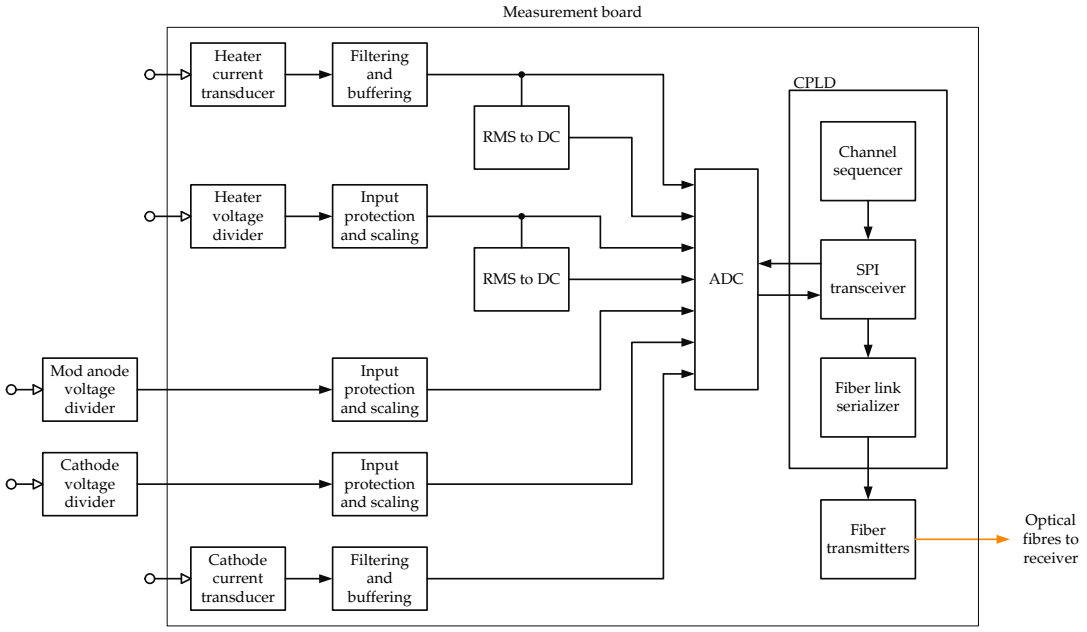

Figure 3.6: Block diagram of the measurement card

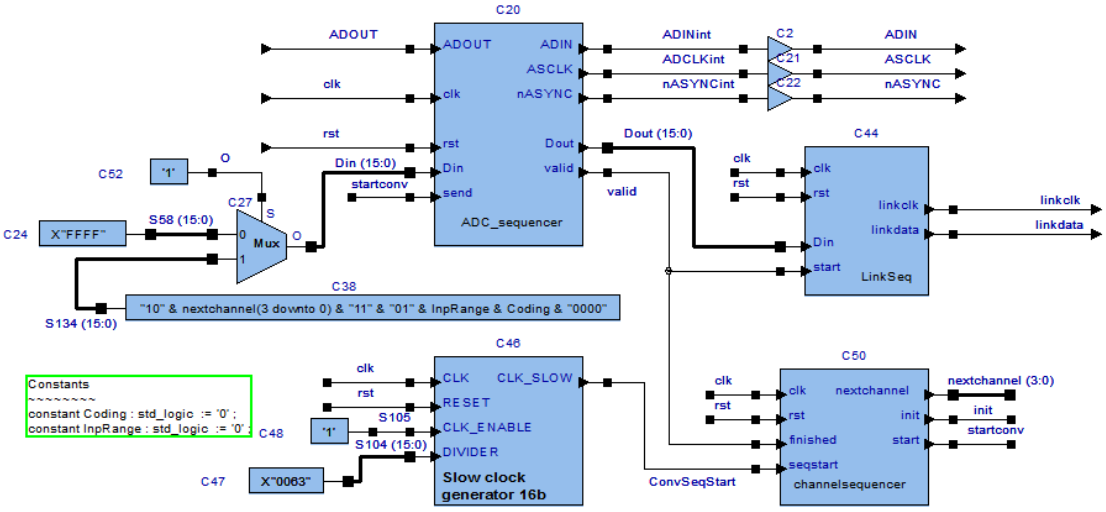

Figure 3.7: Block diagram of the CPLD internals in Visual Elite

As the CPLD has only limited hardware resources available, the CPLD code was heavily optimized to squeeze both the ADC readout and the link sequencing into the chip. For example, reading the ADC channels in the sequence 0-1-2–7 would take much more resources than sampling them in the sequence 7-6-5–0. A similar optimization was done for the temporary 16-bit buffer between the ADC and the link sequencer. Without these optimizations, the code would not fit in the CPLD.

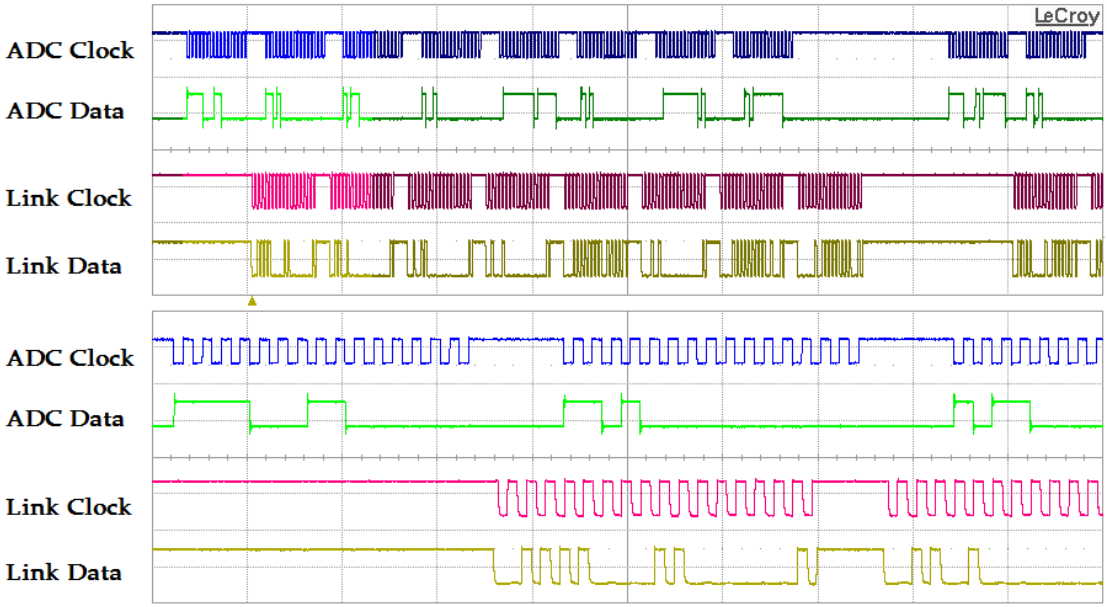

Figure 3.8: Oscilloscope view of the ADC SPI bus and the fibre link, upper traces are 50 μs per division, lower traces are 10 μs per division

Figure 3.8 shows the data and clock lines between the ADC and CPLD, and the serial link outputs of the CPLD. The upper traces show all eight measurement channels being transmitted. The lower traces show the transmission of the individual measurement channels in closer detail.

The serial data is converted to optical signals using two Avago HFBR-series fibre transmitters [15]. A Maxim MAX6304 microprocessor supervisory circuit holds the CPLD in reset for 250 ms to allow the supply voltage rails to stabilize [16]. Power input to the board is rectified, smoothed and fed to Traco THL3-series isolated DC/DC converters to generate the different supply rails for the measurement electronics. These converters have an input voltage range of 9–36 V DC [17].

Currents are sensed using LEM HX-series open loop current transducers [18]. The voltage signals from the current transducers and voltage dividers are filtered. A 2.5 V offset is added to the AC measurement channels to centre them around the middle of the ADC input voltage range. Analog Devices AD8436 RMS-to-DC converters are used to calculate the RMS value of the filament voltage and current [19].

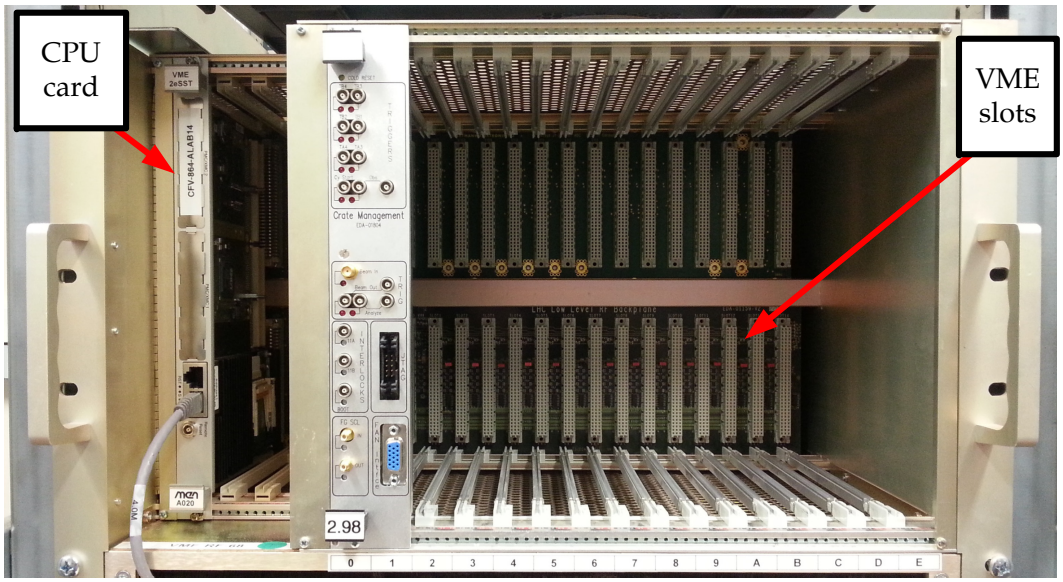

Figure 3.9: VME crate used for Low level RF systems in the LHC

VME form factor cards are used for the Low Level RF systems in the LHC [20]. The cards are mounted in custom rack-mount crates that each hold up to 15 cards with a 16-bit VME bus, and up to 5 cards with a 32-bit VME bus, shown in Figure 3.9. The VME bus is a parallel computer bus commonly used in industry, which was originally developed from the Motorola MC68000 processor bus. FESA is the Front End Software Architecture, which is a software framework used at CERN to integrate hardware such as measurement and control systems into the machine control system. A processor card mounted in the VME crate runs the FESA server, reading data from the measurement card when requested.

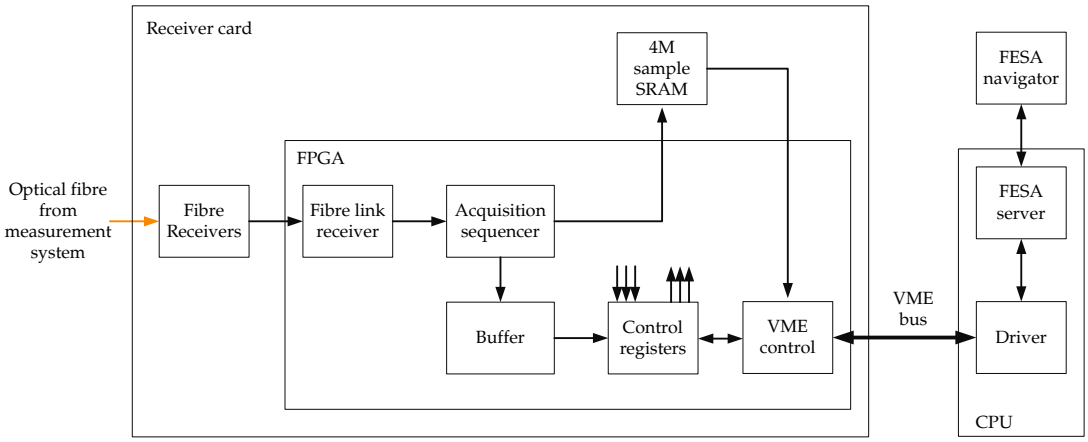

Figure 3.10: Block diagram of the receiver

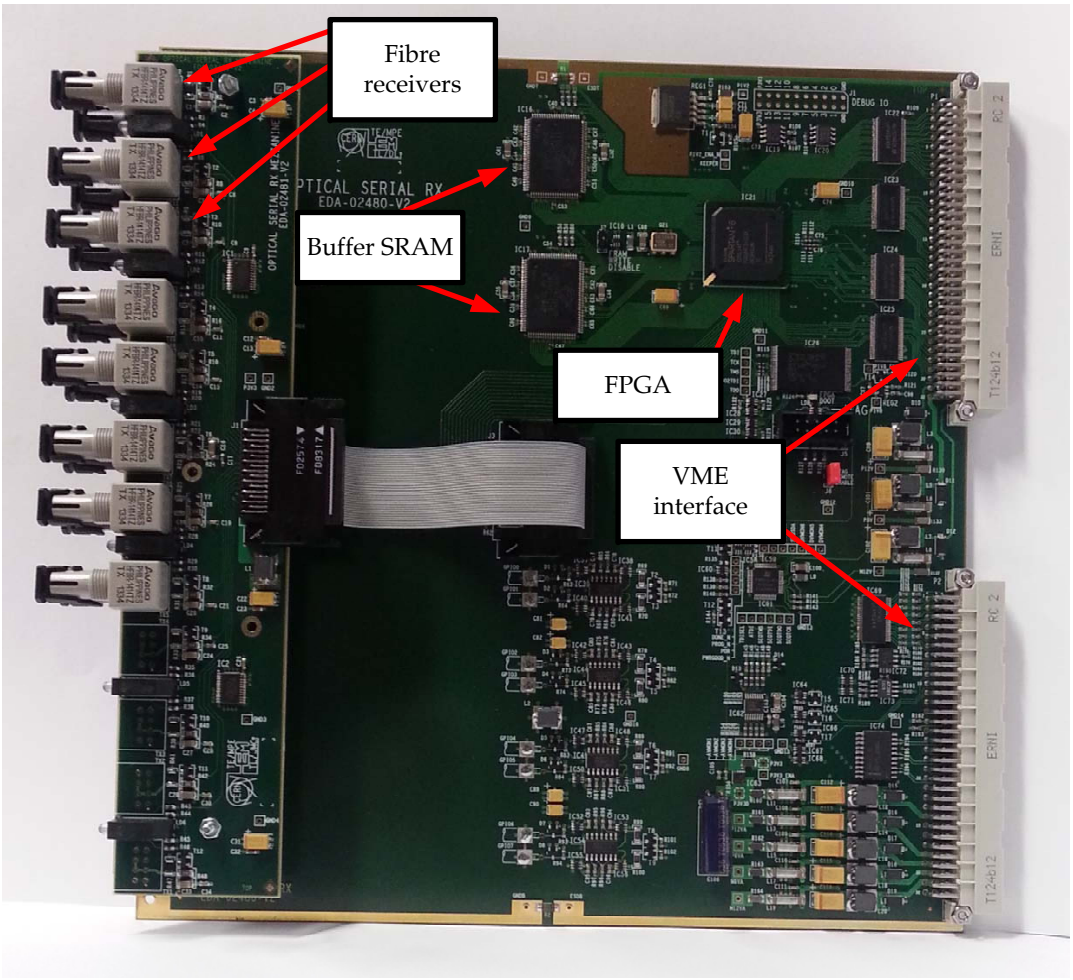

Figure 3.11: Revision 2 of the serial receiver card

The receiver card can receive data from up to four measurement cards. The optical serial link is converted to electronic signals using Avago HFBR-series fibre optic receivers [15]. The serial data is received by a Xilinx XC6SLX45 Spartan 6 FPGA, which deserializes it and stores it in a circular buffer in two external SRAM chips. The last measured values are also stored in a buffer in the FPGA for real-time readout of measured values. Measurement data is read out of the card over a 16-bit VME bus. A block diagram of the receiver card is shown in Figure 3.10 and the receiver card itself is shown in Figure 3.11.

4. Prototype modifications and testing

4.1 Prototype modifications

A number of modifications were made to the prototype measurement system, in order to make it perform to the required specifications

To improve rejection of common-mode noise on the voltage inputs, instrumentation amplifiers were added and the measurement across the low-side resistor of the divider was made differentially. The AD8226 instrumentation amplifier was chosen for this purpose based on availability, low offset voltage and the ability of the inputs to handle voltages beyond the rails [21].

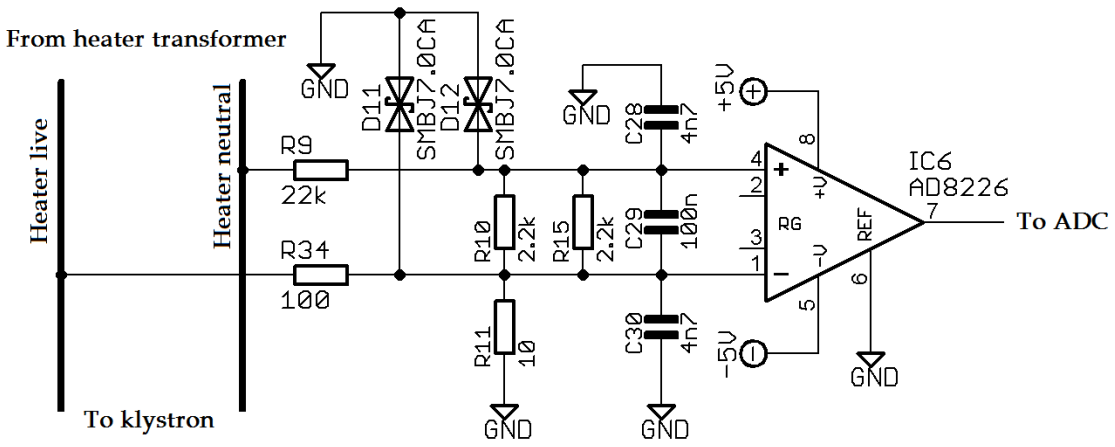

Figure 4.1: Protection circuit used for the heater voltage input

Due to the harsh conditions during klystron arcing, additional protection circuits were added to the modulation anode, cathode and heater voltage sensing inputs. The schematic of the updated protection circuit for the heater voltage measurement is shown in Figure 4.1. The protection circuits for the modulation and cathode voltage input are identical. The protection circuit consists of series resistors R9 and R34 and transient voltage suppressors D11 and D12. The series resistors limit the current flowing into the inputs in case of high voltages on the input, and the transient voltage suppressors clamp the voltage seen by the instrumentation amplifier to a safe level. Capacitors C28, C29 and C30 form a low pass filter along with the resistors, attenuating common-mode and differential-mode high frequency noise.

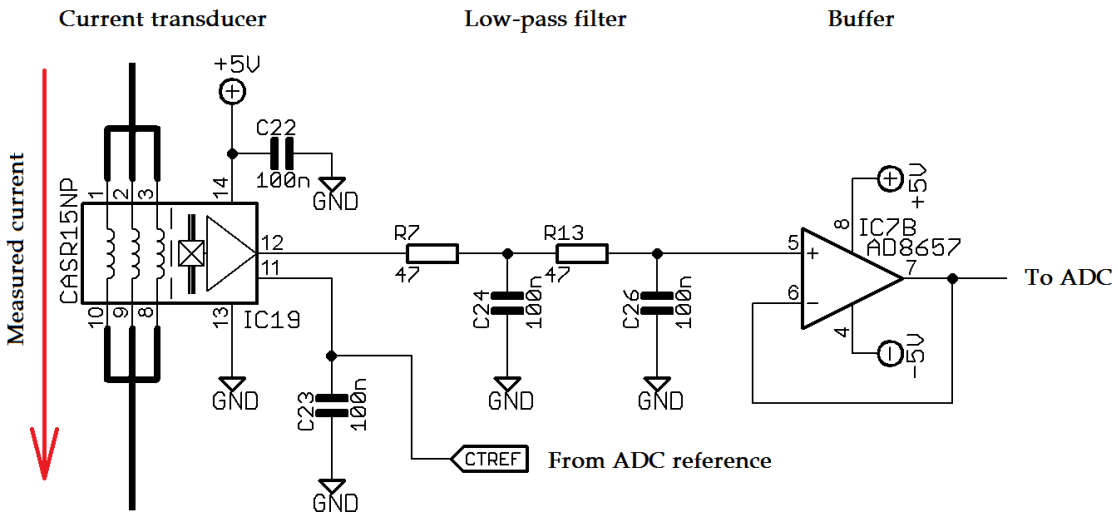

Figure 4.2: Filter and buffer circuit for the current transducers

The LEM HX-series current transducers used in the prototype need a power supply of ±15 V DC. No other parts of the measurement system utilize these supply rails. To simplify the design, these current transducers were replaced with LEM CASR-series current transducers, which can be powered from the existing +5 V supply used for the analogue section. This allowed the removal of the ±15 V DC/DC converter. The CASR-series current transducers have the added benefit of improved linearity, with a specified linearity error of maximum ±0.1% [22] compared to ±1.0% for the HX-series [18].

The CASR-series current transducers have a bipolar current range, measuring both positive and negative currents. The output voltage is centred around an internally generated reference voltage of 2.5 V, and it swings from 0.375 V to 4.625 V. This makes them directly compatible with the input voltage range of the ADC, so no offset addition or scaling needs to be performed. Second order RC low-pass filters were added to the current transducer outputs. Any difference between the internal reference voltage of the current transducer and the reference voltage for the ADC will appear as an offset on the ADC reading. The CASR-series transducers have a reference input, which allows the ADC reference voltage to be used as the reference voltage for the current transducer, eliminating this offset. The circuitry between the current transducers and the ADC is shown in Figure 4.2.

Component values for the measurement voltage dividers were chosen to get the required measurement ranges. Scaling factors and measurement range for the different channels is shown in table 4.1. The current transducers are provided with three isolated measurement windings, to allow for different full-scale current ranges by connecting them in series or parallel. The CASR-15NP provided a measurement range of ±17 A with all three windings in series, and a range of ±50 A with all windings in parallel. This allowed the same current transducers to

be used for both heater current measurement and cathode current measurement, minimizing the number of different parts used in the design.

Measurement parameter	Scaling factor	Range
Heater voltage	25.6 mV/LSB	±52.5 V
Heater voltage RMS	25.6 mV/LSB	52.5 V RMS
Heater current	29.3 mA/LSB	±60.0 A
Heater current RMS	29.3 mA/LSB	60.0 V RMS
Cathode current	9.77 mA/LSB	20.0 A
Cathode voltage	24.4 V/LSB	100 kV
Mod. anode voltage	24.4 V/LSB	100 kV

Table 4.1: Scaling and range for measurement channels after modifications

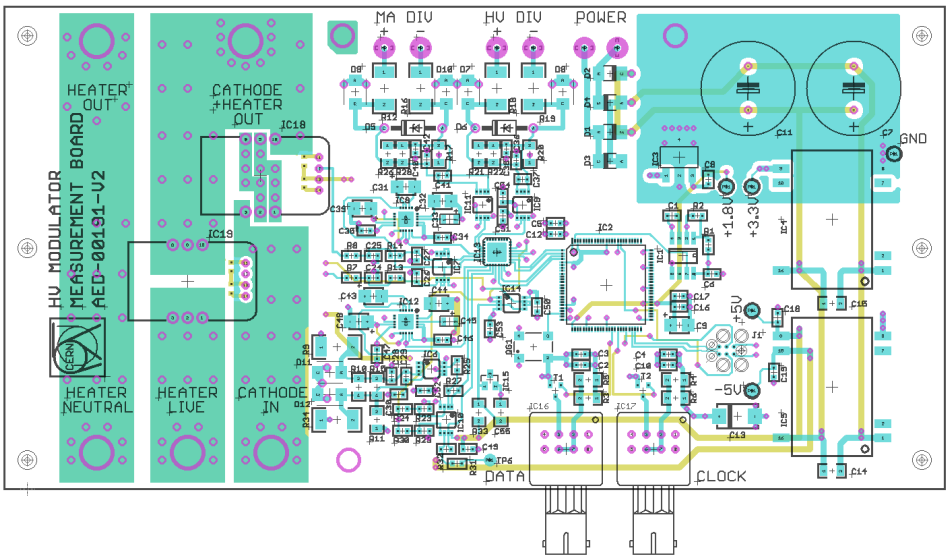

Figure 4.3: Circuit board layout

To be able to test the measurement system in the modulator, the prototype board design was updated to reflect the modifications made to the prototype version. The size of the circuit board and the position of the mounting holes was not changed, to allow the new board to use the shielding plates made for the prototype. The free board space gained by removing the ±15 V DC/DC converter allowed larger diameter and shorter electrolytic capacitors to be used, which lowered the overall board height. The updated layout is shown in in Figure 4.4 and the manufactured circuit board is shown in Figure 4.4.

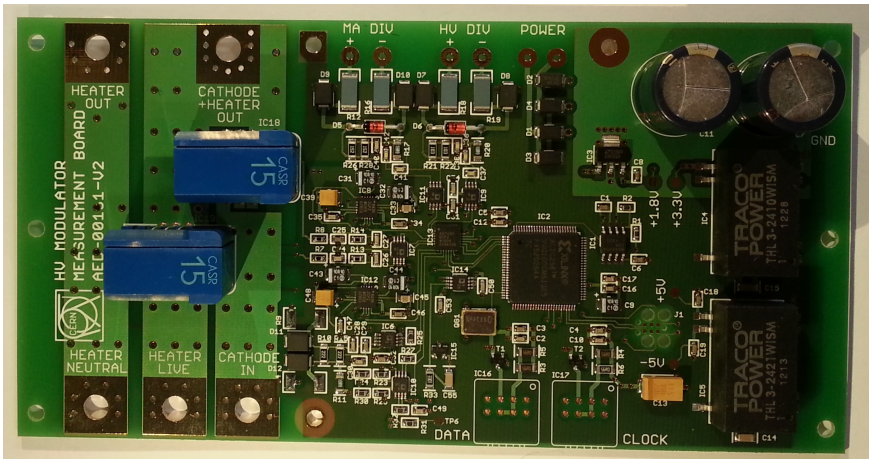

Figure 4.4: Manufactured circuit board

4.2 Accuracy determination

To determine the accuracy of the system, all measurement channels were compared to values measured with known accurate instruments. These tests were performed in lab conditions without high voltage. Table 4.2 summarizes the measurement results.

The accuracy of the multimeter used for reference measurements is specified as 0.5% for AC voltage and current measurements [23]. This is similar to the expected accuracy of the measurement system. For this reason, it is impossible to accurately determine the accuracy of the system using this meter, but the relative difference between the measurements gives a good indication of the accuracy of the system. The relative difference was calculated as a fraction of the full scale, according to equation 4.1.

$$\text{Relative difference} = \frac{\text{Measurement}}{\text{Reference}} * 100\% \tag{4.1}$$

To verify the accuracy of the heater voltage measurement, AC voltage was applied across the filament connections of the measurement system using a signal generator. The signal from the generator was observed on a LeCroy WaveRunner 64Xi oscilloscope [24], and compared to the data from the measurement system. The result is shown in Figure 4.5. The measurement was confirmed by installing the measurement system in a modulator and applying voltage to the heater transformer using a variable transformer, while observing the data from the measurement system. The heater voltage was measured with a Fluke 87 V multimeter for reference. The RMS reading from the multimeter was compared to the value from the ”Heater Voltage RMS” channel and the calculated RMS value of the ”Heater Voltage” channel.

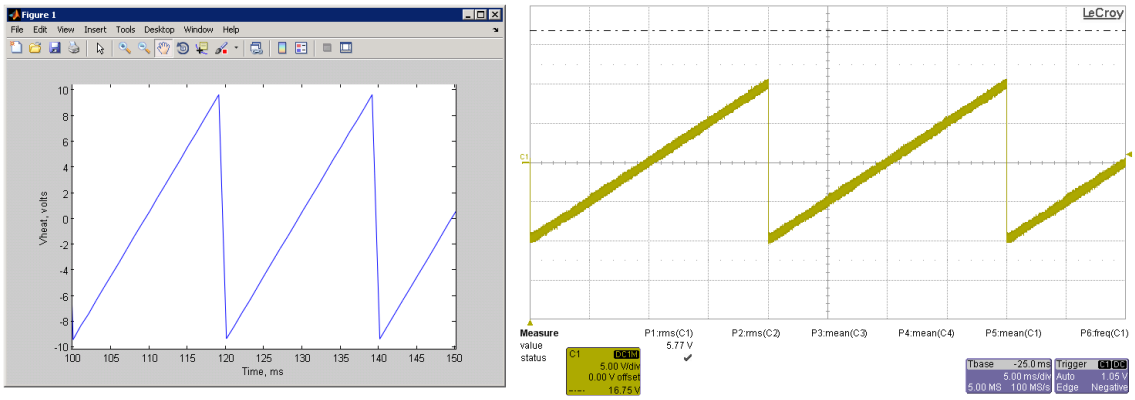

Figure 4.5: 20 Hz 20 Vpp sawtooth measured by measurement system and oscilloscope

To verify the accuracy of the heater current measurement, AC current was passed through the heater current transducer by connecting an adjustable resistor in place of the klystron heater and applying an adjustable voltage to the input of the heater transformer. A Fluke 87 V multimeter connected in series with the resistor served as the reference for the measurement. The RMS reading from the multimeter was compared to the value from the "Heater Current RMS" channel and the calculated RMS value of the "Heater Current" channel.

To verify the accuracy of the cathode current measurement, an adjustable bench power supply was used to pass a DC current through the cathode current transducer. A Fluke 87 V multimeter connected in series with the power supply served as the reference.

To verify the accuracy of the cathode and modulation anode measurements, an adjustable bench power supply was used to apply a DC voltage across the low-side resistor in the measurement divider. The voltage used was 4 V, corresponding to 80 kV with the dividers in place. A Fluke 87 V multimeter connected in parallel with the power supply served as the reference

Measured parameter	Fluke 87V	Measurement system	Relative difference
Heater voltage	7.05 V AC	7.04 V AC	0.1 %
Heater voltage RMS	7.05 V AC	7.01 V AC	0.6 %
Heater current	9.76 A AC	9.75 A AC	0.1 %
Heater current RMS	9.76 A AC	9.73 A AC	0.3 %
Cathode current	8.11 A DC	8.13 A DC	0.2 %
Cathode voltage	4.01 V DC	4.01 V DC	0.0 %
Mod. anode voltage	4.01 V DC	4.01 V DC	0.0 %

Table 4.2: Results of accuracy measurements after modifications to prototype

4.3 Oil compatibility testing

The modulator is a high voltage device, therefore it is mounted in an oil-filled tank. Two different types of oil are currently in use in the CERN RF HV systems, Midel 7131, which is ester-based, and Rhodorsil 47-series oil, type 604V50, which is silicone-based. Both of these oils are used at CERN on account of their lower fire hazard as compared with more traditional mineral oil dielectric fluids. There is no information on oil compatibility in the datasheets of the electronic components used in the design, and no information on materials compatibility in the Midel oil datasheet. There is some information on materials compatibility in the Rhodorsil datasheet:

> "In spite of being highly chemically inert, Rhodorsil Oils 47 can have an effect on certain materials to varying extents. Materials containing plasticizers can be affected by immersion in a silicone oil. The effect will vary according to the oil viscosity, the material composition, the immersion temperature." [25, p.22]

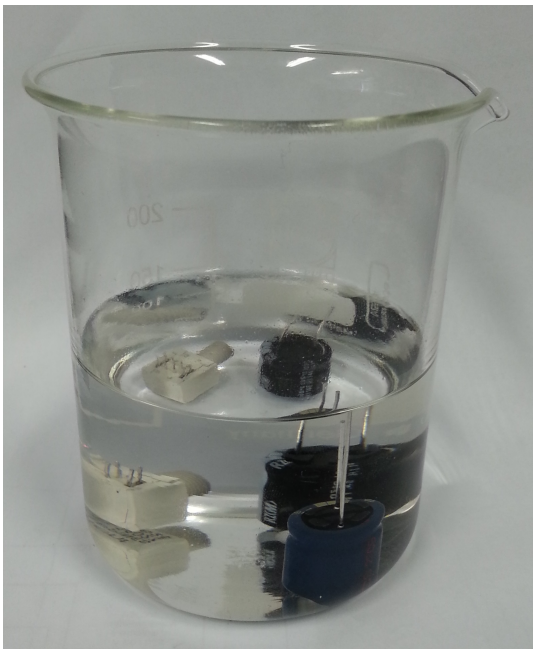

Figure 4.6: Components in Rhodorsil 604V50 for long term testing

To determine whether the chosen components were compatible with the different oils, a test was carried out. Samples of both dielectric oils were obtained, and an operating measurement board was immersed in the oil and observed for correct operation after several days under oil. This test was carried out for both oils. In addition, plasticiser-containing components from the design were left in

oil for a longer period, shown in Figure 4.6. The measurement board operated correctly in both types of oil, and no electrical or mechanical degradation was observed during or after the test. During later high voltage testing, the modulator with the measurement board was immersed in Rhodorsil 604V50 for several weeks. No electrical or mechanical degradation was observed during or after these tests.

4.4 Optical fibre evaluation

To verify whether the optical fibres used in the prototype version would be sufficient for the installation in UX45, optical power losses were calculated for the installation. The longest distance between the modulators and the receiver card is approximately 30 m, as shown in Figure 4.7. The actual length of the fibres will be longer in practice, due to the height difference between the cable trays and the modulators, and the additional lengths of fibre inside the modulators. To give some safety margin, loss calculations are done with a fibre length of 40 m. The fibres going to the receiver cards pass through a patch panel with one fibre-to-fibre connection, and there is an additional fibre-to-fibre connection where the fibre exits the modulator tank.

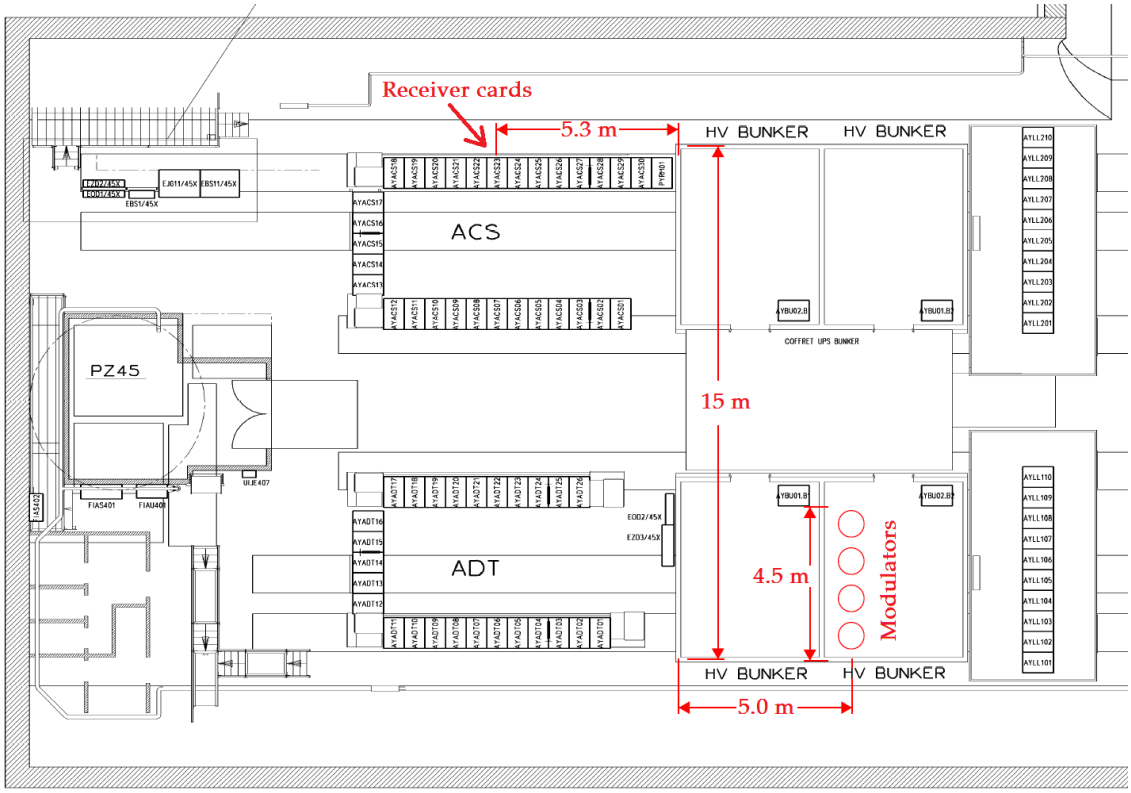

Figure 4.7: Distance between receivers and modulators in the underground cavern UX45, where the LHC accelerating systems are installed

Fibre type	1mm plastic	62.5 μm glass	50 μm glass
RX type	HFBR-2505AFZ	HFBR-24X2	HFBR-24X2
TX type	HFBR-1505AFZ	HFBR-14X4	HFBR-14X4
RX/TX loss budget	14.6 dB [26]	8.0 dB [15]	4.2 dB [15]
Connector loss (2x)	5.6 dB [27]	1.5 dB [28]	1.5 dB [28]
Cable loss (40 m)	9.2 dB [27]	0.14 dB [28]	0.14 dB [28]
Loss margin	-0.2 dB	6.4 dB	2.6 dB

Table 4.3: Loss calculations for the installation

Table 4.3 summarizes the main optical power budget consumers for the three most popular fibre types in industry. The 1mm plastic optical fibre used in the prototype would exceed the loss budget if used in this installation, so the other options were evaluated. Both 62.5 μm and 50 μm glass multi-mode give acceptable loss budgets for the projected installation, using the HFBR-24X2 receiver and HFBR-14X4 transmitter. 50 μm glass multi-mode was selected after consulting with the Electrical Engineering group at CERN, EN-EL-CF, due to wide usage in existing installations at CERN. The HFBR-24X2 receiver and HFBR-14X4 transmitter are available with different fibre connectors, SMA, ST, FC and SC. ST connectors were chosen based on the all-metal construction and positive locking action providing a solid mechanical connection in the oil tank, and wide usage in existing installations at CERN.

5. Integration into modulator

5.1 High voltage compatibility testing

To verify that the system would work correctly under high voltage conditions, initial tests were performed at the high voltage test stand in building A5 (285). The purpose of these tests was to verify that the measurement system would operate correctly under conditions like those encountered in normal modulator operation in the LHC, and that it would survive common fault conditions without damage or degradation of performance.

This lab is independent from the accelerator, allowing us to test the measurement system under different conditions without affecting critical operational systems of the accelerator. The lab is equipped with an overhead crane, making it possible to remove the modulator from the oil tank for modifications between tests. The high voltage test stand is enclosed in a cage for safety reasons, shown in Figure 5.2, and there are interlock switches on the door of the cage that remove the high voltage, in case the high voltage is left on by accident when entering the test area.

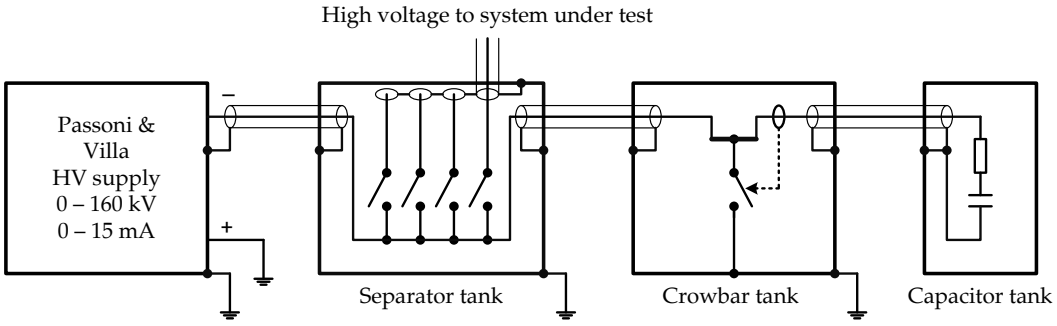

Figure 5.1: The high voltage test setup in building A5

To provide high voltage for the test, an adjustable power supply was used. The power supply was a Passoni & Villa 0–160 kV 0–15 mA unit, configured for negative output polarity. This power supply has adjustable output voltage and current limit, and also adjustable voltage and current trip points that will trigger a shut down of the supply. The control panel of the power supply is shown in Figure 5.3. This power supply can deliver a maximum of 15 mA whereas the ones in the LHC can deliver up to 40 A. 15 mA was sufficient for our tests as we were

not powering an actual klystron. The decoupling capacitor in this installation has a capacitance of 2 μF, whereas the ones in the LHC have a capacitance of 4 μF. This affects the charge deposited in the crowbar but the peak current through the modulator is the same in case of a klystron spark. The crowbar in the test stand is of the recently developed thyristor type [4], as opposed to the thyratron based crowbars that are used in the LHC. This is an advantage, as the thyristor crowbar is planned to be installed in the LHC before the measurement system is installed. A general overview of the setup in the A5 high voltage test stand is shown in Figure 5.1.

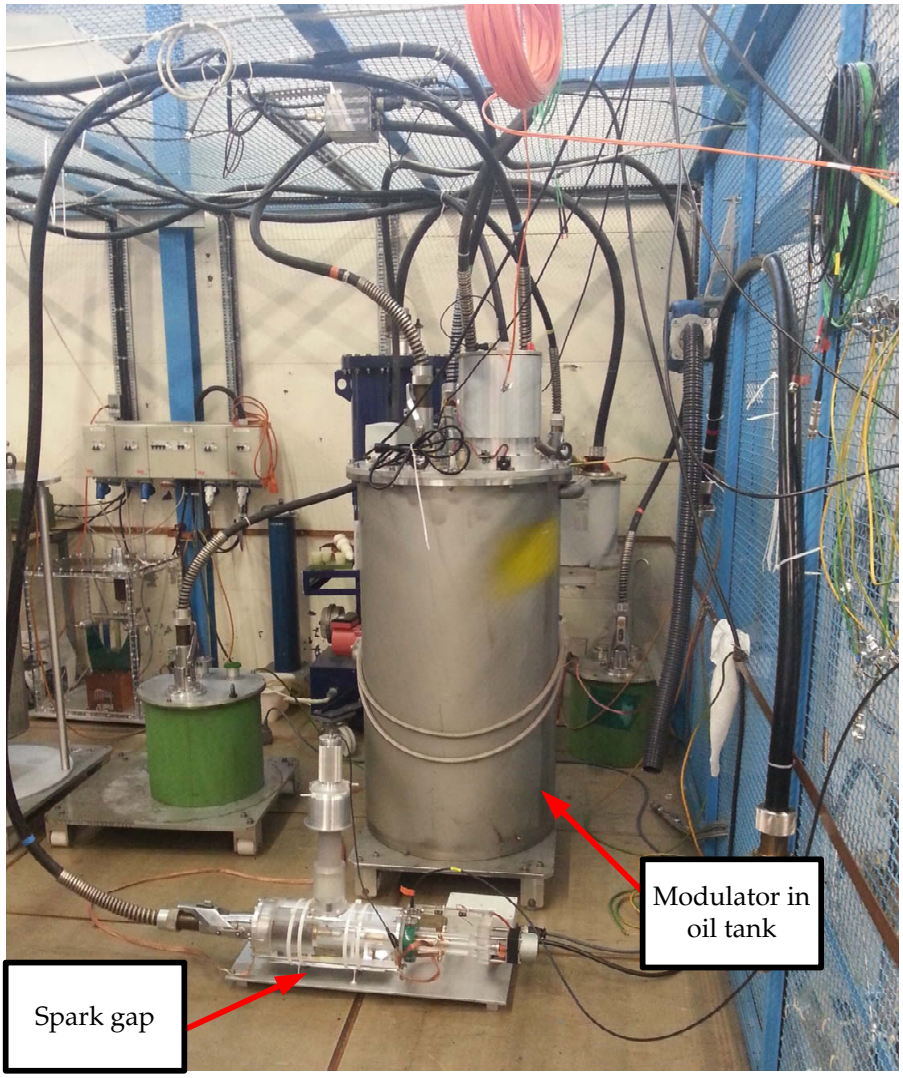

Figure 5.2: Test setup in high voltage cage with modulator and spark gap

Figure 5.3: Control panel of the high voltage power supply used for testing

The MAC10 modulator used for the tests did not have the full modulation anode control system mounted. To generate a reasonable modulation anode voltage for testing, a fixed resistance voltage divider was used. To make this divider, two 5 MΩ resistors were each constructed using seven 35M Ω 105 W resistors in parallel. This gives a voltage on the modulation anode that is half of the cathode voltage. With a klystron connected to the modulator, the modulation anode voltage will be lower due to the current drawn by the modulation anode.

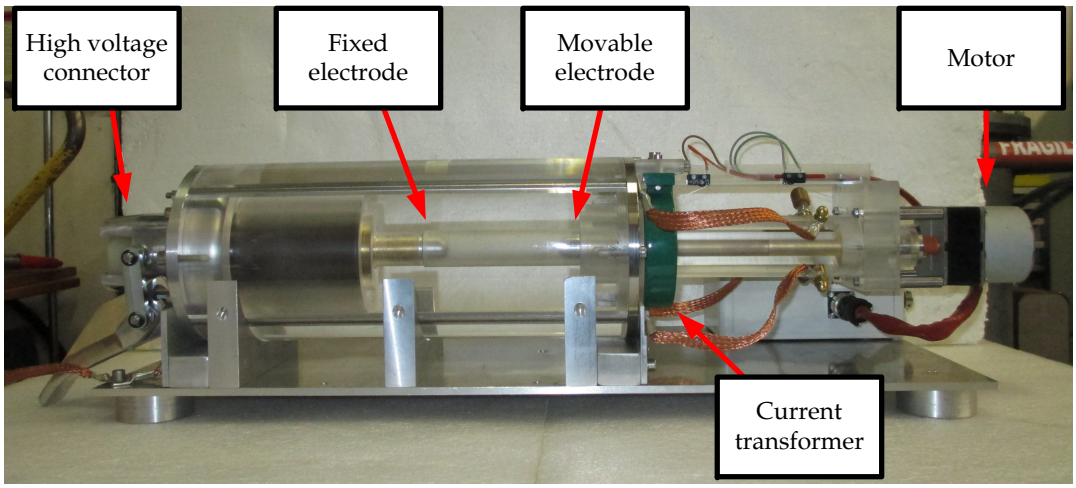

Figure 5.4: Adjustable spark gap as used in testing

An adjustable spark gap, shown in Figure 5.4, was used to simulate klystron arcing. The spark gap is motorized, and the distance between the electrodes can be adjusted remotely from 0 mm to 110 mm. This corresponds to a breakdown voltage range of 0 V to approximately 80 kV. There is a permanently mounted cur-

rent transformer on the spark gap to measure the spark current. This is a Pearson model 150, with a -3 dB bandwidth of 40 Hz–20 MHz. The output scaling of the current transformer is 0.5 V/A into an open circuit, and the output impedance is 50 Ω [29]. To scale this down to a voltage that the oscilloscope can handle, a 50 Ω termination and a 10:1 attenuator was used, giving a scaling factor of 25 mV/A.

There is no VME crate in the A5 test stand, so it was not possible to monitor or log the data from the measurement system using the receiver card. To allow functional verification and data readout, a converter was built to convert the serial fibre optic signal from the measurement system into electrical signals that could be monitored on an oscilloscope. The oscilloscope used was a Tektronix model DPO5034 [30]. Setting up the "pulse width" trigger of the oscilloscope to trigger on the dead-time between transmissions, it was possible to get a stable image of the serial data packets, allowing manual reading of the measured values. To check the condition of the measurement system during spark gap testing, the spark gap current transducer was also connected to the oscilloscope. The oscilloscope was set to trigger on the spark gap current, and the time scale was set so that it would capture several serial data packets before and after the spark event. An example of such a measurement is shown in Figure 5.5.

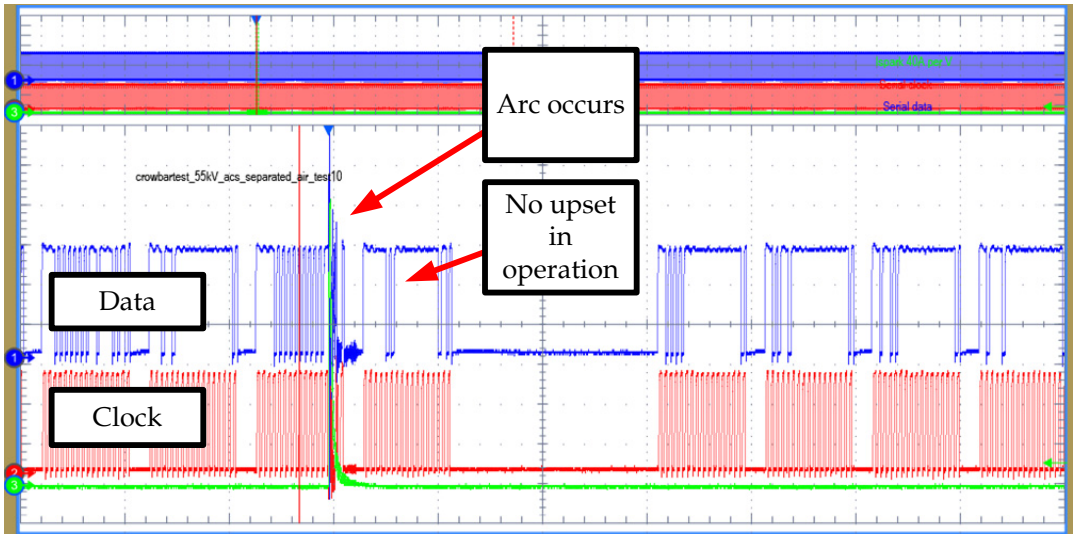

Figure 5.5: Oscilloscope image showing an arc event and no upset in system operation, 40 microseconds per horizontal division

During testing, several problems were discovered and solved.

1. With the original mounting of the measurement system, problems were encountered with signs of high voltage breakdown when the modulator was operated in air. This was solved by enclosing the measurement system in an aluminium box with rounded corners.

2. During crowbar firings, with the spark gap connected to the output of the modulator, the ADC crashed. This was caused by the routing of the power traces to the current transducers, and the solution was a modification of the board to change the location of these traces.

3. Occasionally during crowbar firings, the measurement system reset itself. This was caused by the lack of grounding on the secondary of the low voltage transformer.

4. Occasionally after crowbar firings crystal oscillator was upset. This was caused by the lack of grounding on the secondary of the low voltage transformer.

5. The current transducers acquired offsets and occasionally sustained damage when the crowbar fired. The high currents encountered when the spark gap fired exceeded the maximum rating for the current transducers used. Adding a circuit to bypass the spark current from the current transducers solved this issue.

These problems and remedies are further discussed in the following chapters.

5.2 Test procedures

To verify the high voltage integrity of the modulator with the measurement system mounted, high voltage was applied with the modulator in air, and the setup was observed for signs of electrical breakdown. The first signs of electrical breakdown manifest themselves as a hissing sound and fluctuations in the current drawn from the power supply. For these tests, the modulator was connected to the high voltage power supply through the separator, the crowbar and capacitor were not connected, as shown in Figure 5.6. The high voltage was adjusted until the sound of partial discharge was evident and current fluctuations were observed, and the voltage was noted.

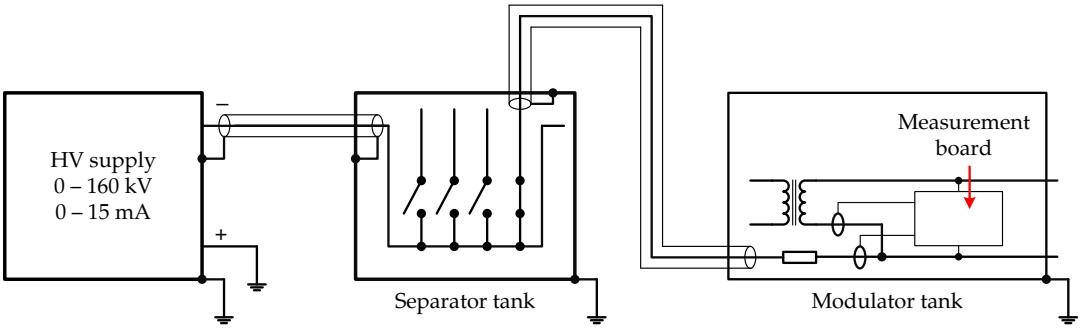

Figure 5.6: Test setup for high voltage breakdown testing

When the crowbar fires, the high voltage bus will collapse in microseconds, and the common mode dV/dt seen by the board is very high. To verify that the measurement system is not negatively affected during this event, testing was performed. For these tests, the modulator was connected to the separator, and the spark gap was connected to a different output on the separator, as shown in Figure 5.7. A 10 Ω resistor was placed in series with the spark gap to substitute for the 10 Ω resistor in the modulator of the arcing klystron. The crowbar and 2 μF capacitor were connected to the separator. For tests at voltages under 55 kV, the modulator was in air for practical reasons, and for tests above 55 kV, the modulator was immersed in a tank with Rhodorsil 604V50 oil. The spark gap was separated so that it would not break down at the test voltage, and the power supply voltage was slowly increased until the test voltage was reached. When the capacitor was charged and the voltage had stabilized, the power supply output current limit was set to a higher value than the over-current trip point. This ensured that the power supply turned off when the spark gap fired. The spark gap electrodes were brought closer together until breakdown occurred.

If an arc forms in the klystron connected to the modulator, the spark current will flow through the measurement system until the crowbar removes the high voltage. To verify that the measurement system is not negatively affected during this event, testing was performed as described in the previous paragraph, with the difference that the spark gap was connected to the cathode output of the modulator, as shown in Figure 5.8.

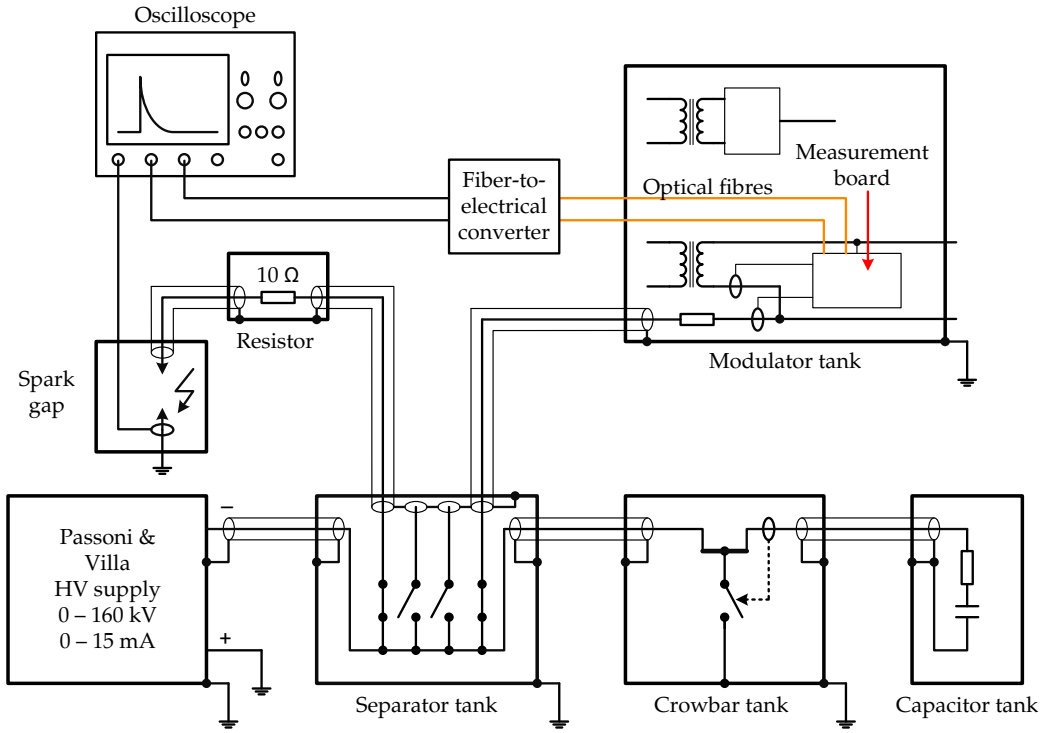

Figure 5.7: Test setup for emulating arc in other klystron on same separator

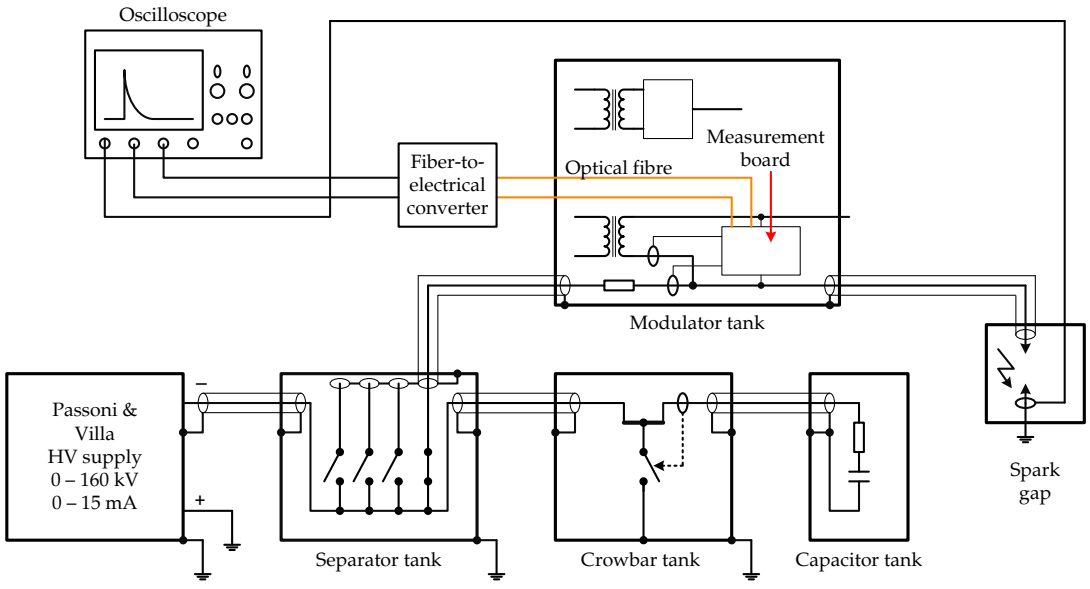

Figure 5.8: Test setup for emulating arc in the klystron connected to the measurement system

Certain problems only occurred after multiple tests. To verify that these prob-

lems were solved, reliability testing was performed. This testing consisted of many repeated spark gap firings with the spark gap connected to the cathode output of the modulator. The spark gap was set to a fixed width corresponding to a breakdown voltage of around 70 kV, and the high voltage was increased until the spark gap broke down. This allowed the test to be repeated rapidly, as there was no need to wait for the spark gap to move to the correct position for each test. 160 spark firings have been performed, showing reliability of the modified ruggedized measurement system.

5.3 Mounting in modulator

During initial high voltage testing, the measurement system board was mounted on a fibreglass plate above the transformers. Circuit boards with a solid copper layer were mounted above and below the measurement system and connected to the reference potential of the measurement system, -58 kV, to shield the sensitive electronics from electric fields, as shown in Figure 5.9. Rigid 6 mm^2 copper wire with solder lugs was used for the filament transformer and klystron connections between the measurement system and the modulator. During initial tests with high voltage, signs of partial discharge started at 35 kV in air, whereas the modulator on its own could be operated at up to 50 kV in air before signs of partial discharge, without the measurement system mounted.

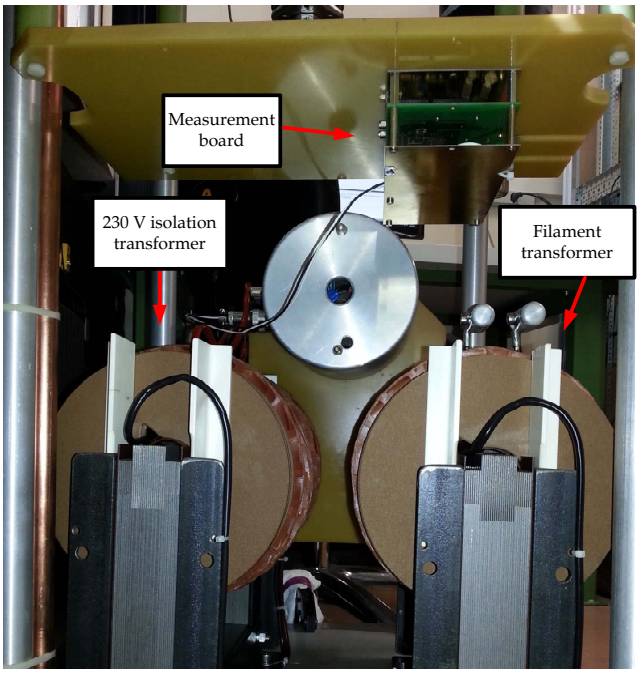

Figure 5.9: Initial measurement system mounting

To remedy this problem, the measurement system board was mounted in a cast aluminium box with rounded corners, as shown in Figure 5.10. To simplify mounting and removal of the measurement system, the hard-wired connections between the measurement system and the modulator were replaced with connectors. For the filament transformer and klystron connections, Multi-Contact B6AR-series 100 A connectors were selected. These connectors are already used in the modulators, they were selected for this project based on sufficient current handling capacity and availability. For the cathode and modulation anode dividers, SMC connectors were chosen on account of their shielded nature and compact dimensions.

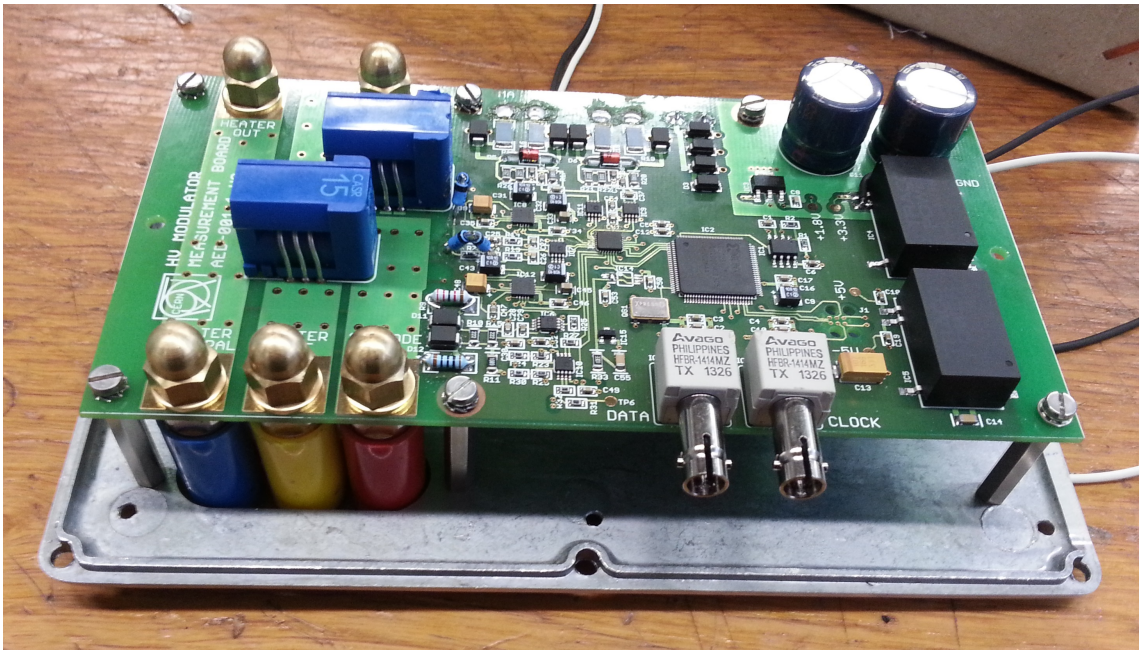

Figure 5.10: Measurement system mounted in aluminium shielding box

During later tests, measurement system crashes were experienced. These were suspected to be caused by induced currents in the circuit board ground plane from the spark current flowing in the cathode current transducer. To check if this was the problem, the current transducers were moved to a separate box, as shown in Figure 5.11 and Figure 5.12. The connection between the current transducers and the rest of the measurement card was done using a shielded cable and Lemo series 2S 6-pin circular connectors [31].

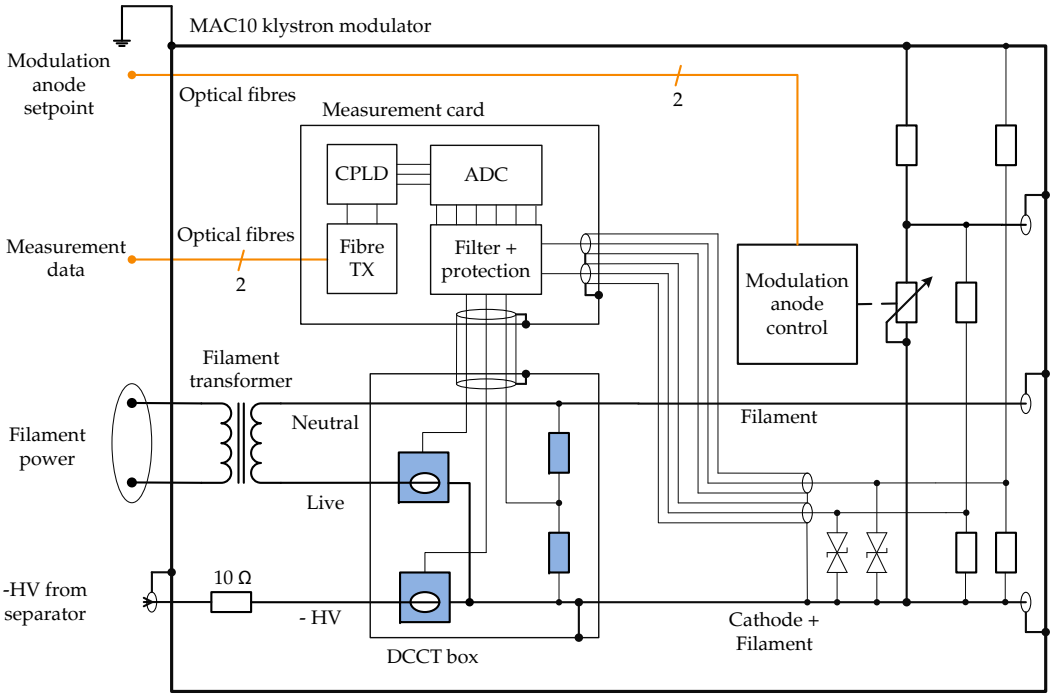

Figure 5.11: Diagram of measurement card and current transducers mounted in separate boxes

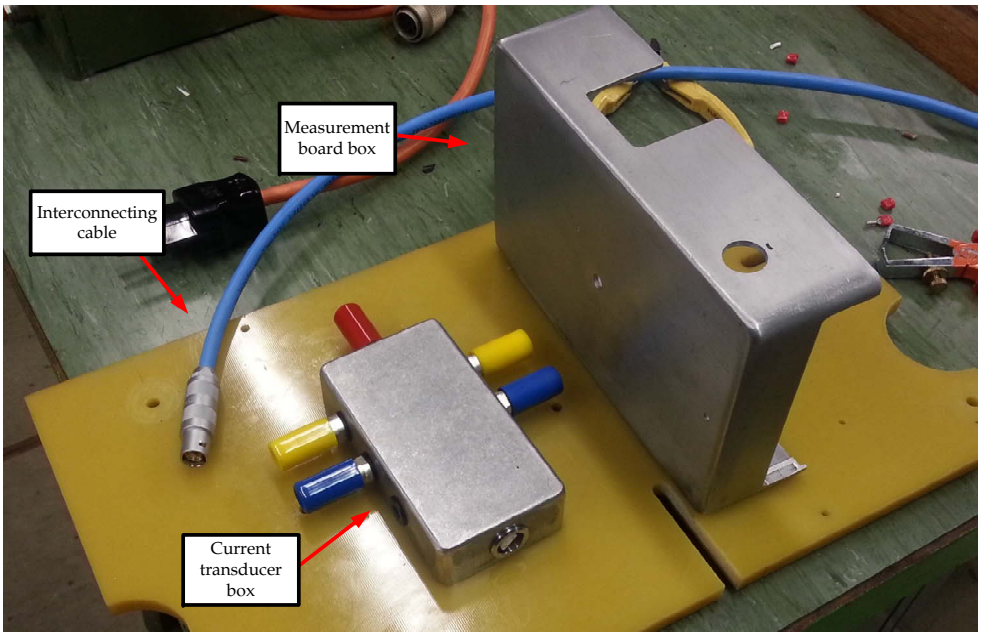

Figure 5.12: Measurement card and current transducers in separate boxes

5.4 Signal routing and interference

During early testing with the spark gap connected to the cathode output of the modulator, the measurement system crashed when the spark gap fired at voltages of 35 kV and higher. After crashing, the board continued correctly outputting serial data, but the transmitted value was 0xFFFF for all measurement channels, shown on the oscilloscope picture in Figure 5.13. The corrupt output data started appearing on the second data word transmitted after the arc occurred. Removing and reapplying power to the board restored normal operation.

These symptoms were diagnosed to be caused by an upset of the analogue-to-digital converter. Removing power to the input section of the ADC in the lab replicated the symptoms. The first data word after the arc is not affected. This data word corresponds to a measurement that was performed before the arc occurred, and the correct data were still stored in the link sequencer shift register.

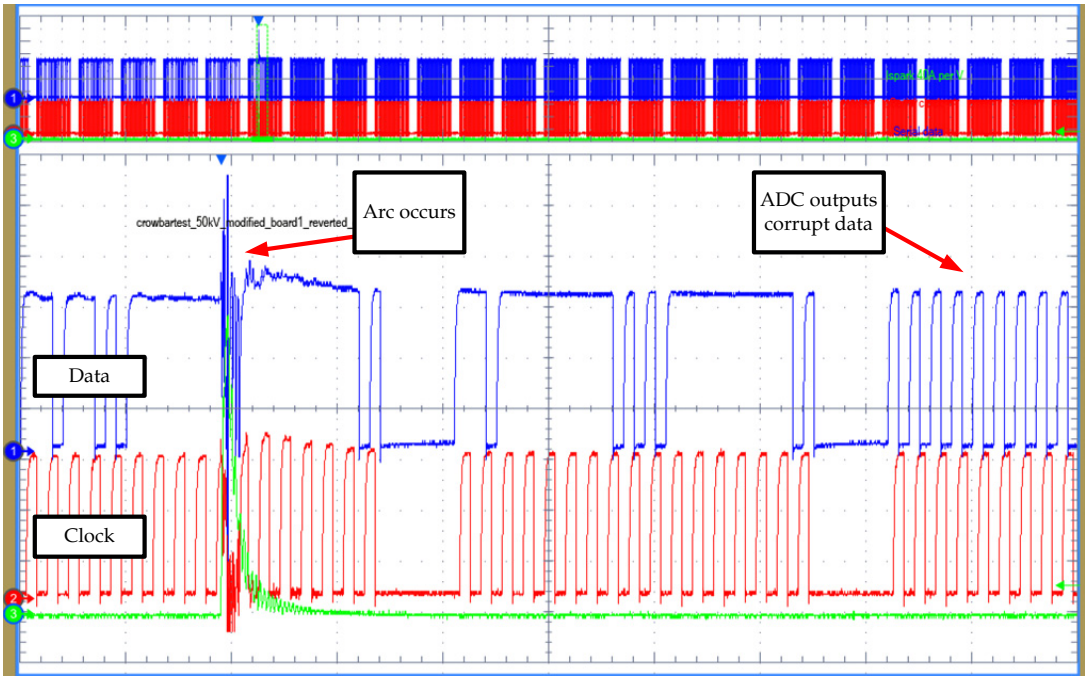

Figure 5.13: Oscilloscope image showing an arc event and data corruption, 10 microseconds per horizontal division

When further tests were performed with the inputs of the ADC disconnected, the data corruption still occurred. The same tests were performed with the current transducers completely disconnected from the rest of the measurement system. In this case, there was no data corruption at a test voltage of 53 kV, which was the highest voltage we could apply without immersing the modulator in

oil. The traces going to the current transducers were examined, and a loop of the +5 V trace supplying the current transducers was found to be sensitive to induced currents from the spark current flowing in the trace next to it. These induced currents created spikes on the +5 V rail powering the analogue section and the ADC, leading to the upset of the ADC. The loop is shown in Figure 5.14.

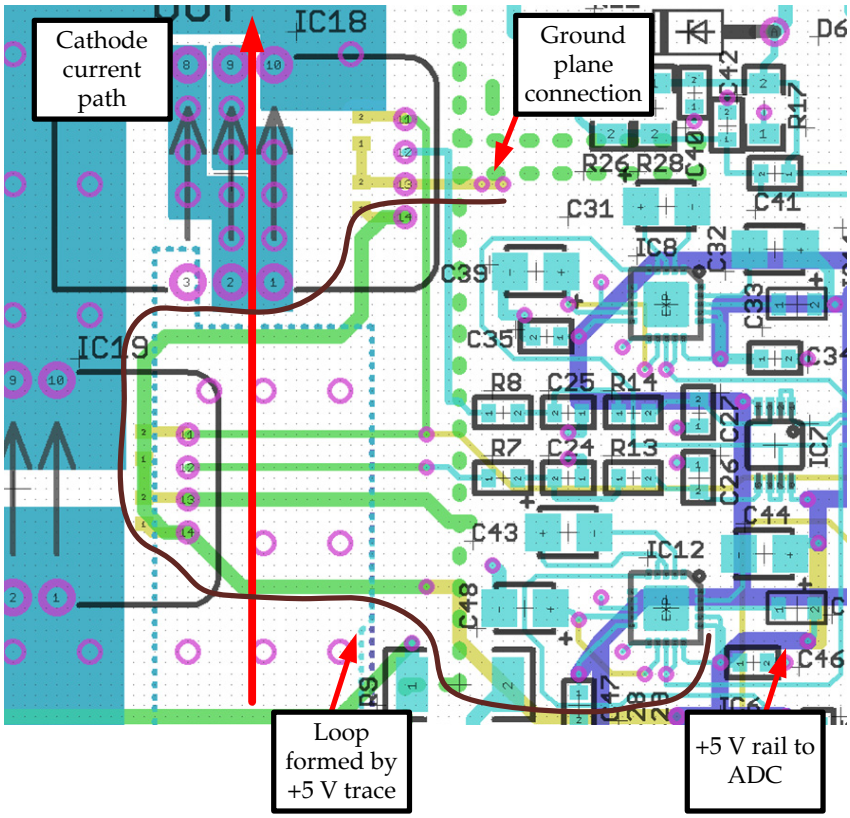

Figure 5.14: Current loop formed by +5 V trace under cathode current trace

As the loop was on an inner layer, breaking the loop was accomplished by drilling a hole through the circuit board in a location without any other traces. The cut trace was replaced by short wires on the underside of the board, running perpendicularly to the high current trace to minimize inductive coupling. After the modification, the board did not crash at 53 kV. The modulator was immersed in oil to allow testing at higher voltages, and the test was continued at voltages up to 70 kV. ADC crashing and subsequent data corruption was not observed in tests after the modification was performed.

5.5 System grounding

After the +5 V loop under the cathode current trace was cut, a different failure mode was occasionally observed. Around one in every ten spark events resulted in the measurement system resetting, when the spark gap was connected to the cathode output of the modulator. This is shown on the oscilloscope picture in Figure 5.15.

A different failure mode was also observed, where the data transmission rate increased by a factor of 20 after a spark event. Normal operation was resumed when power was removed and reapplied. This failure mode occurred more rarely, approximately once in every 20 spark events. This is shown on the oscilloscope picture in Figure 5.16.

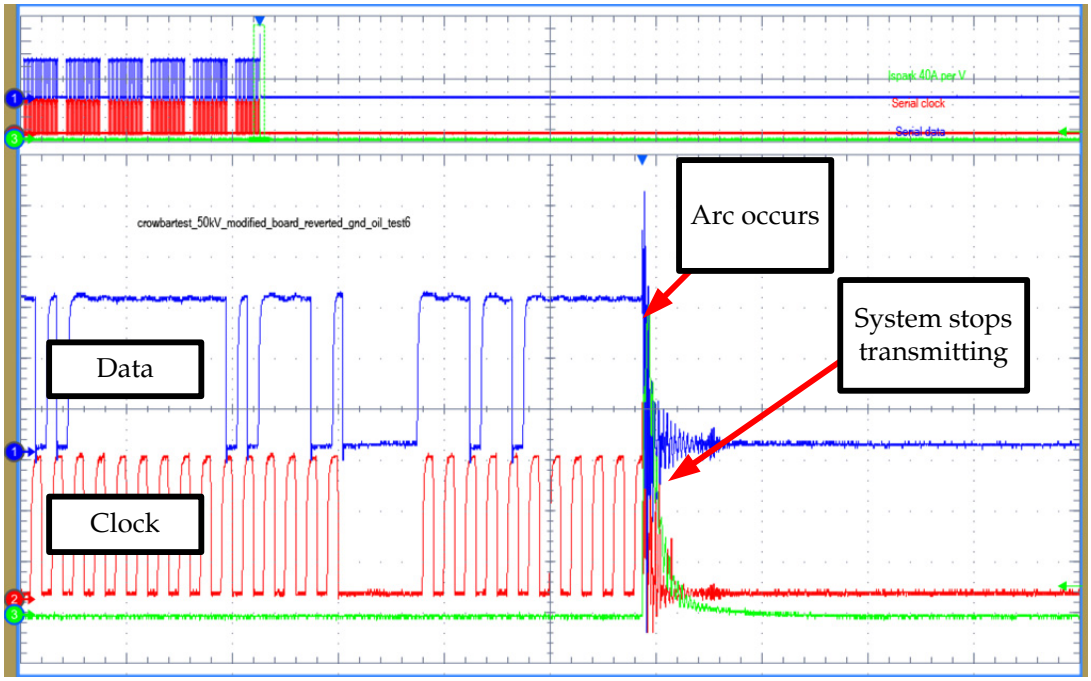

Figure 5.15: Oscilloscope image showing an arc event and system resetting, 10 microseconds per horizontal division

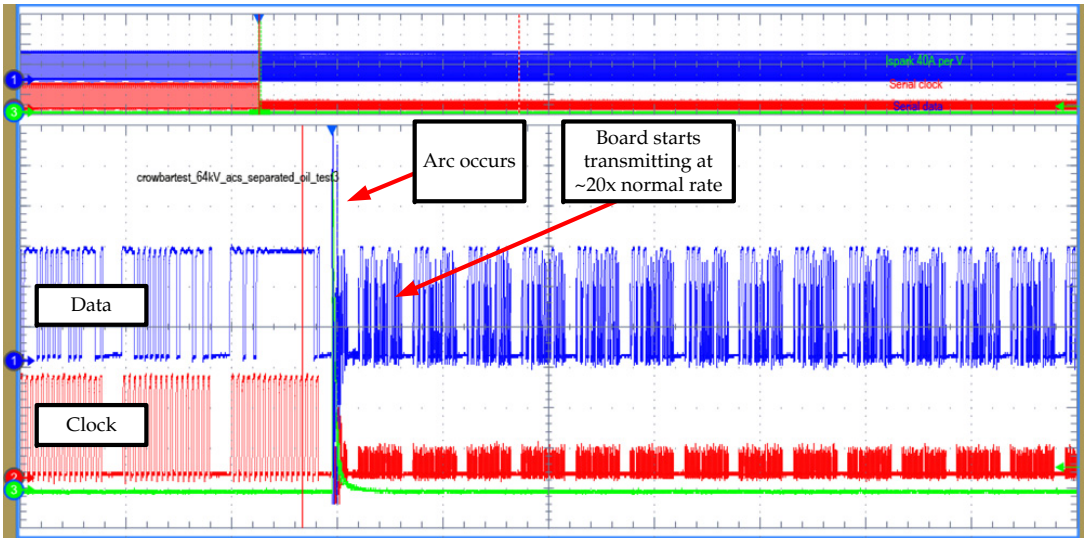

Figure 5.16: Oscilloscope image showing an arc event and oscillator upset, 40 microseconds per horizontal division

The reset line of the CPLD is controlled by a Maxim MAX6304 microprocessor supervisory circuit. The data transmission rate is governed by the crystal oscillator, the link clock rate is half of the oscillator frequency. The only nodes shared between these two devices are ground and +3.3 V, which indicated that the upset was most likely caused by noise on these nodes. Additional decoupling capacitors were added between ground and +3.3 V, but this did not improve the situation.

The cause was suspected to be currents induced in the ground plane of the circuit board. To verify this, the high current traces were separated from the rest of the board by moving the current transducers to a separate shielded box. This did not improve the situation, but it simplified the search for the cause of the upset, as it allowed the current transducer section to be isolated from the rest of the measurement system by unplugging the cable between them.

The upset still occurred after the current transducer section was disconnected and the cathode and modulation anode voltage dividers were disconnected. At this point, the only thing connected to the measurement system was the low voltage transformer. The secondary winding used for powering the measurement system was floating relative to the ground of the measurement system, shown in Figure 5.17. The power input section of the measurement system is also floating, on account of the isolated DC/DC converters used to power the board. This isolated circuit section could conceivably pick up interference and couple it into the +3.3 V rail through the parasitic capacitance of the DC/DC converter.

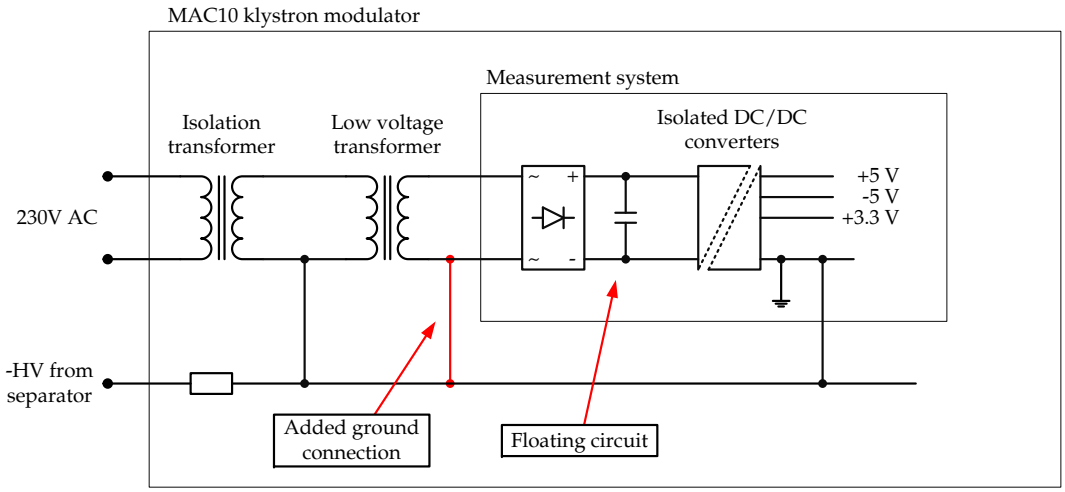

Figure 5.17: The floating circuit formed by the LV transformer secondary and the added ground connection to solve the problem

To test this hypothesis, one end of the low voltage transformer secondary was connected to the same potential as the ground of the measurement system. System resetting and oscillator upset was not observed in subsequent testing, which included over 160 spark events.

This problem also opened a question of component selection. The 1 MHz crystal oscillator used is of the type XpressO FXO [32]. This oscillator is a generic type, with the internal oscillator running at 4.096 MHz. It contains a PLL and a divider to synthesize the output frequency, based on a configuration word programmed into it by the manufacturer [33]. This allows the manufacturer to provide the oscillator in a range of different standard and custom frequencies using a single production line. As it turned out during testing, the frequency programming word can be altered by interference on the supply rail for the oscillator. A fundamental mode oscillator should be used instead, to avoid this problem.

5.6 Current transducer protection

Different models of current transducers based on different technologies were evaluated in the measurement system, shown in table 5.1.

It was observed that all types of transducers tested had significant DC measurement offsets after the cathode current output was grounded through the spark gap. From spark gap current measurements, it was estimated that the peak current through the cathode current transducer was in excess of 1 kA. The offset was observed to decay to close to zero over a period of hours. On repeated spark gap firings, the offset increased after each firing. On top of that, the LEM LTS-15 and CASR-15 current transducers stopped working after tens of spark gap firings.

Manufacturer	LEM	LEM	Allegro
Model number	LTS-15 [34]	CASR-15 [22]	ACS710-12 [35]
Current range	$\pm$17 A	$\pm$17 A	$\pm$12.5 A
Technology	Closed loop hall effect	Closed loop fluxgate	Open loop hall effect
Failure mode	Offsets Destruction	Offsets Destruction	Offsets

Table 5.1: Current transducers used in testing

The offsets were suspected to be caused by the high peak current magnetising the core of the current transducers. The magnetic offset in the core was then converted to an electrical offset by the transducer. Destruction was suspected to be caused by high currents being induced in the DC injection winding by the current pulse. To avoid these problems, a method was needed to bypass the high current pulse from the current transducer, without affecting normal operation.

To evaluate the relative merits of different protection schemes, SPICE models were prepared and simulations were run. To get realistic results out of the simulation, the actual measured spark gap current was used as the spark current in the simulation. This was accomplished by measuring the spark gap current with an oscilloscope, exporting the waveform from it and converting it to piecewise linear file that could be imported into SPICE. To simulate the current transducer, inductance and resistance values were taken from the LEM LTS-15 data sheet [34]. The inductance is specified as 120 nH when configured for a range of $\pm$17 A, and the DC resistance is 1.6 mΩ.

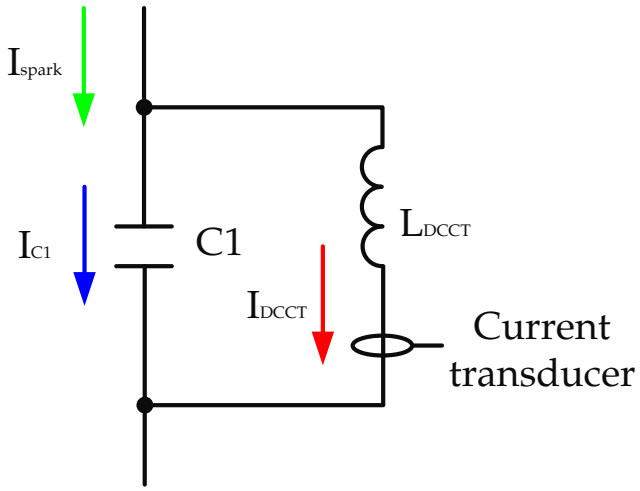

Figure 5.18: Current paths in current transducer protected with capacitor

The first method evaluated was a capacitor in parallel with the current transducer, as shown in figure 5.18. This bypassed the start of the current pulse, but the resonance set up between the current transducer inductance and the capacitor lead to an increase in the peak current seen by the transducer, shown in the plot in figure 5.19.

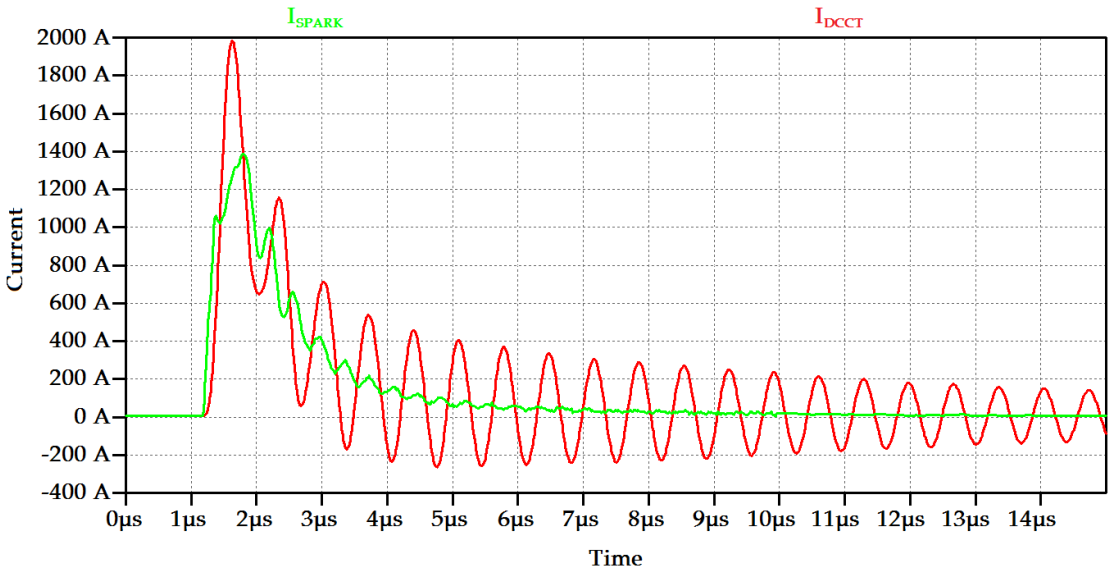

Figure 5.19: SPICE simulation result of capacitor-based current transducer protection

The plot shows the result with 100 nF of parallel capacitance, but other capacitance values were also used in simulation without better results. To damp this resonance and limit the peak current through the transducer to a reasonable value, a resistor in the order of 10 Ω is needed in series with the current transducer. This is an unacceptable solution, as the resistor would dissipate several hundreds of watts from the cathode current passing through it in normal operation.

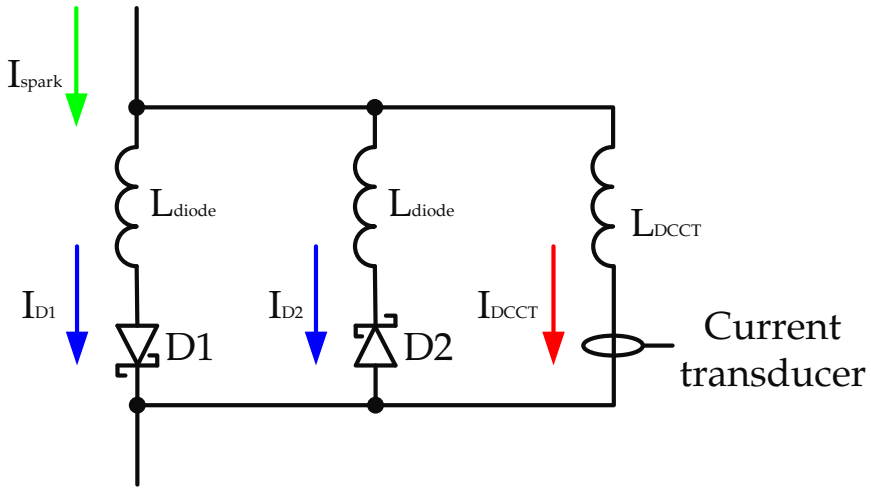

Figure 5.20: Current paths in current transducer protected with diodes

The second method evaluated was anti-parallel fast diodes connected across the current transducer, as shown in Figure 5.20. The current through a diode is an exponential function of the voltage across it, as described by the Shockley diode equation $I_d = I_s(e^{V_D/nV_T} - 1)$. This means that the voltage across the diode varies very little for large changes in current. As the diodes clamp the voltage across the transducer inductance, the rate of rise of current through the transducer is also limited. Schottky diodes were selected based on their low voltage drop and fast turn-on and turn-off characteristics.

This solution performed well in simulation. The peak current through the transducer significantly reduced. Figure 5.21 shows the simulation result, green trace is the current through the spark gap, the blue trace is the current through the protection diodes, and the red trace is the current through the LEM transducer. As can be seen from the simulation result, the peak current through the transducer is limited to less than 10 % of the spark current.

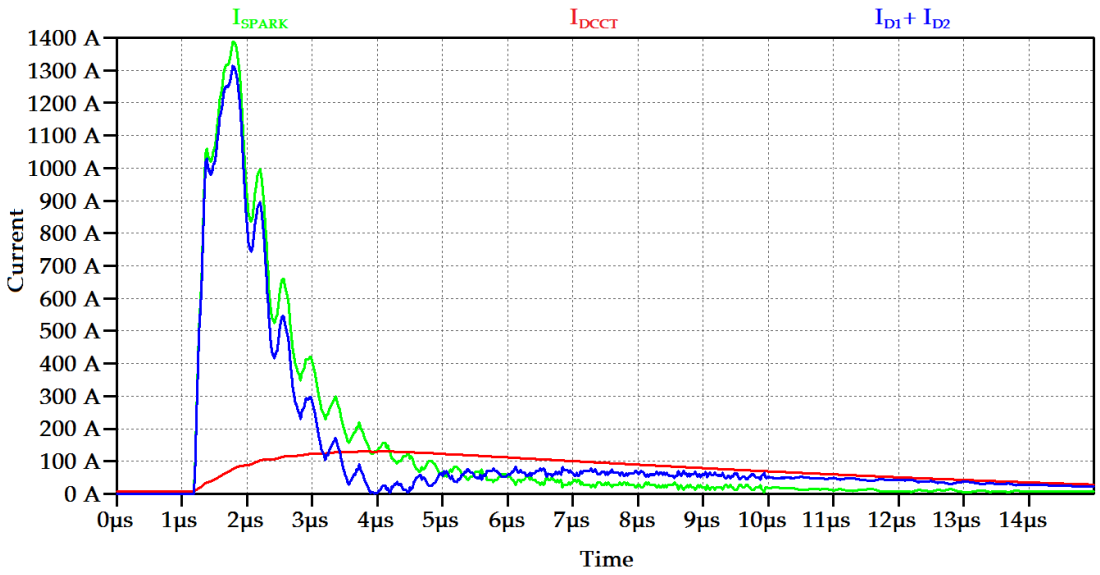

Figure 5.21: SPICE simulation result of diode-based current transducer protection

The diode-based transducer protection was tested by placing two antiparallel Vishay 15MQ040 Schottky diodes in parallel with the LTS-15 cathode current transducer in the measurement system, as illustrated in Figure 5.20. In subsequent reliability testing, the spark gap was fired over 160 times while connected to the cathode output of the modulator. No offsets were observed during or after testing, using LEM LTS-series current transducers, and the current transducers performed according to specifications afterwards. The final protection diode selection is ongoing, to gain some margin, more robust protection diodes will be used.

5.7 Final hardware implementation

Figure 5.22 shows the final implementation of the measurement card, after all the modifications mentioned in the previous sections were performed. The current transducers are protected using diodes, and mounted in a separate box. Figure 5.23 shows the measurement card box and the current transducer box, along with the connection to the cathode voltage divider.

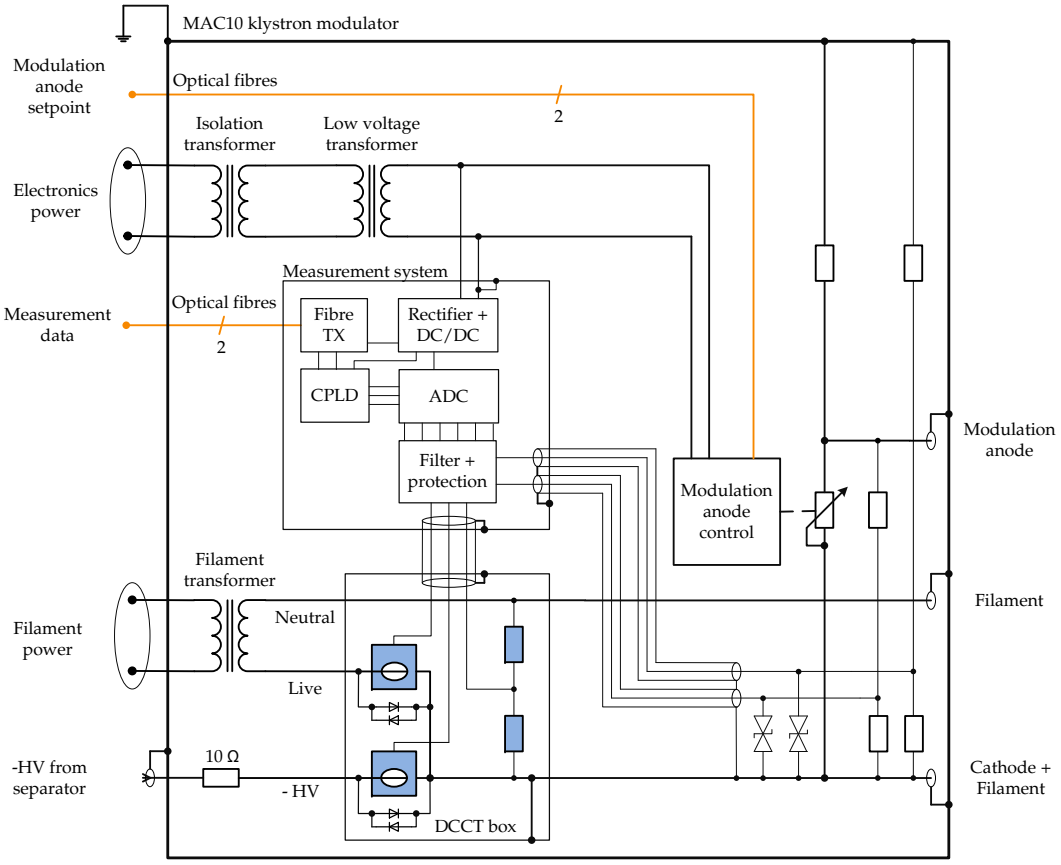

Figure 5.22: Final implementation of the measurement card in the modulator

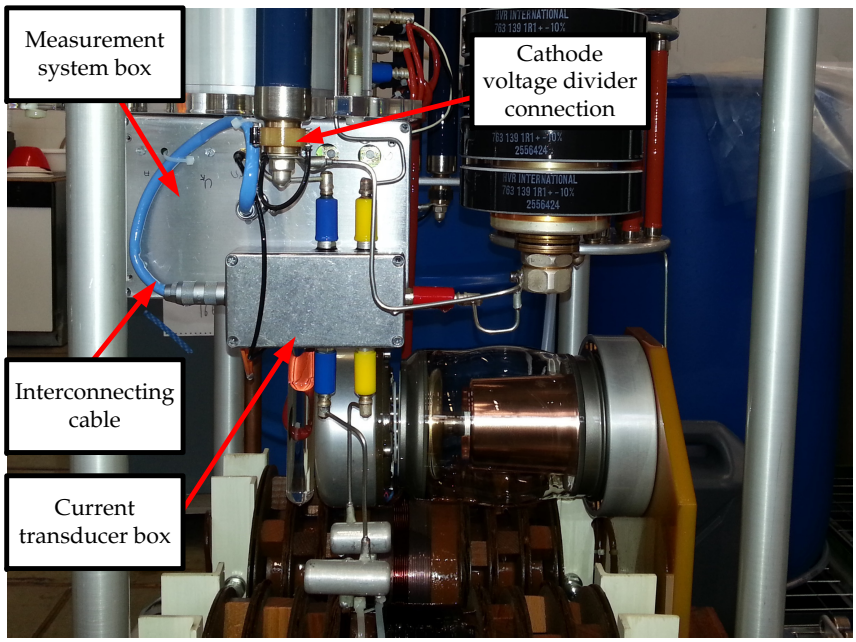

Figure 5.23: Measurement card mounted in modulator

5.8 Accuracy verification

To verify the accuracy of the measurement system after it had been mounted inside the modulator, operating under high voltage conditions, a test was carried out. Measured values from the system were compared with reference measurements from a Fluke 87 V multimeter [23] and the built-in metering in the Passoni & Villa high voltage power supply. The measurement error was calculated as a fraction of the full scale, according to equation 4.1. The relative differences in the measurements are higher than in the low voltage bench tests in section 4.2, this is to be expected as the measurements are now being performed in a more electrically noisy environment. In addition, the low voltage bench tests were performed without the high voltage dividers connected. The tolerance of these resistors will also add to the measurement error. Results are summarized in table 5.2.

Measured parameter	Reference measurement	Measurement system	Relative difference
Heater voltage RMS	20.0 V RMS	19.8 V RMS	1.0 %
Heater current RMS	20.6 A RMS	20.7 A RMS	0.5 %
Cathode current	2.80 A DC	2.79 A DC	0.4 %
Cathode voltage	20.0 kV DC	20.0 kV DC	0.0 %
Mod. anode voltage	40.0 kV DC	39.8 kV DC	0.5 %

Table 5.2: Values measured with the measurement system mounted in the modulator

To verify the heater voltage and current measurements, power was applied to the filament transformer through an adjustable autotransformer (variac). For the voltage measurement, the variac was adjusted so that a Fluke 87 V multimeter connected across the filament transformer secondary showed 20.0 V RMS. For the current measurement, a 1.1Ω resistor was connected between the filament and cathode outputs of the modulator, and the variac was adjusted to get a current of just over 20 A RMS through the filament transformer.

To verify the cathode current measurement, an adjustable DC power supply was connected between the modulator HV input and the cathode output. The voltage was adjusted so that a current of 2.80 A was flowing through the cathode current transducer.

To verify the accuracy of the cathode and modulation anode voltage measurement, high voltage was applied to the modulator using the Villa & Passoni 0–160 kV 0–15 mA power supply. The power supply was set to 40.0 kV.

6. Measurements

6.1 Measurements in a real klystron system

The modified modulator equipped with the measurement system was moved to a full scale klystron test facility in building 112, to verify that the measurement system would work correctly while connected to an operating klystron. The test setup is shown in Figure 6.1. This test stand is equipped with klystrons of the same model as used in the LHC, with the infrastructure to run them under the same conditions as in the LHC. The power supply for the test stand is based on the same technology as those in the LHC, but the current rating is 25 A. The crowbar in the test stand was replaced with the new solid state model, as these are planned to be in use in the LHC installation when the measurement systems are installed. The sample rate of the measurement system was set to 2.5 kHz, giving a nyquist frequency limit of 1.25 kHz. This allowed the 600 Hz ripple from the power converter to be observed.

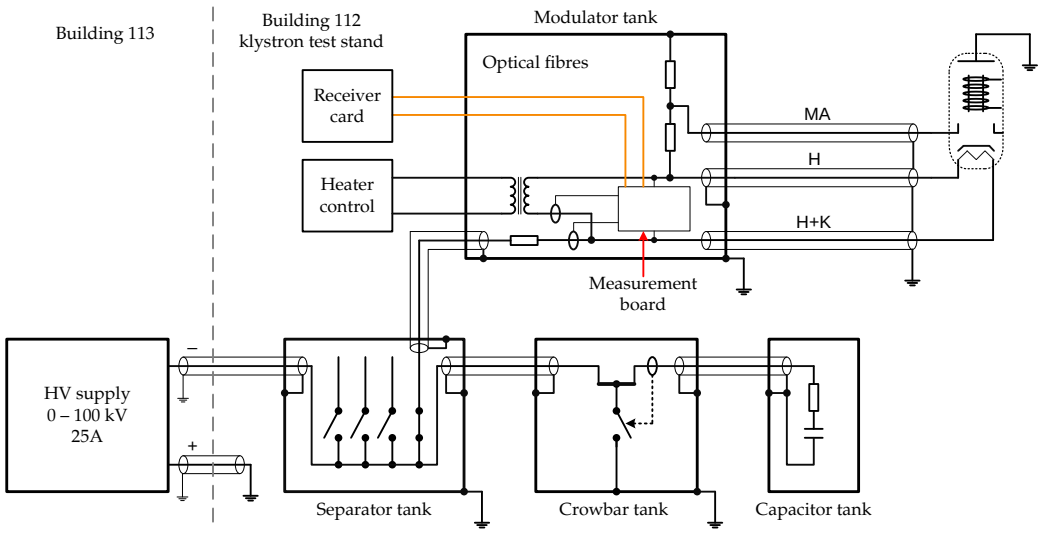

Figure 6.1: The test setup used to test the measurement system with a klystron connected

A receiver card was installed in the VME crate at the test stand, and connected to the measurement system using 57 m of 50 μm multimode glass fibre optic cable, with two fibre-to-fibre interconnections. This allowed monitoring and logging

of the data from the measurement system, and verification of the optical power budget with a realistic length of fibre. Data from the sample buffers was loaded into MATLAB for further processing and analysis.

Power was gradually applied to the klystron heater, and it was allowed to warm up for 20 minutes before high voltage was applied to the klystron cathode. The measured values from the system were observed while high voltage was gradually applied to the cathode of the klystron. The cathode voltage was increased stepwise until -58 kV was reached, the highest voltage the TH2167 klystron is specified for operation at. The measured values were allowed to stabilize between each voltage step. The receiver card buffers were allowed to fill up with measured data at cathode voltages of -30 kV, -40 kV, -50 kV and -58 kV, and the data was saved for further analysis.

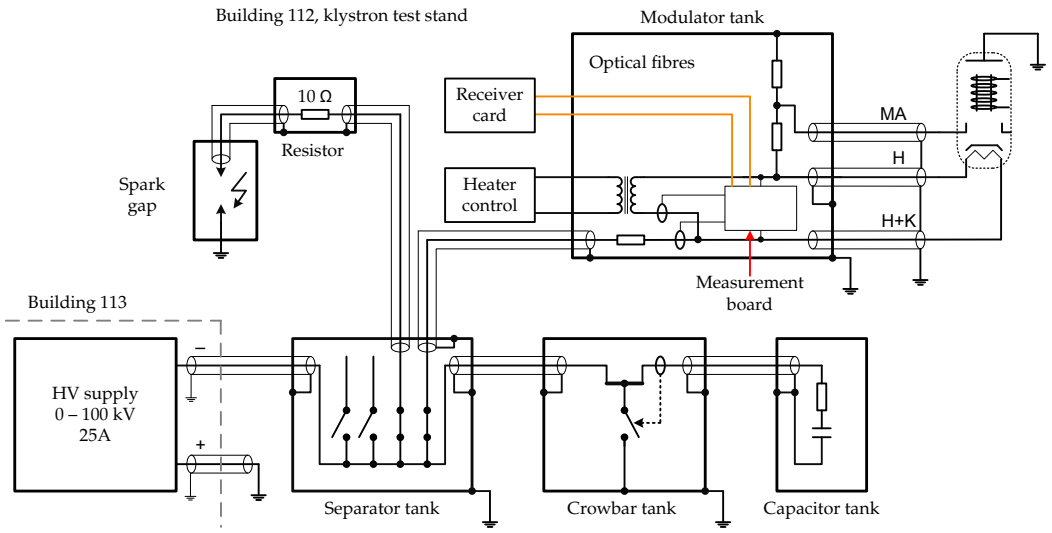

Figure 6.2: The test setup used to trigger the crowbar while capturing measurement data

To be able to observe the data captured by the measurement system during a crowbar firing, the crowbar was triggered while the klystron was operating. To trigger the crowbar, a spark gap in series with a 10 Ω resistor was connected between one of the separator outputs and ground. The setup is shown in figure 6.2

The same test was performed with the spark gap connected between the cathode output of the modulator and ground, to be able to observe the data captured by the measurement system during an arc in the klystron. The klystron was connected to a second modulator that was connected to the same separator. The setup is shown in Figure 6.3.

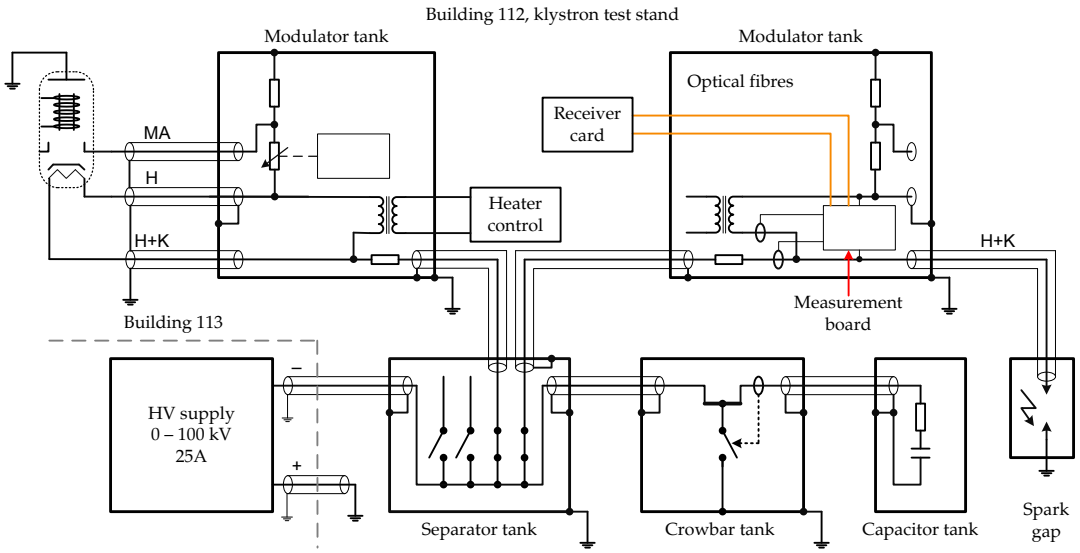

Figure 6.3: The test setup used to capture measured data during spark gap firing

6.2 Measurement results

Figure 6.4 shows a plot of the filament current and filament voltage during the beginning of filament warm-up. Tungsten has a positive thermal coefficient of resistance. This means that the resistance of the tungsten filament increases as the cathode structure heats up. The current is held constant by the filament current regulator, and the rise in filament resistance manifests itself as a rise in filament voltage, as can be seen in the plot.

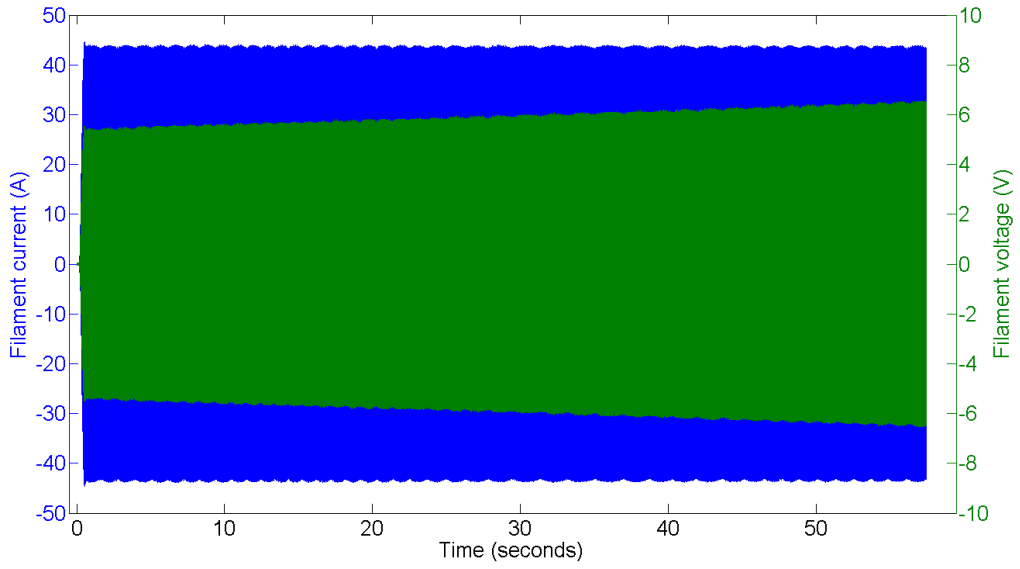

Figure 6.4: Filament current and voltage during the start of filament warm-up

Figure 6.5 shows the heater current and voltage waveforms on a shorter time scale. The shape of the current and voltage deviating from a sine wave is caused by the filament current controller, which chops the mains waveform using a thyristor, to regulate filament current. The filament voltage and current waveforms are in phase due to the resistive nature of the klystron cathode heater.

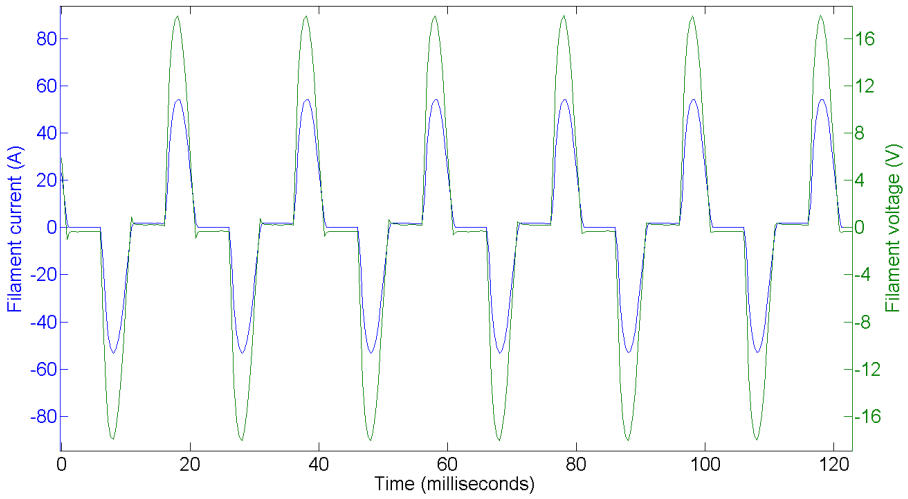

Figure 6.5: Filament voltage and current waveform

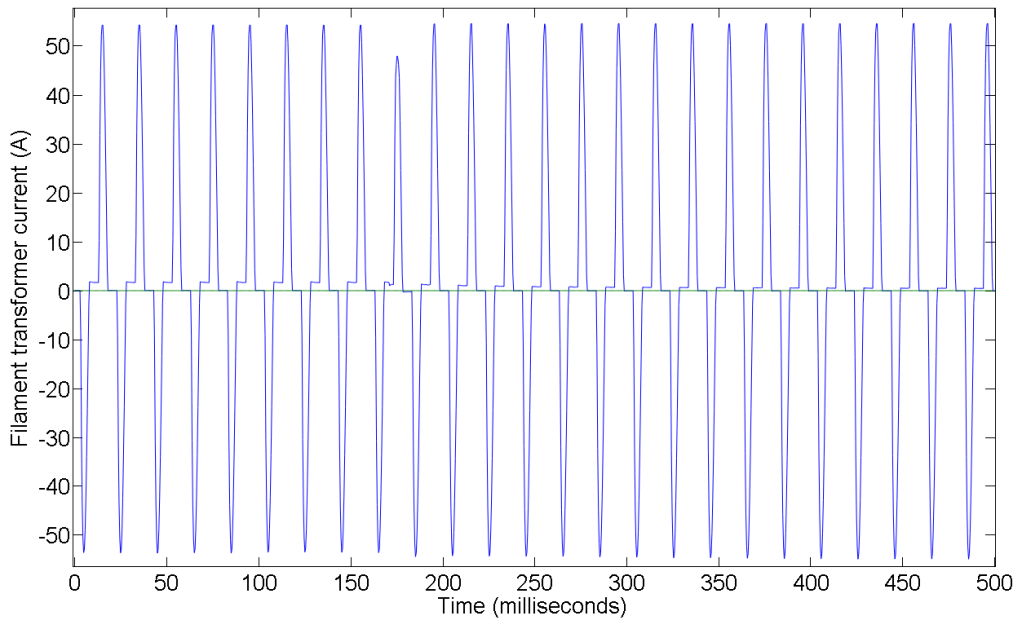

Figure 6.6: Filament current with part of the cathode current flowing through the filament transformer

Figure 6.6 shows a plot of the current flowing through the filament transformer during a test where the crowbar was fired. There is 7.4 A of cathode current flowing until 170 ms into the plot, where the crowbar fires, and no cathode current after this. Part of the cathode current is flowing through the filament transformer, as evidenced by the DC offset during the flat parts of the current waveform.

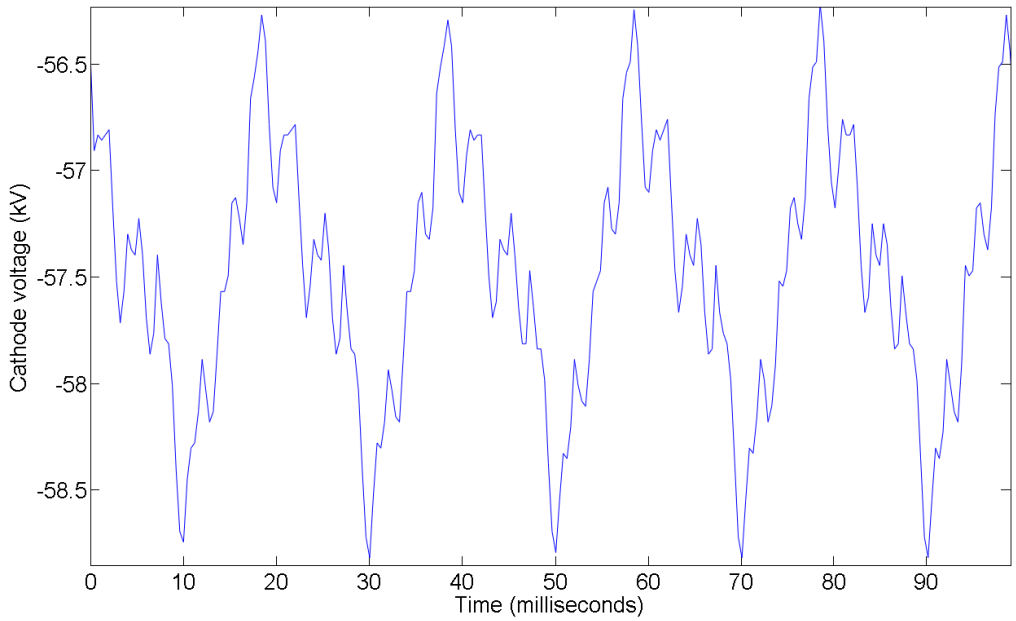

Figure 6.7: Ripple on the high voltage supply in the time domain

Figure 6.7 shows a plot of the cathode voltage as a function of time, with the klystron running at -58 kV and 7.4 A of cathode current. The high voltage supply used in these tests is known to have a large amount of ripple on the output, and the measurement system confirmed this, indicating a ripple voltage of approximately 2.5 kV peak-to-peak. To confirm the ripple waveform and the magnitude of ripple, the cathode voltage was measured using a Tektronix DPO5034 [30] oscilloscope and a North Star PVM-5 [36] 1000:1 high voltage probe. This measurement showed the same ripple magnitude and waveform of ripple.

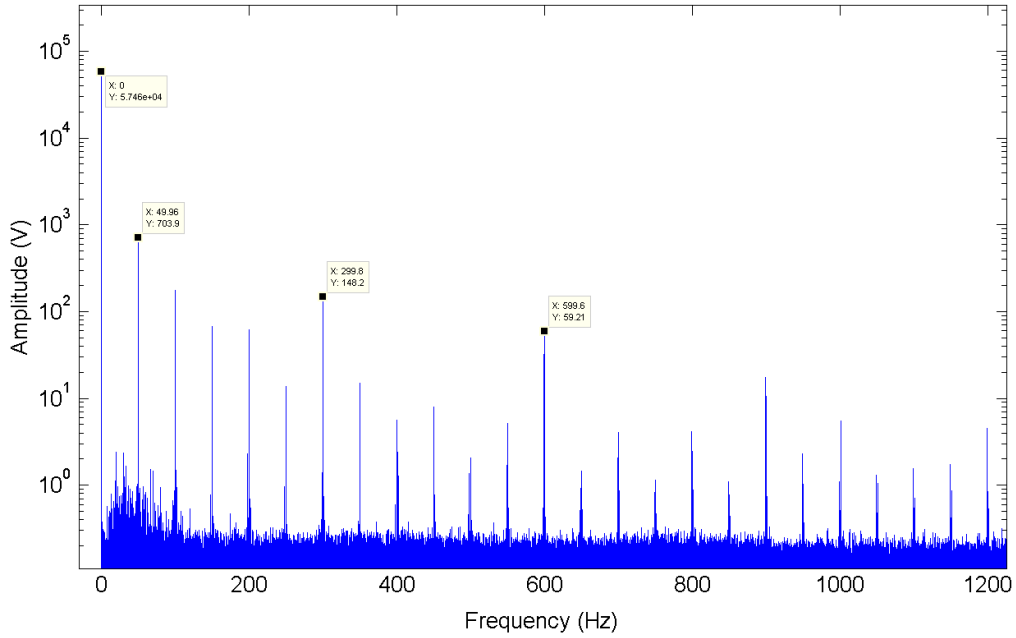

Figure 6.8: Ripple on the high voltage supply in the frequency domain

The cathode voltage waveform was converted to the frequency domain by using the Matlab FFT function and a Hamming window, the result is shown as a logarithmic plot in Figure 6.8. The amplitude of the 50 Hz component of the ripple is over 700 V RMS. In the ideal case, a 12-pulse converter does not have any ripple components below 600 Hz, but any phase asymmetry or difference in switching time between the different phases results in lower frequency ripple components, as can be seen here. These measurements give important clues on the state of the power converter, facilitating repairs and adjustments.

7. Conclusion

A measurement system has been developed which allows critical parameters of klystron operation to be monitored and logged with improved accuracy and a sample rate three orders of magnitude higher than the existing measurement systems. The receiver card provides a buffer of the last 262144 measurements for each channel. The data in the buffer is frozen if a fault triggers the interlock system, and the data stored in the buffer can give valuable clues to the cause of the fault, and the events leading up to the fault.

The measurement system is floating at the klystron cathode potential, and communication to the receiver board is over optical fibres. Errors in cathode current measurement are eliminated, due to the fact that cathode current is measured directly at the klystron cathode.

Components for the design have been tested to be compatible with the oil types used in the modulator. Fibre losses have been calculated for the installation in underground cavern UX45, and a fibre type has been selected to satisfy the loss requirements.

The measurement system has been integrated into an LHC klystron high voltage modulator, and extensive testing has been performed to verify that it will survive expected fault conditions. Modifications have been performed to eliminate interference issues during klystron arcing. A protection scheme has been developed to bypass high fault currents from the current transducers during klystron arcing, to avoid magnetisation and damage of the current transducers. Reliability testing has been performed to verify that the system will withstand repeated fault conditions.

The modulator with the measurement system has been tested in a real klystron setup, and measurement values have been logged and analyzed during klystron operation. These measurements show aspects of klystron operation that can not be observed with the present measurement systems.

References

[1] Laurent Guiraud. Working on an LHC superconducting cavity. Travail effectu sur une cavit supraconductrice. Aug 2000.

[2] Private. Image from the CERN RF picture archives. Nov 2009.

[3] Hans W. Isch. *Power converter for RF klystrons 100 KV, 40 A: some aspects of the design of the power circuit*. Geneva, 1984.

[4] G. Ravidà, O. Brunner, and D. Valuch. Performance of the Crowbar of the LHC High Power RF System. *Conf. Proc.*, (CERN-ATS-2012-149), Apr 2012.

[5] L. Arnaudon, P. Baudrenghien, O. Brunner, and A. Butterworth. Operation experience with the LHC RF system. (CERN-ATS-2010-192), May 2010.

[6] Paul Proudlock and Hans W. Isch. The power converters for the RF klystrons of LEP. (CERN-SL-90-33-PC), Jun 1990.

[7] A. Delizee, J. C. Carlier, and Paul Proudlock. The realization of the power converters for the CERN RF system of LEP. (CERN-SL-90-54-PC), Jun 1990.

[8] Thales. TH2167 specifications.

[9] Thales. *TH 5184, TH 5186, TH 5188, Switching and regulation tetrodes*.

[10] D. Valuch. High voltage tetrode replacement in the LHC klystron modulator. 2010.

[11] C. Roderick, L. Burdzanowski, and G. Kruk. *The CERN Accelerator Logging Service- 10 Years in Operation: A Look at the Past, Present and Future* . Geneva, Oct 2013.

[12] LEM. *Isolated current and voltage transducers, Characteristics - Applications - Calculations*.

[13] Analog Devices. *AD7490, 16-Channel, 1 MSPS, 12-Bit ADC with Sequencer*.

[14] Xilinx. *CoolRunner-II CPLD Family*.

[15] Avago. *Low Cost, Miniature Fiber Optic Components with ST, SMA, SC and FC Ports Data Sheet*.

[16] Maxim Integrated. *MAX6304, +5V, Low-Power μP Supervisory Circuits with Adjustable Reset/Watchdog*.

[17] Traco Power. *DC/DC Converters, THL 3WI(SM) Series, 3 Watt*.

[18] LEM. *Current Transducer HX 05..15-NP*.

[19] Analog Devices. *AD8436, Low Cost, Low Power, True RMS-to-DC Converter*.

[20] A. Butterworth, L. Arnaudon, P. Baudrenghien, and J. Molendijk. RF Issues and Developments at the LHC Machine. 2007.

[21] Analog Devices. *AD8226, Wide Supply Range, Rail-to-Rail Output Instrumentation Amplifier*.

[22] LEM. *Current Transducer CASR series*.

[23] Fluke. *80 Series V Multimeters*.

[24] LeCroy. *Waverunner XI seris Oscilloscopes Operators Manual*.

[25] Bluestar Silicones. *Rhodorsil Oils 47 Technical information*.

[26] Avago. *Full Metal Fiber Optic Transmitters and Receivers for SERCOS, PROFIBUS and INTERBUS-S Applications*.

[27] Avago. *Plastic Optical Fiber Cable and Accessories for Versatile Link*.

[28] TELECOMMUNICATIONS INDUSTRY ASSOCIATION. *Optical Fiber Cabling Components Standard TIA/EIA-568-B.3*.

[29] Pearson. *Pearson current monitor model 150*.

[30] Tektronix. *MSO5000B, DPO5000B Series Datasheet*.

[31] Lemo. *Unipole and multipole connectors*.

[32] Fox Electronics. *XpressO HCMOS 7 x 5mm 3.3V Oscillator*.

[33] Fox Electronics. *Crystal Oscillator history and development*.

[34] LEM. *Current Transducer LTS 15-NP*.

[35] Allego Microsystems. *ACS710, 120 kHz Bandwidth, High Voltage Isolation Current Sensor with Integrated Overcurrent Detection*.

[36] North Star High Voltage. *PVM Series Portable High Voltage Probes to 60 kV DC*.

Acronyms and abbreviations

CERN	the European Organization for Nuclear Research
LHC	Large Hadron Collider
SPS	Super Proton Synchrotron
PS	Proton Synchrotron
PSB	Proton Synchrotron Booster
LINAC	Linear Accelerator
HV	High Voltage
CPLD	Complex Programmable Logic Device
ADC	Analog-to-digital converter
DCCT	DC current transducer
CW	Continous Wave
RF	Radio Frequency
LLRF	Low Level Radio Frequency

Appendices

A. Acceptance test data for Thales TH2167 klystron

Heating :

Vf = 7 V
If = 29 A

Solenoid current :

I1 = 9.8 A

Solenoid voltage :

V1 = 260 V

Cooling :

	Water flow			Power / °C	
Body + Output cavity =	**15**	**dm^3/min**	**x 0.07 =**	**1.05**	**kW/°C**
Collector =	**450**	**dm^3/min**	**x 0.07 =**	**31.5**	**kW/°C**
Load =	**335**	**dm^3/min**	**x 0.07 =**	**23.45**	**kW/°C**

Window Air flow = 90 m^3/h

Gun Air flow = 90 m^3/h

OUTPUT POWER MODE II (300 kW cw - 54 kV - 9 A)

PARAMETRES *PARAMETERS*	SYMBOLE *SYMBOL*	UNITE *UNIT*	LIMITES *LIMITS*		VALEURS MESUREES *MEASURED VALUES*
			MIN	MAX	
TENSION DE CHAUFFAGE **Heater voltage**	Vf	V	-	12	**29**
COURANT DE CHAUFFAGE **Heater current**	If	A	-	30	**29**
TENSION FAISCEAU **Beam voltage**	Vk	kV	-	54	**54**
COURANT FAISCEAU **Cathode current**	Ik	A	-	9	**9**
TENSION ANODE **Anode voltage**	Va	kV	-	35	**31.7**
PERVEANCE CANON **Gun Perveance**	k	$\mu A/V^{3/2}$	1.5	1.65	**1.59**
COURANT D'ANODE **Anode current**	Ia	mA	-	2.5	**-0.3**
PUISSANCE RF SORTIE **RF output power**	Ps	kW	300	-	**302**
PUISSANCE RF ENTREE **RF drive power**	Pe	W	-	60	**42**
GAIN **Gain**	G	dB	37	-	**38.6**
FREQUENCE RF **RF frequency**	fo	MHz	400.8		**400.8**
PUISSANCE CORPS & CAVITE **Body and output cavity power**	Pbody	kW	-	10	**5.8**
RENDEMENT **Efficiency**	η	%	62	-	**62.1**
PUISSANCE RF REFLECHIE **RF reflected power**	Pref	kW	-	-	**0.68**
ROS CHARGE **VSWR load**	VSWR	-	-	1.1	**1.1**
COURANT FOCALISATEUR 1 **Solenoidl current 1**	Isol1	A	-	12	**9.8**
COURANT POMPE IONIQUE **Ion pump current**	Ipi	µA	-	10	**0.5**

OUTPUT POWER MODE II (300 kW cw - 58 kV - 8.4 A)

PARAMETRES *PARAMETERS*	**SYMBOLE** *SYMBOL*	**UNITE** *UNIT*	**LIMITES** *LIMITS*		**VALEURS MESUREES** *MEASURED VALUES*
			MIN	**MAX**	
TENSION DE CHAUFFAGE **Heater voltage**	Vf	V	-	12	**7**
COURANT DE CHAUFFAGE **Heater current**	If	A	-	30	**29**
TENSION FAISCEAU **Beam voltage**	Vk	kV	-	58	**58**
COURANT FAISCEAU **Cathode current**	Ik	A	-	8.4	**8.4**
TENSION ANODE **Anode voltage**	Va	kV	-	35	**29.9**
PERVEANCE CANON **Gun Perveance**	k	$\mu A/V^{3/2}$	1.5	1.65	**1.62**
COURANT D'ANODE **Anode current**	Ia	mA	-	2.5	**-0.2**
PUISSANCE RF SORTIE **RF output power**	Ps	kW	300	-	**302**
PUISSANCE RF ENTREE **RF drive power**	Pe	W	-	-	**61**
GAIN **Gain**	G	dB	-	-	**36.9**
FREQUENCE RF **RF frequency**	fo	MHz	400.8		**400.8**
PUISSANCE CORPS & CAVITE **Body and output cavity power**	Pbody	kW	-	10	**5.6**
RENDEMENT **Efficiency**	η	%	62	-	**62.0**
PUISSANCE RF REFLECHIE **RF reflected power**	Pref	kW	-	-	**0.68**
ROS CHARGE **VSWR load**	VSWR	-	-	1.1	**1.1**
COURANT FOCALISATEUR 1 **Solenoidl current 1**	Isol1	A	-	12	**9.8**
COURANT POMPE IONIQUE **Ion pump current**	Ipi	µA	-	10	**0.5**

OUTPUT POWER MODE I (200 kW cw)

PARAMETRES *PARAMETERS*	SYMBOLE *SYMBOL*	UNITE *UNIT*	LIMITES *LIMITS*		VALEURS MESUREES *MEASURED VALUES*
			MIN	MAX	
TENSION DE CHAUFFAGE **Heater voltage**	Vf	V	-	12	**7**
COURANT DE CHAUFFAGE **Heater current**	If	A	-	30	**29**
TENSION FAISCEAU **Beam voltage**	Vk	kV	-	46	**46**
COURANT FAISCEAU **Cathode current**	Ik	A	-	8	**8**
TENSION ANODE **Anode voltage**	Va	kV	-	35	**29.5**
PERVEANCE CANON **Gun Perveance**	k	$\mu A/V^{3/2}$	1.5	1.65	**1.58**
COURANT D'ANODE **Anode current**	Ia	mA	-	2.5	**-0.2**
PUISSANCE RF SORTIE **RF output power**	Ps	kW	200	-	**206**
PUISSANCE RF ENTREE **RF drive power**	Pe	W	-	40	**25**
GAIN **Gain**	G	dB	37	-	**39.2**
FREQUENCE RF **RF frequency**	fo	MHz	400.8		**400.8**
PUISSANCE CORPS & CAVITE **Body and output cavity power**	Pbody	kW	-	10	**4.6**
RENDEMENT **Efficiency**	η	%	55	-	**56.0**
PUISSANCE RF REFLECHIE **RF reflected power**	Pref	kW	-	-	**0.29**
ROS CHARGE **VSWR load**	VSWR	-	-	1.1	**1.08**
COURANT FOCALISATEUR 1 **Solenoidl current 1**	Isol1	A	-	12	**9.8**
COURANT POMPE IONIQUE **Ion pump current**	Ipi	µA	-	10	**0.5**

OUTPUT POWER MODE TEST (330 kW cw)

PARAMETRES *PARAMETERS*	SYMBOLE *SYMBOL*	UNITE *UNIT*	LIMITES *LIMITS*		VALEURS MESUREES *MEASURED VALUES*	
			MIN	MAX	To	To + 1 hour
TENSION DE CHAUFFAGE **Heater voltage**	Vf	V	-	12	**7**	**7**
COURANT DE CHAUFFAGE **Heater current**	If	A	-	30	**29**	**29**
TENSION FAISCEAU **Beam voltage**	Vk	kV	-	58	**58**	**58**
COURANT FAISCEAU **Cathode current**	Ik	A	-	10	**10**	**10**
TENSION ANODE **Anode voltage**	Va	kV	-	-	**34.2**	**34.2**
PERVEANCE CANON **Gun Perveance**	k	$\mu A/V^{3/2}$	1.5	1.65	**1.58**	**1.58**
COURANT D'ANODE **Anode current**	Ia	mA	-	2.5	**-0.3**	**-0.3**
PUISSANCE RF SORTIE **RF output power**	Ps	kW	330	-	**339**	**339**
PUISSANCE RF ENTREE **RF drive power**	Pe	W	-	-	**42**	**42**
GAIN **Gain**	G	dB	-	-	**39.1**	**39.1**
FREQUENCE RF **RF frequency**	fo	MHz	400.8		**400.8**	**400.8**
PUISSANCE CORPS & CAVITE **Body and output cavity power**	Pbody	kW	-	10	**8.3**	**8.3**
RENDEMENT **Efficiency**	η	%	-	-	**58.4**	**58.4**
PUISSANCE RF REFLECHIE **RF reflected power**	Pref	kW	-	-	**0.83**	**0.83**
ROS CHARGE **VSWR load**	VSWR	-	-	1.1	**1.1**	**1.1**
COURANT FOCALISATEUR 1 **Solenoidl current 1**	Isol1	A	-	12	**9.8**	**9.8**
COURANT POMPE IONIQUE **Ion pump current**	Ipi	µA	-	10	**0.5**	**0.5**

1 - RF frequency = 400.8 MHz
Ik = **8.4** A
Va = 29.9 kV
and Pe for 1 dB below saturated Output

Vk (value of mode II)	Vk (kV)	Phase (°)	Output power (kW)
	58	**0**	**302**
	57	**-15**	**293**
	56	**-30**	**289**

$\frac{\text{Vk max - Vk min}}{\text{Vk average}}$ = 3.5 %

RF output power variation = **0.05** dB/% (max. = 0.1 dB/%)
RF phase variation = **-8.6** deg/% (max. = 10 °/%)

2 - RF frequency = 400.8 MHz
Vk = **54** kV (value of mode II)
Pe = **42** W (value at saturation of mode II)

Va (kV)	Ik (A)	Phase (°)	Output power (kW)
31.7	9	**0**	**302**
28.9	8	**5**	**278**
26.1	7	**15**	**234**
23.2	6	**25**	**176**
19.9	5	**37**	**121**
18.4	4	**45**	**78**
13	3	**50**	**50**
8.9	2	**60**	**35**
4.2	1	**67**	**24**

RF phase variation = **8.4** deg/A (max. = 15 °/A)

3 - Mode II
2 nd Harmonic = **-64** (≤ - 30 dB)
3 rd Harmonic = **-61.5** (≤ - 30 dB)

4 - Signal ratio of fundamental to other discrete frequencies within bandwith **= 62** (≥ 60 dB)

-1 dB Bandwith and Group Delay

Mode I :

0 dB = Saturated Output power = 200 kW

- 1 dB = 158 kW

- 2 dB = 126 kW

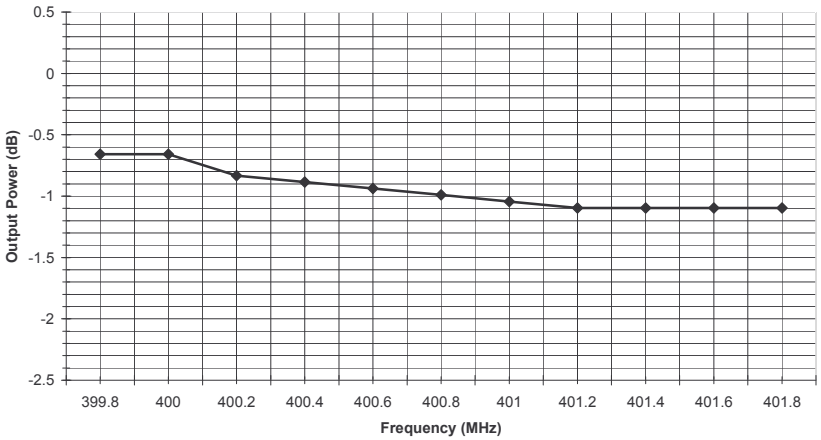

- 1 dB Bandwith = -0.44 (≥ ± 1 MHz)
Group Delay (fo ± 1 MHz) = 139 (≤ 120 ns)

Frequency (MHz)	399.8	400	400.2	400.4	400.6	400.8	401	401.2	401.4	401.6	401.8
Output power (kW)	177	177	170	168	166	164	162	160	160	160	160
Phase (°)	65	50	35	24	10	0	-12	-45	-35	-48	-60

-1 dB Bandwith and Group Delay

Mode II :

0 dB = Saturated Output power = 300 kW

- 1 dB = 238 kW

- 2 dB = 189 kW

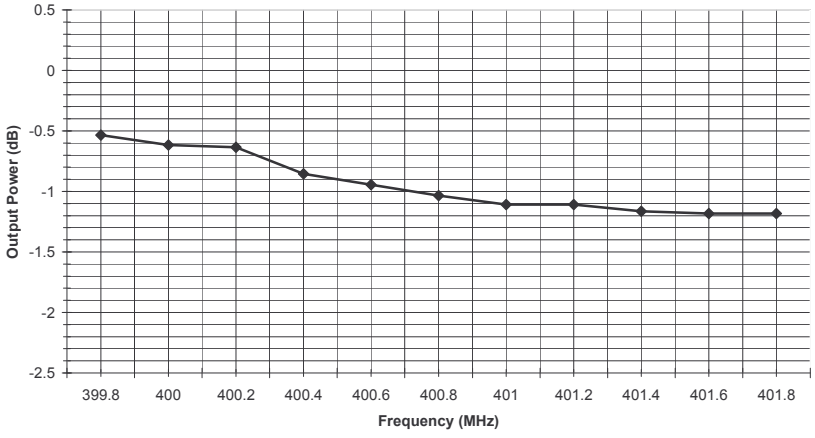

- 1 dB Bandwith = -0.65 (≥ ± 1 MHz)
Group Delay (fo ± 1 MHz) = 133 (≤ 120 ns)

Frequency (MHz)	399.8	400	400.2	400.4	400.6	400.8	401	401.2	401.4	401.6	401.8
Output power (kW)	267	262	261	248	243	238	234	234	231	230	230
Phase (°)	65	50	40	29	15	0	-10	-20	-35	-45	-56

Test Collector :

Beam Power ≥ 500 kW (54 kV - 9.3 A)

Duration = 20 min.

Ipi = 1,5 µA at To

Ipi = 1,5 µA at To + 20 min.

DC Test Voltages (cold cathode) :

Cathode / Modulation Anode to ground	≥ 65 kV for 15 min.	Result =	250 µA
Cathode to Modulation Anode	≥ 65 kV for 15 min.	Result =	700 µA

X-Radiation (MODE II and test power) :

Maximum X-Radiation at any klystron surface = 4 µSv/h (≤ 5)

RF Radiation (MODE II and test power) :

RF Radiation from any Surface = 0 mW / cm^2 (≤ 0.1)

Magnetic Field :

1 m from Klystron Axis = 0 mT (≤ 0.5)

Rieke Diagram

Vk = 58 kV Va = 29.9 kV
Ik = 8.4 A Pe = 61 W

Position cm	Ia mA	P sortie kW	P refl. kW	TOS	η %	Gain dB	Ipi µA	P corps+cavité kW
0	**-0.2**	**282**	**1.6**	**1.16**	**57.9**	**36.6**	**<1**	**5.4**
5	**-0.2**	**284**	**2**	**1.18**	**58.3**	**36.7**	**<1**	**5.4**
10	**-0.2**	**286**	**1.9**	**1.18**	**58.7**	**36.7**	**<1**	**5.4**
15	**-0.2**	**295**	**1.5**	**1.15**	**60.6**	**36.8**	**<1**	**5.5**
20	**-0.2**	**304**	**0.95**	**1.12**	**62.4**	**37.0**	**<1**	**5.7**
25	**-0.2**	**306**	**0.4**	**1.08**	**62.8**	**37.0**	**<1**	**5.9**
30	**-0.2**	**310**	**0.13**	**1.04**	**63.6**	**37.1**	**<1**	**5.9**
35	**-0.2**	**304**	**0.18**	**1.05**	**62.4**	**37.0**	**<1**	**5.6**
40	**-0.2**	**291**	**0.26**	**1.06**	**59.7**	**36.8**	**<1**	**5.4**
45	**-0.2**	**280**	**0.28**	**1.07**	**57.5**	**36.6**	**<1**	**5.4**
50	**-0.2**	**278**	**0.37**	**1.08**	**57.1**	**36.6**	**<1**	**5.4**

Rendement max. = 63.6%

Calcul du rendement :

Electrique : (Psortie - Prefl.) / Vk * Ik
Thermique : P charge / (P corps & cavité + P collecteur + P charge)

B. Complete schematics of measurement system

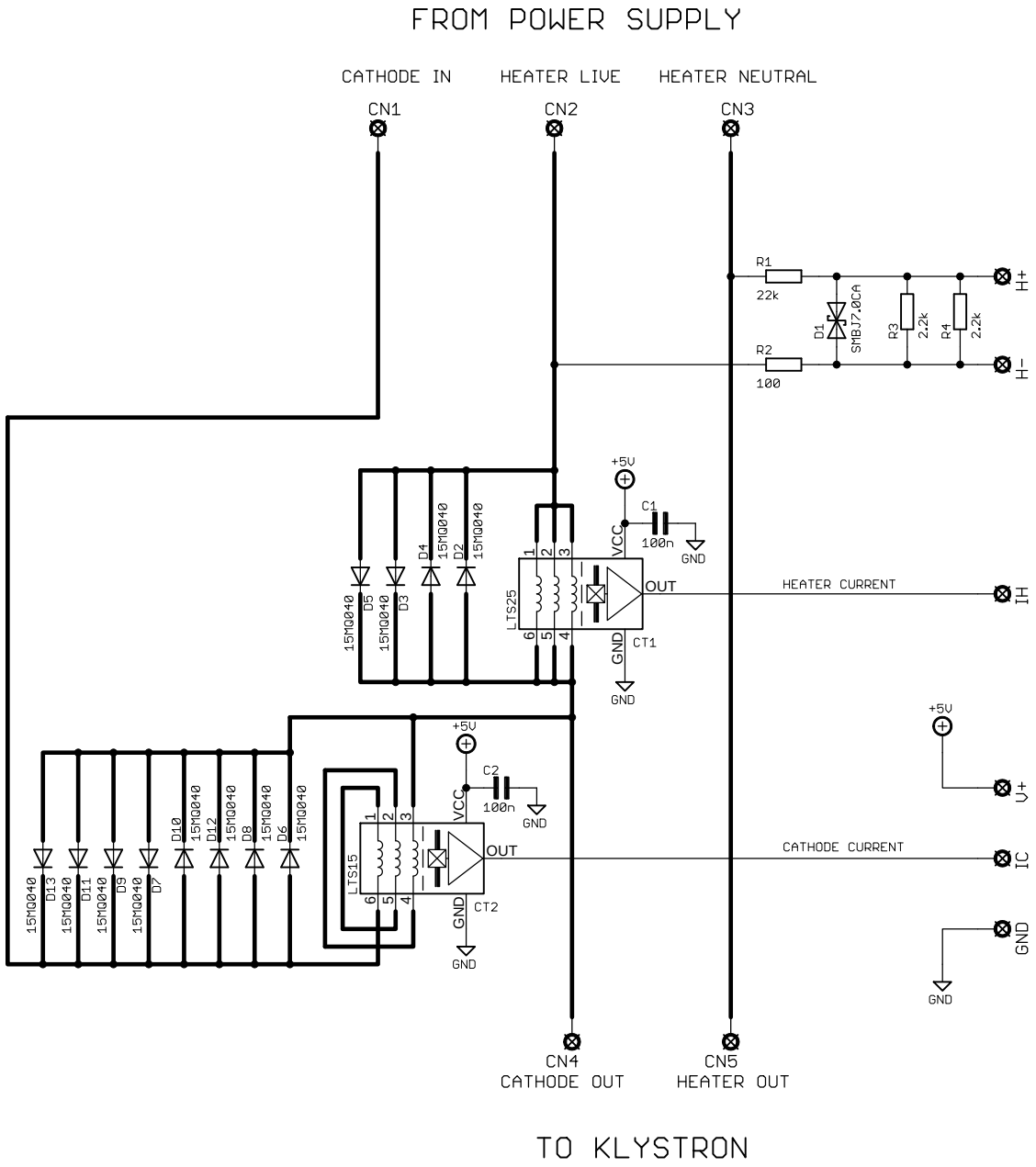

Projet/ Project: LHC modulator measurement system		Resp.:	
Ensemble/ Set:	Echelle/ Scale	Designer:	AM/DV
Sous-ensemble Underset:		Drawn:	AM/DV
Document: HV MEASUREMENTS SENSOR CARD		MODA:	
		MODB:	
		File:	IND.
LAB. EUROPEEN POUR LA PHYSIQUE DES PARTICULES EUROPEAN LABORATORY FOR PARTICLE PHYSICS GENEVE/GENEVA	Ref: nb	AED-00202-V1	

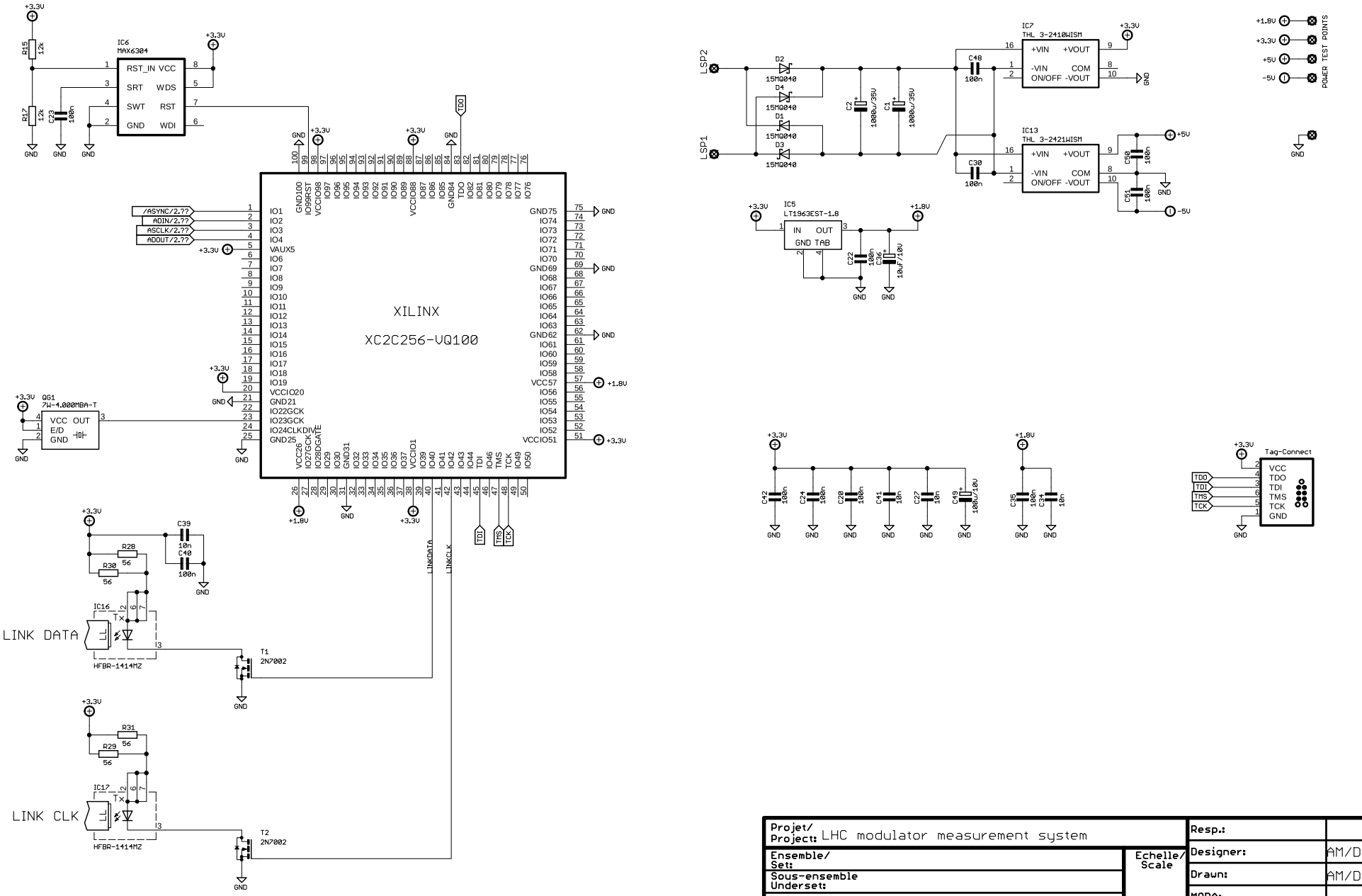

Projet/ Project: LHC modulator measurement system		Resp.:	
Ensemble/ Set:	Echelle/ Scale	Designer:	AM/DV
Sous-ensemble Underset:		Draun:	AM/DV
Document: HV MEASUREMENTS TRANSMITTER CARD		MODA:	
		MODB:	
		File:	IND.
LAB. EUROPEEN POUR LA PHYSIQUE DES PARTICULES EUROPEAN LABORATORY FOR PARTICLE PHYSICS GENEVE/GENEVA	Ref: nb	AED-00191-V3	

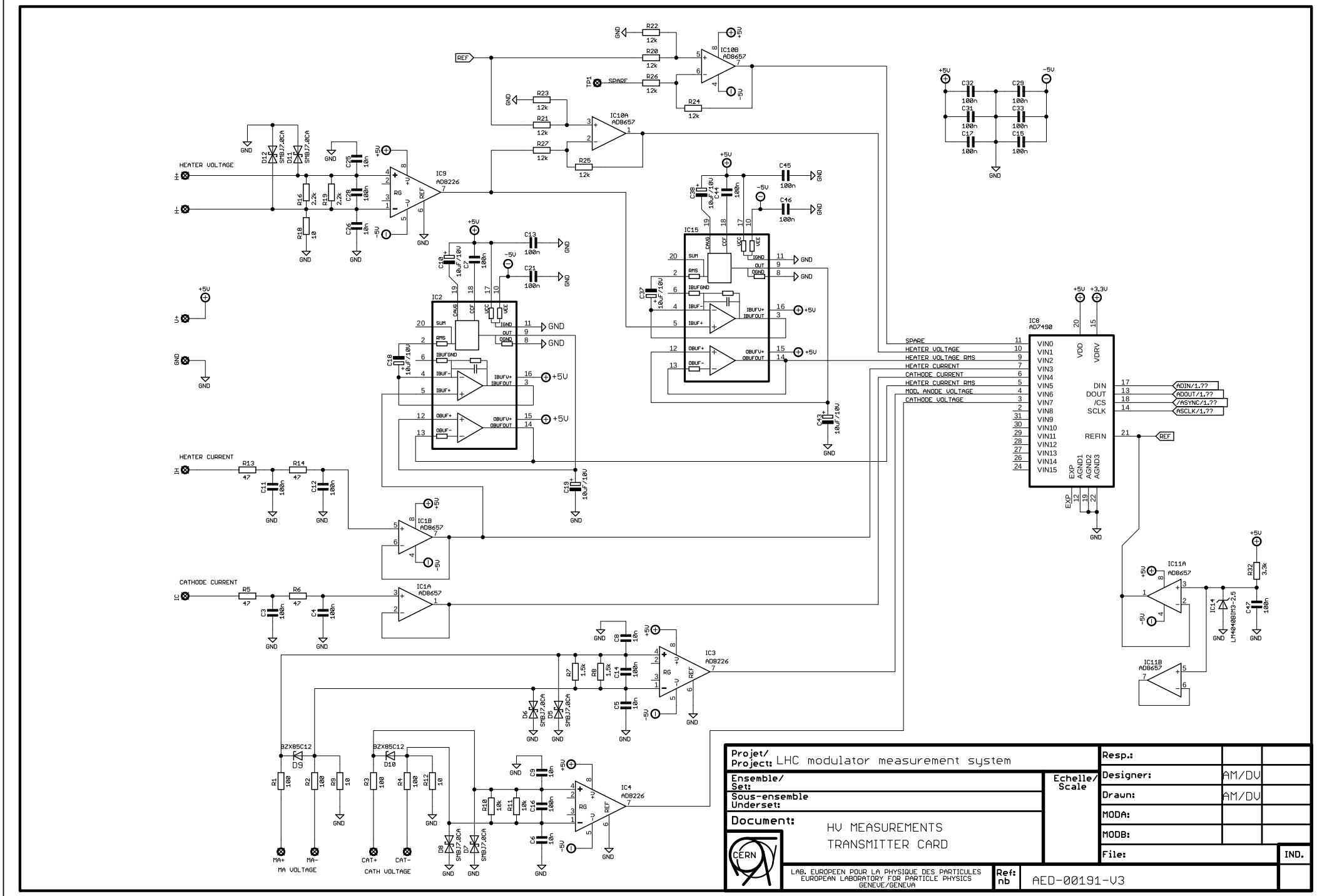
HEATER VOLTAGE
H+
H-
HEATER CURRENT
IH
CATHODE CURRENT
IC
U+
GND
MA VOLTAGE
MA+
MA-
CATH VOLTAGE
CAT+
CAT-
REF
SPARE
TP1
IC1A AD8657
IC1B AD8657
IC2
IC3 AD8226
IC4 AD8226
IC9 AD8226
IC10A AD8657
IC10B AD8657
IC11A AD8657
IC11B AD8657
IC15
IC8 AD7490
D5 SMBJ7.0CA
D6 SMBJ7.0CA
D7 SMBJ7.0CA
D8 SMBJ7.0CA
D9 BZX85C12
D10 BZX85C12
D11 SMBJ7.0CA
D12 SMBJ7.0CA
IC14 LM4040BIM3-2.5
SPARE
HEATER VOLTAGE
HEATER VOLTAGE RMS
HEATER CURRENT
CATHODE CURRENT
HEATER CURRENT RMS
MOD. ANODE VOLTAGE
CATHODE VOLTAGE
ADIN/1.??
ADOUT/1.??
/ASYNC/1.??
ASCLK/1.??
REF
Projet/ Project: LHC modulator measurement system
Ensemble/ Set:
Sous-ensemble Underset:
Document: HV MEASUREMENTS TRANSMITTER CARD
Echelle/ Scale
Resp.:
Designer: AM/DV
Draun: AM/DV
MODA:
MODB:
File:
IND.
LAB. EUROPEEN POUR LA PHYSIQUE DES PARTICULES
EUROPEAN LABORATORY FOR PARTICLE PHYSICS
GENEVE/GENEVA
Ref: nb
AED-00191-V3

C. Measurement system installation in LHC MAC10 klystron modulator

AED-00202-V1 DCCT box assembly

Required parts for assembly of AED-00202-V1 DCCT box			
Part	**Type**	**Part number**	**Amount**
Circuit board, assembled	AED-00202-V1		1
Die-cast aluminium box	Hammond manufacturing 1590BS		1
Connector	Multi-Contact B6AR-NS	01.0200	5
Connector jacket	Multi-contact IH6AR (yellow)	14.5006-24	2
Connector jacket	Multi-contact IH6AR (blue)	14.5006-23	2
Connector jacket	Multi-contact IH6AR (red)	14.5006-22	1
Nut	Brass, M6		5
Washer	Brass, M6		5
Connector	Lemo ERA.2S.306.CLL		1
Hexagonal spacer	25mm long, M3		4
Screw	M3, 10mm countersunk machine screw		4
Screw	M3, 10mm machine screw		4

The box for the measurement system is type 1590BS from Hammond Manufacturing. Drill four 3.2mm holes in the lid for the mounting of the boards. All dimensions in the drawings are in millimetres

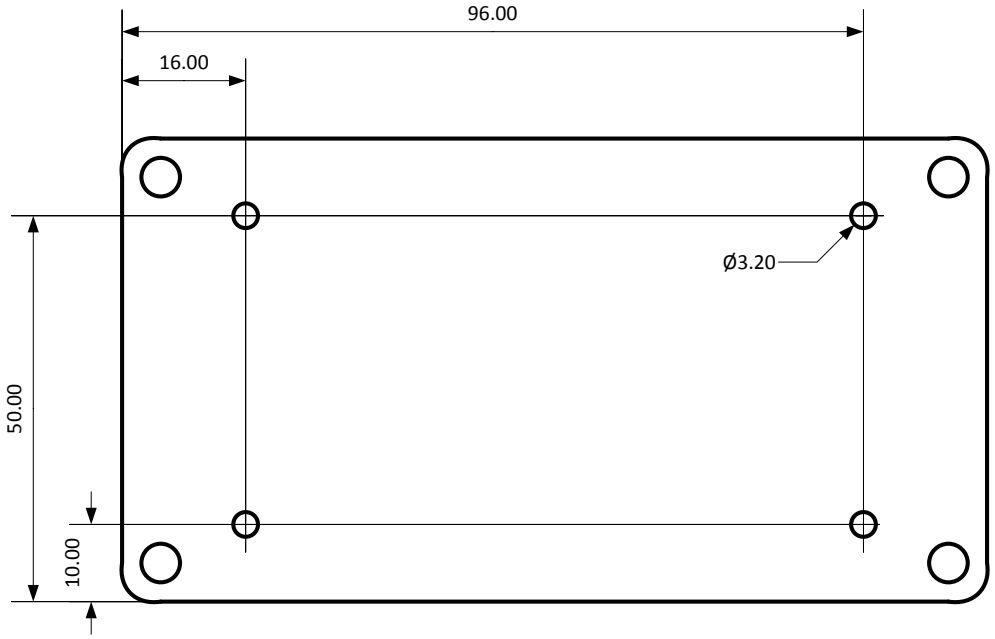

Drill six 15mm holes in the lid for the connectors.

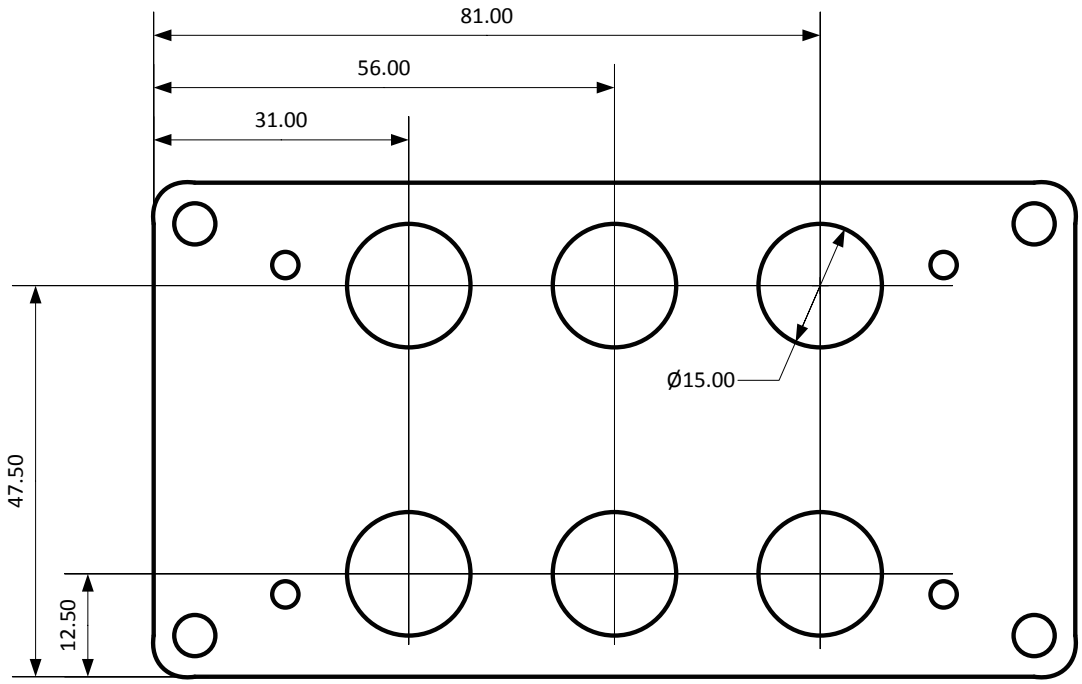

Mount the Lemo connector in the box lid, in the upper centre 15mm hole, using the mounting hardware supplied with the connector.

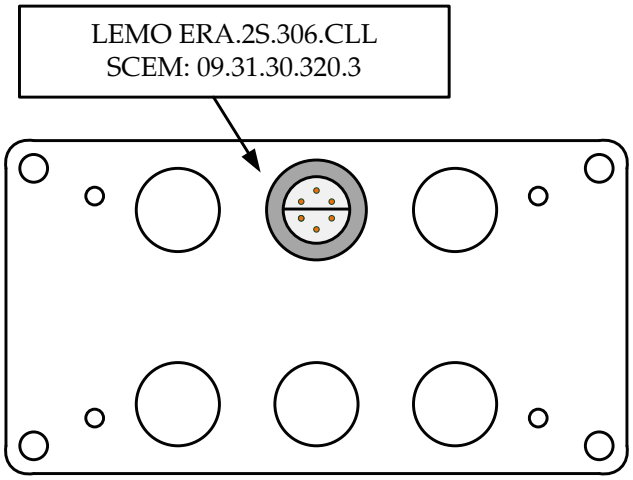

Prepare 5 Multi-contact banana connectors by cutting the threaded part to 8mm. Two connectors should have yellow jackets, two should have blue jackets, and one should have a red jacket.

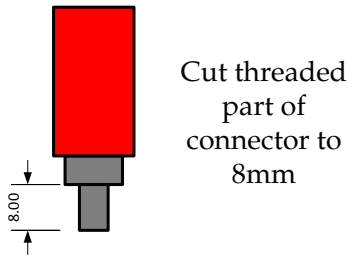

Mount the Multi-contact connectors to the circuit board as shown, using M6 brass nuts and brass washers. Mount one 25mm long M3 hexagonal spacer in each corner of the board.

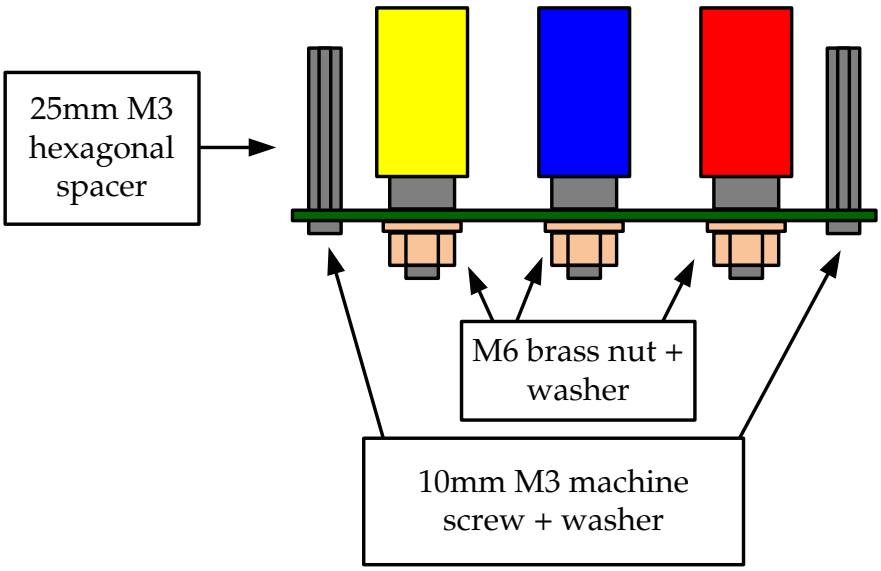

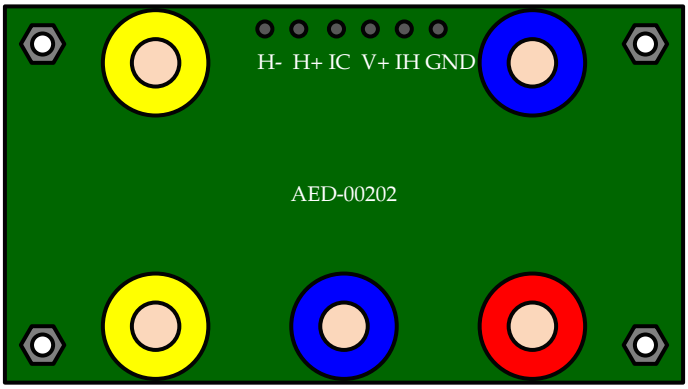

Connect the LEMO connector to the circuit board, following the listed pinout:

LEMO connector pin	Circuit board pad
1	H-
2	V+
3	GND
4	IC
5	IH
6	H+

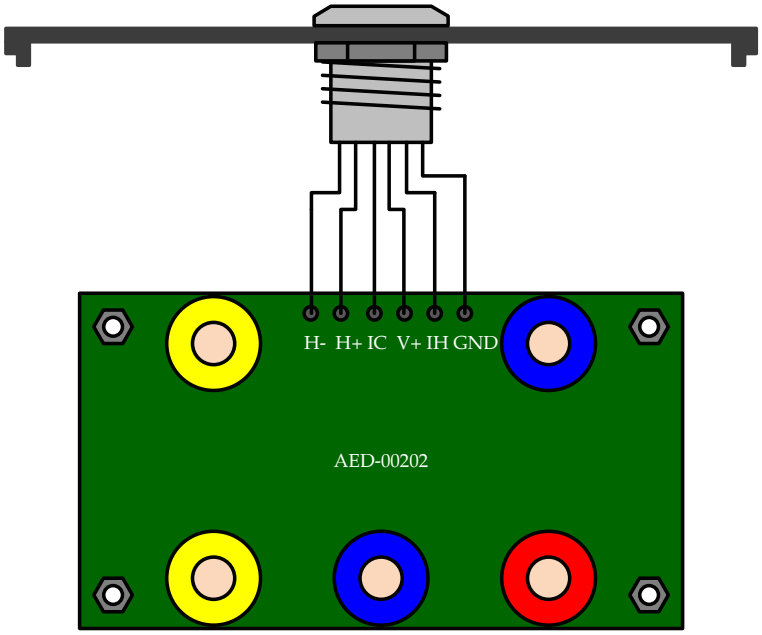

Mount the circuit board to the box lid using four 10mm long countersunk M3 screws.

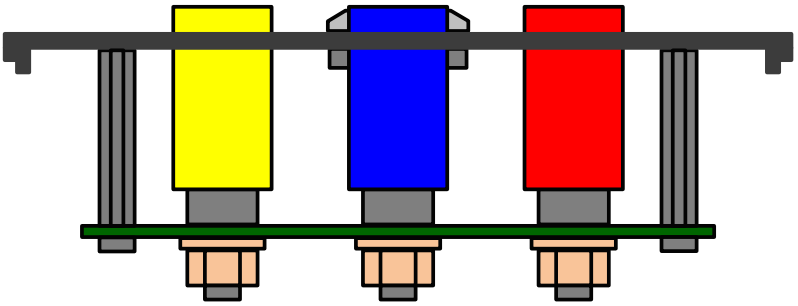

Assemble the box, using 6-32 x ½'' UNC screws supplied with the box.

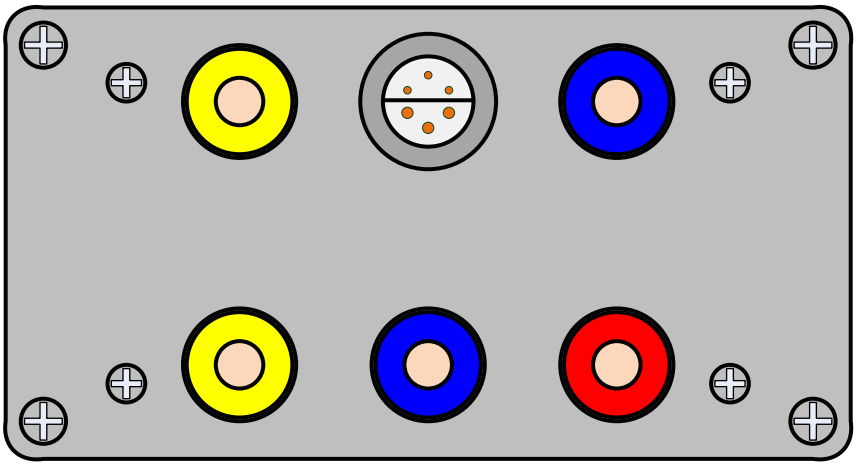

AED-00191-V3 measurement box assembly

Required parts for assembly of AED-00191-V3 measurement system box		
Part	**Type**	**Amount**
Circuit board, assembled	AED-00191-V3	1
Die-cast aluminium box	Hammond manufacturing 1590BB	1
Coaxial cable	Huber + Suhner Enviroflex 316	20 cm
SMC connector, male	Huber + Suhner 24_SMC-50-2-110/111_NE	2
Lemo connector, 2 pin	Lemo ERA.2S.302.CLL	1
Lemo connector, 6 pin	Lemo ERA.2S.306.CLL	1
Hexagonal spacer	25mm long, M3	4
Screw	M3, 10mm countersunk machine screw	4
Screw	M3, 10mm machine screw	4

The box for the measurement system is type 1590BB from Hammond Manufacturing. Drill four 3.2mm holes in the lid for the mounting of the boards. All dimensions are in millimetres

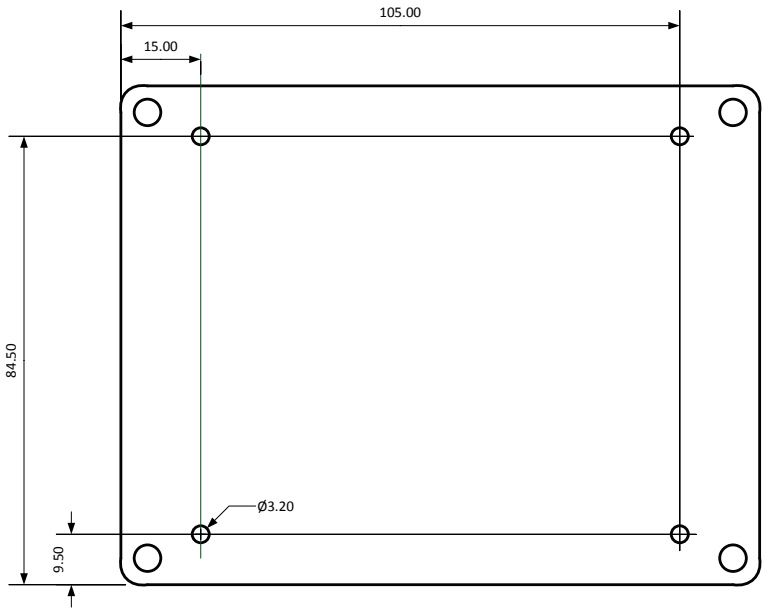

Drill holes in the lid for the connectors.

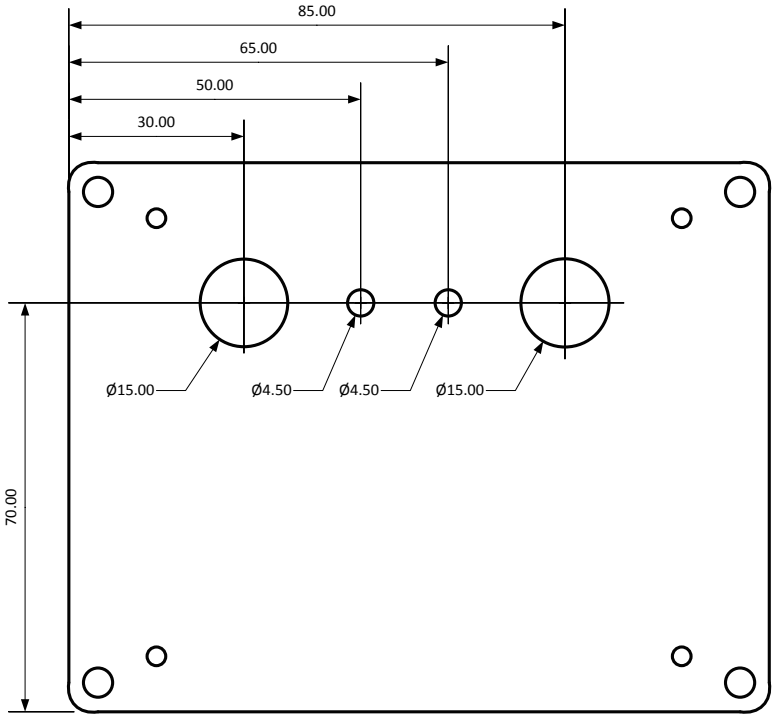

Drill holes for the fibre optic transmitters in the side of the box.

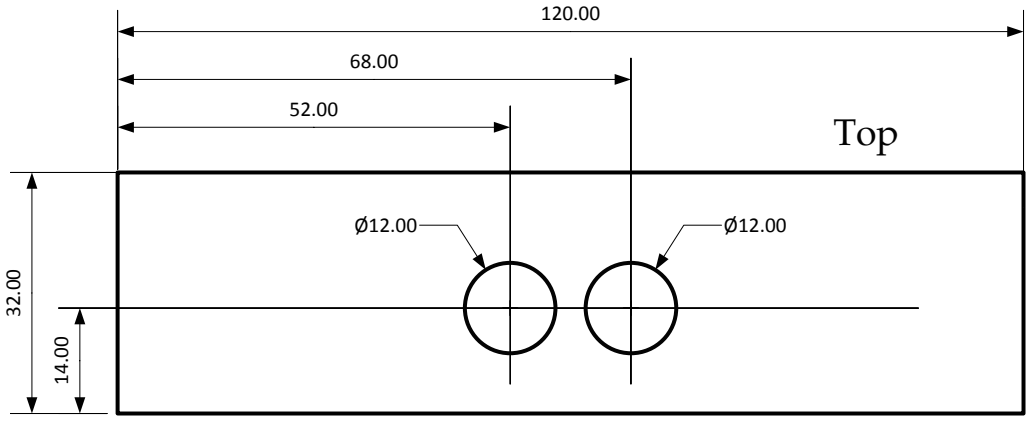

Mount the Lemo connectors in the box lid, using the mounting hardware supplied with the connectors.

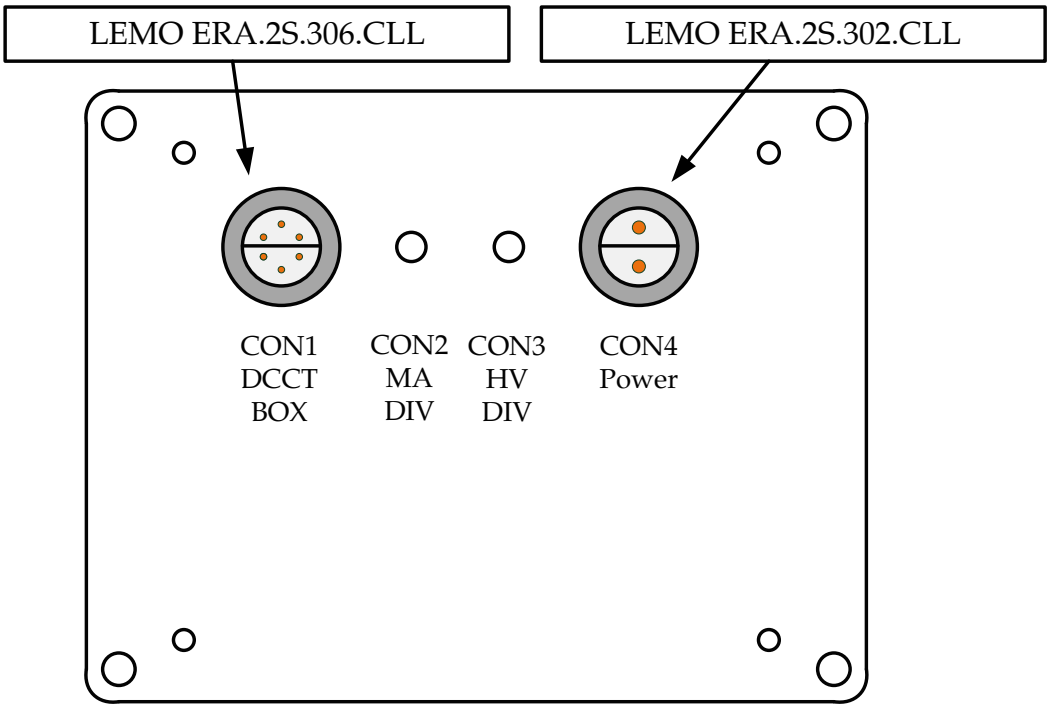

Mount one 25mm long M3 hexagonal spacer in each corner of the board.

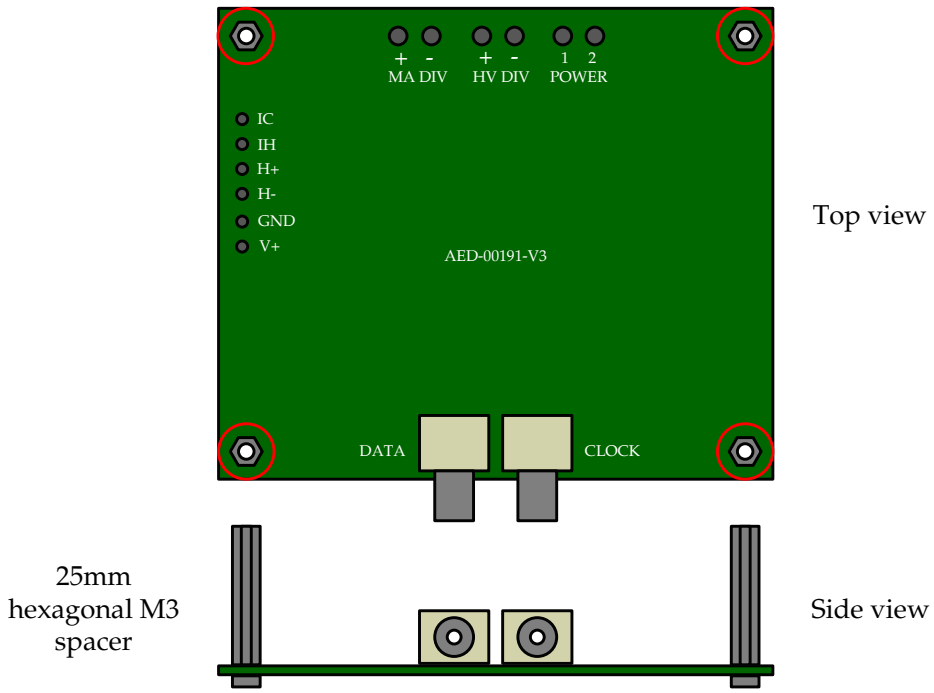

Prepare two pieces of Enviroflex 316 coaxial cable, each 10 cm long. Crimp the SMC connectors to the coaxial cable.

2x

Connect the connectors to the circuit board, following the listed pinouts:

CON1: Lemo ERA.2S.306.CLL	
Lemo connector pin	Circuit board pad
1	H-
2	V+
3	GND
4	IC
5	IH
6	H+

CON2: Huber + Suhner SMC male	
SMC connector pin	Circuit board pad
Centre	MA DIV +
Shield	MA DIV -

CON3: Huber + Suhner SMC male	
SMC connector pin	Circuit board pad
Centre	HV DIV +
Shield	HV DIV -

CON4: Lemo ERA.2S.302.CLL	
Lemo connector pin	Circuit board pad
1	Power 1
2	Power 2

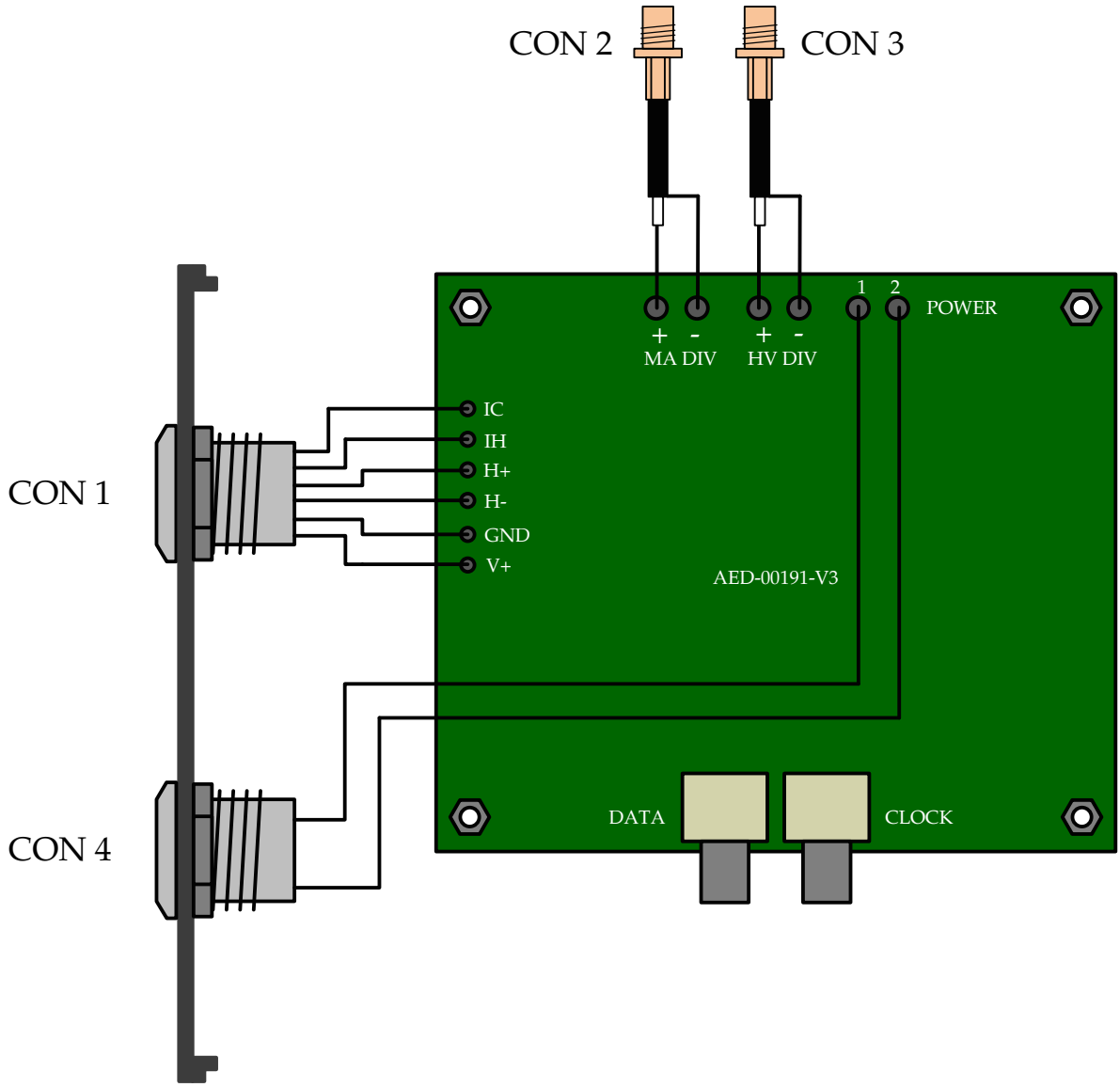

Mount the SMC connectors in the holes in the box lid, using hardware supplied with the connectors.
Mount the circuit board to the box lid, using the 10mm long countersunk M3 screws

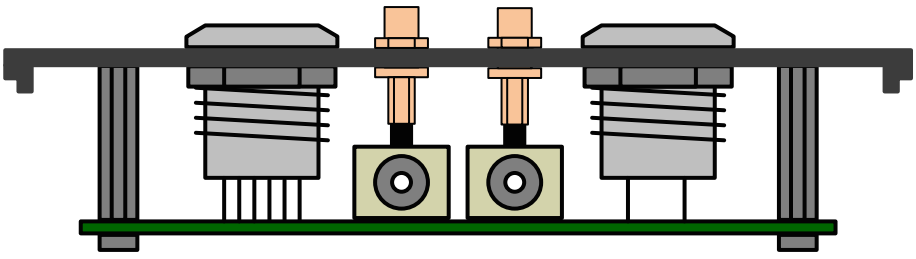

Assemble the box.

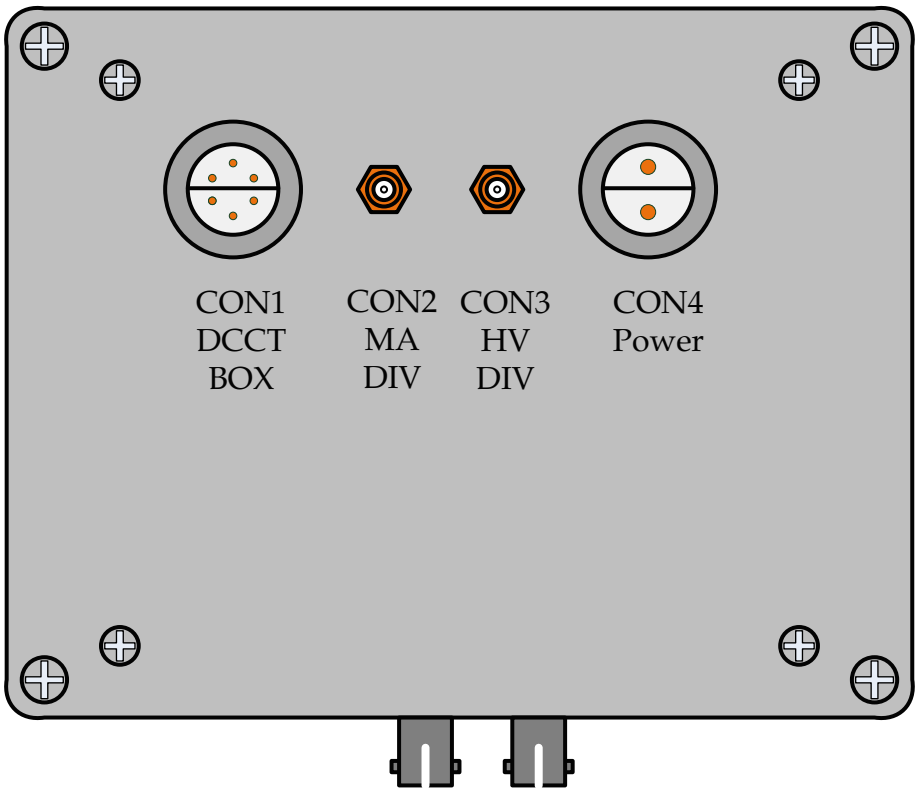

Interconnecting cable assembly

Required parts for assembly of measurement system interconnecting cable		
Part	**Type**	**Amount**
Connector	Lemo FFA.2S.306.CLA C.87	2
Shielded cable	CERN MCA08	

Prepare the interconnecting cable. The length of the cable should be determined depending on the distance between the measurement system and the current transducer box in the modulator.

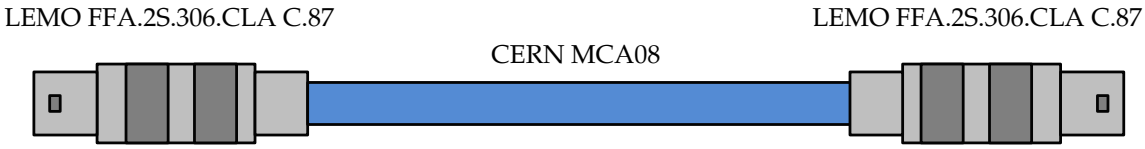

Cable stripping lengths for multipole connectors (S series)

M1 straight plugs and sockets with cable collet, clamping type C (solder or crimp contacts)

M3 elbow plugs (90°) with cable collet, clamping type C (solder or crimp contacts)

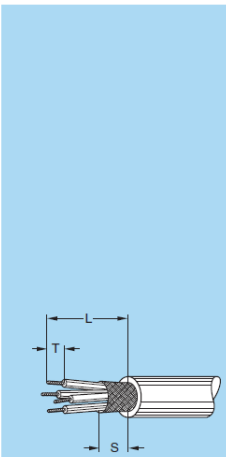

Connector		ø contact A (mm)	Cable stripping lengths (mm)											
			M1						M3					
			Solder			Crimp			Solder			Crimp		
Series	Type		L	S	T	L	S	T	L	S	T	L	S	T
0S	302	0.9	10	5	3.5	15	5	4.0	10	5	3.5	15	5	4.0
	303/304	0.7	10	5	3.5	15	5	4.0	10	5	3.5	15	5	4.0
1S	302	1.3	12	8	3.0	17	8	4.0	14	8	3.0	17	8	4.0
	303/304	0.9	12	8	3.0	17	8	4.0	14	8	3.0	17	8	4.0
	305	0.9	12	8	3.0	17	8	4.0	14	8	3.0	17	8	4.0
		0.7	12	8	2.5	17	8	4.0	14	8	2.5	17	8	4.0
	306	0.7	12	8	2.5	17	8	4.0	14	8	2.5	17	8	4.0
2S	302	1.6	18	9	4.5	22	9	5.5	18	9	4.5	22	9	5.5
	303/304/305/306	1.3	18	9	4.0	22	9	4.0	18	9	4.0	22	9	4.0
	307	1.3	18	9	4.0	22	9	4.0	18	9	4.0	22	9	4.0
		0.9	18	9	4.0	22	9	4.0	18	9	4.0	22	9	4.0
	308/310	0.9	18	9	4.0	22	9	4.0	18	9	4.0	22	9	4.0
3S	302/303/304	2.0	21	9	5.0	–	–	–	–	–	–	–	–	–
	305	2.0	21	9	5.0	–	–	–	–	–	–	–	–	–
		1.3	21	9	4.0	–	–	–	–	–	–	–	–	–
	306/307/308/310	1.3	21	9	4.0	–	–	–	–	–	–	–	–	–
	312/313/314/316/318	0.9	21	9	4.0	–	–	–	–	–	–	–	–	–
	302	4.0	25	9	7.0	–	–	–	–	–	–	–	–	–
	303/304	3.0	25	9	6.0	–	–	–	–	–	–	–	–	–

Measurement system installation in modulator

Required parts for installation of measurement system into modulator		
Part	**Description**	**Amount**
Fibre optical cable	Duplex ST-ST, 50/125 multimode	2 m
Fibre optical feedthrough	ST-ST	2
TVS diode	1.5KE6.8CA	2
Coaxial cable	Huber + Suhner Enviroflex 316	
SMC connector, female	Huber + Suhner 11_SMC-50-2-11/111_NE	2
Lemo connector	Lemo FFA.2S.302.CLAC.72	1
Burndy female pin		2
Burndy male pin		2

Install two additional pins into the female 4-pin Burndy connector in the transformer housing. Connect these pins to the transformer as shown in the diagram.

Red lines are new connections

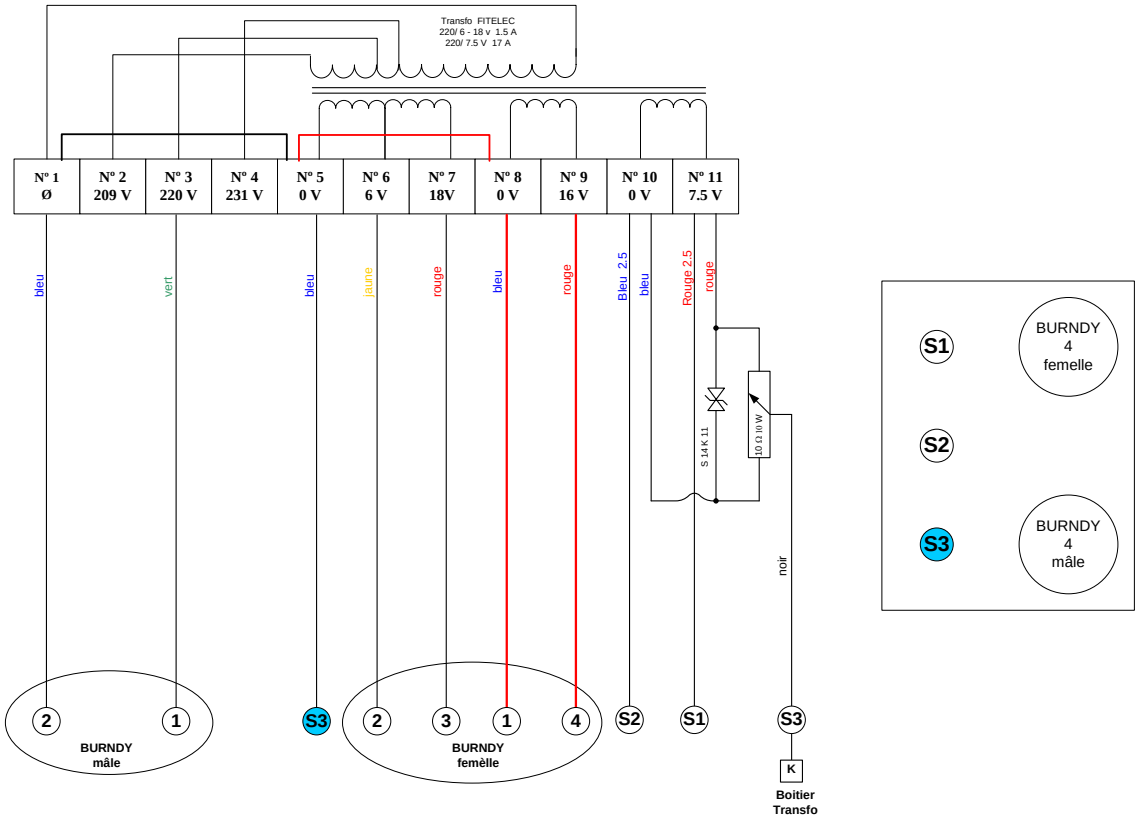

Install two additional pins into the 4-pin Burndy male wire connector that supplies the modulation anode control system. Wire these pins to the Lemo FFA.2S.302.CLAC.72 connector.

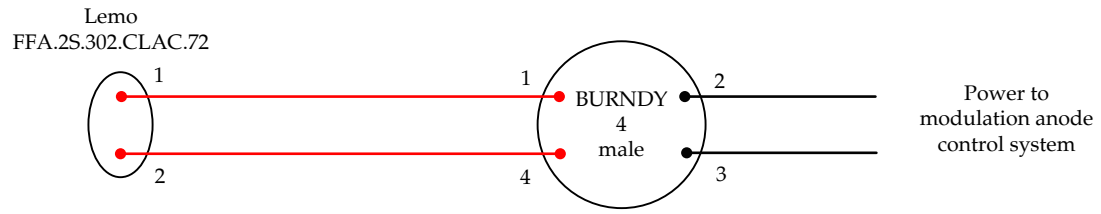

Prepare two pieces of Enviroflex 316 coaxial cable. Crimp the SMC connectors to the coaxial cable.

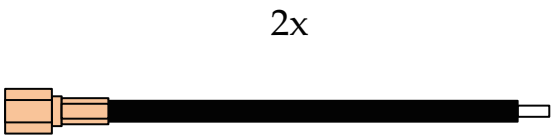

Machine the parts for the voltage divider connections as shown in the diagram.

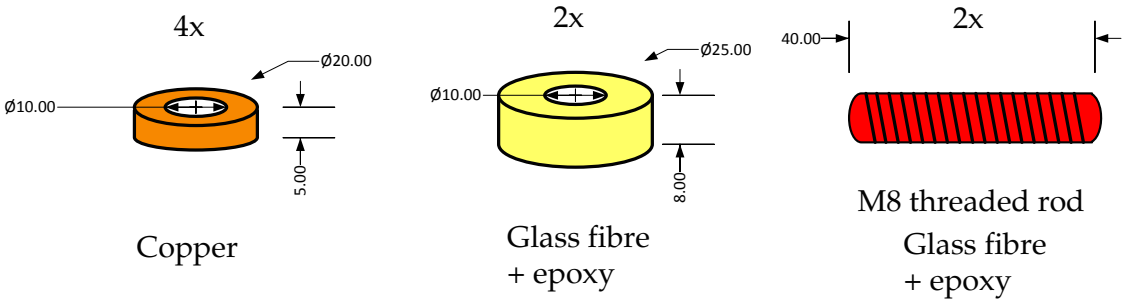

Assemble the connection for the high voltage dividers according to the diagram

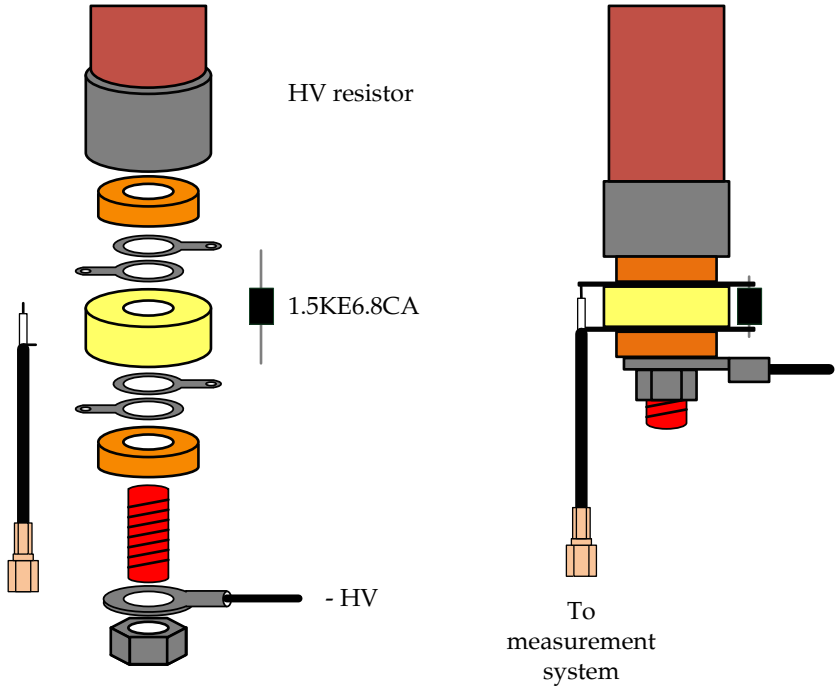

Connect the measurement system to the modulator as shown in the following diagram.

Wiring of MAC10 LHC with measurement system V3

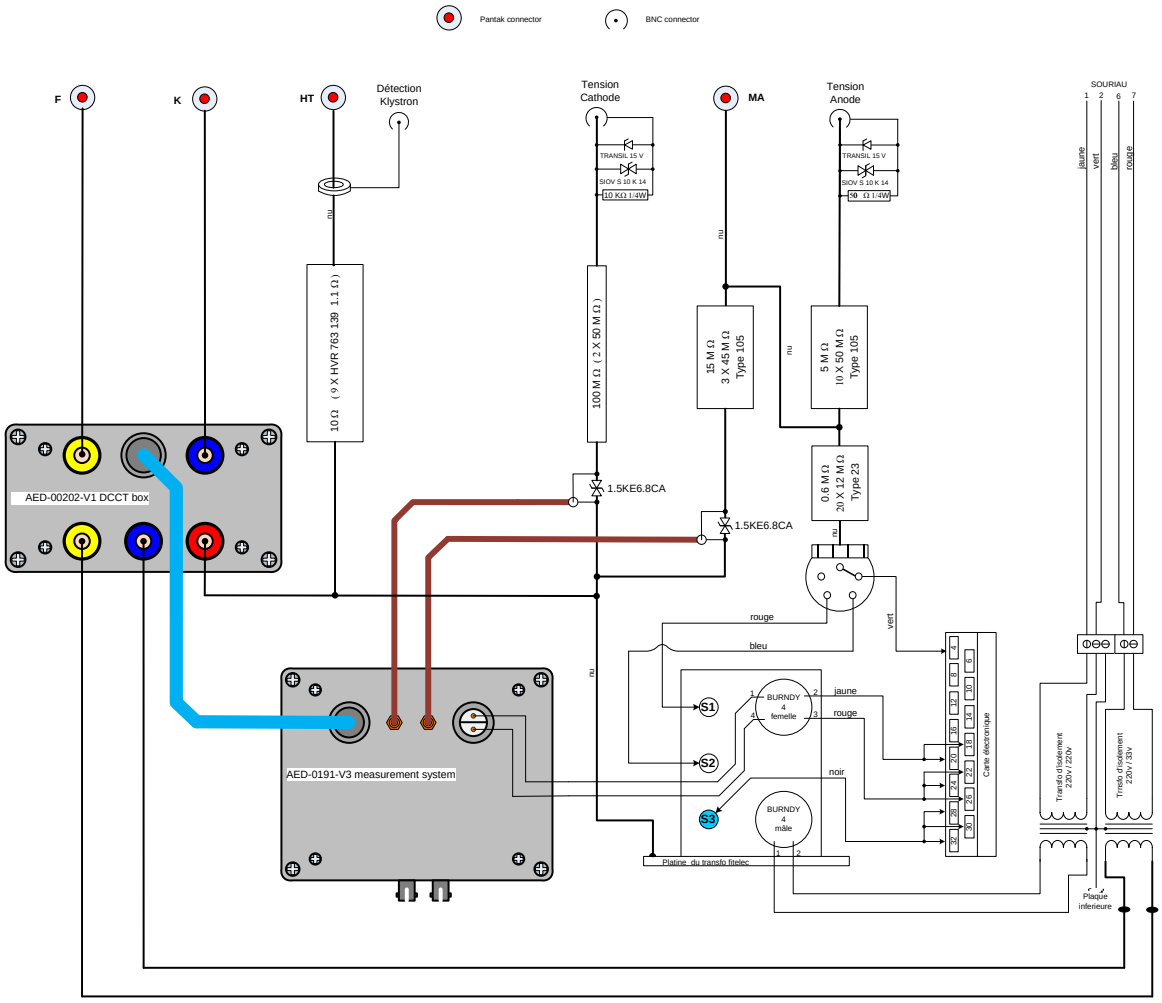

Mount the two ST-ST fibre feedthroughs in the lid of the modulator. Connect them to the measurement system using the 2 m long ST-ST multimode fibre.